Computerized Training of Cryosurgery: Prostate Geometric Modeling and Training Framework

Submitted in partial fulfillment of the requirements for

the degree of

Doctor of Philosophy

in

Mechanical Engineering

Anjali Sehrawat

B.S., Mechanical Engineering, University of Illinois Urbana-Champaign
M.S., Mechanical Engineering, Carnegie Mellon University

Carnegie Mellon University
Pittsburgh, PA

February, 2015

Acknowledgements

I would like to thank my advisors, Professor Yoed Rabin and Professor Kenji Shimada for granting me the opportunity to pursue a Ph.D. degree. Over the past four years they have shown me continuous support, guidance and patience, for which I owe them a huge debt of gratitude. Their mentorship—which extended beyond the purely academic—was integral to providing me with a stellar and comprehensive graduate experience. I can recall so many incidents where a meeting, having begun with an academic question of mine, ended with lessons that integrated advice not just about engineering but also about career and life. I also want to thank my undergraduate advisor, Professor Dimitrios Kryitsis for encouraging me to pursue a Ph.D. degree.

I wish to thank my research committee, Professors Yongjie Jessica Zhang and Phil Campbell, for their invaluable feedback and support throughout my candidacy. I want to thank National Institutes of Health for funding my thesis work. I also wish to express my gratitude to my collaborators, Dr. James McCormick (Allegheny General Hospital) and Dona Wilfong (STAR Center – Allegheny Health Network), whose insights and constant stream of residents were instrumental in completing numerous user-studies.

I want to thank Tomotake Furuhata and Soji Yamakawa for their useful insights on geometric modeling and for their assistance in setting up machines for user-studies. I would like to thank my past and present colleagues in the Biothermal Technology Lab, especially Robert Keelan for developing and modifying many of the cryosurgery computational tools so they may be integrated into the tutoring system; David Eisenberg and Chandrajit Thaokar for their continual support—it has been a pleasure working alongside them. I also want to thank many of my colleagues in the mechanical engineering department for volunteering their time to participate in my pilot studies.

Lastly, I would like to thank my friends and family, especially my mom, Amrita, and brother, Anshu, for their endless love and support through the good, the bad, and the questionable.

Dedicated in loving memory of my nanaji (grandfather), Nawab Singh.

Abstract

This study concerns medical training and education of cryosurgery—the destruction of cancerous tissue by freezing. Minimally invasive cryosurgery is performed by strategically placing an array of cryoprobes within a target region, in order to maximize freezing injury in the target region, while minimizing damage to its surrounding tissues. Cryoprobe placement has yet to be standardized, where cryosurgeons frequently base their practice on their own experience, recommendations made by cryodevice manufacturers, and accepted practices. Suboptimal cryoprobe layouts may leave untreated areas in the target region, lead to cryoinjury in the healthy surrounding tissues, require unnecessarily large numbers of cryoprobes, increase the duration of the surgical procedure, and increase the likelihood of post-cryosurgery complications, all of which affect the quality and cost of the medical treatment. While using prostate cryosurgery as a developmental model for surgical training, this study focuses on two key elements: (i) creating realistic prostate models for training, and (ii) developing training methods for the optimal cryoprobe layout.

Tumor growth pattern in prostates at T3-stage cancer, representative of the cryosurgery candidate population, is characterized in order to identify tumor features that contribute to changes in the prostate shape. Extended free-form deformation (EFFD) is applied on a 3D prostate template geometry to create localized surface changes that resemble cancerous prostates, where key tumor features compiled serve as deformation criteria. The computational technique is demonstrated in three case studies by systematically selecting critical tumor features and deforming the prostate template contour until selected feature parameters are met.

A proof-of-concept for a computerized cryosurgery tutoring system was developed for the simplified case of uniform insertion-depth—2D cryoprobe layout planning. The tutoring system lists geometrical constraints of cryoprobes placement, simulates cryoprobe insertion, displays a rendered shape of the prostate, enables distance measurements, simulates the corresponding thermal history, and evaluates the mismatch between the target region shape and a pre-selected planning isotherm. The quality of trainee planning is measured in comparison with computer-generated planning, created for each case study by previously developed planning algorithms. Two versions of the tutoring system have been tested in the current study using 23 surgical residents: (i) an unguided version, where the trainee can practice cases in unstructured sessions, and (ii) an intelligent tutoring system (ITS), which forces the trainee to follow specific

steps, believed by the authors to potentially shorten the learning curve. Posttest results indicate that the ITS system maybe more beneficial than the non-ITS system, but the proof-of-concept is demonstrated with either system.

Based on the observed effectiveness of the ITS prototype and the learning behaviors of surgical residents, the cryosurgery tutoring system design was modified and extended for the advanced-case of variable insertion-depth—3D cryoprobe layout planning. The objective of the tutoring system remains essentially the same—to develop a cryoprobe layout for a given number of cryoprobes, in order to maximize the match between the resulting frozen region and the target region. The proof-of-concept was demonstrated by measuring learning gains of 18 surgical residents after training on the system. Residents showed significant improvement in minimizing the mismatch between the target region and frozen region.

Table of Contents

List of Figures

List of Tables

Chapter 1. Introduction

The work presented in this thesis is focused on the development of computational tools and methodologies to be used in the computerized training of cryosurgery. This chapter provides an overview of cryosurgery, including the history of cryosurgery, mechanism of tissue injury, modern prostate cryosurgery and current accepted practices. Additionally, challenges in the training of cryosurgery and computerized systems currently used in medical education and training are summarized followed by the specific aims of the thesis.

1.1 History of Cryosurgery

The therapeutic benefits of subjecting tissue to cold temperatures, termed cryotherapy, have been recognized since ancient times. Cryosurgery, a subset of cryotherapy, is the destruction of undesired tissues by freezing, specifically to elicit an inflammatory or necrotic tissue response [1]. At present, cryosurgery is used to treat undesired tissues in various medical specialties, including dermatology, gynecology, oncology, nephrology, urology, neurology, pulmonary medicine, cardiology, and ophthalmology. This section briefly summarizes the evolution of cryosurgery, starting from the first reported case in the mid-19th century through the start of the so-called 'modern-era' of cryosurgery.

In the mid-19th century, an English physician by the name of James Arnott used a mixture of sodium chloride and crushed ice capable of creating a temperature range of -18°C to -24°C, to freeze cervical and skin tumors. Arnott applied the solution to tumors in accessible sites, reporting notable reduction in tumor size and in pain experienced by the patient [2]. A few decades later, advancements in technology, namely the compressing and liquefying of atmospheric gases along with improved cryogen storage methods allowed for the development of several new cryogenic agents: liquid air (-190°C), solid carbon dioxide (–78.5°C), and liquid oxygen (–182.9°C). In the decades surrounding 1900, physicians used these cryogenic agents through various applications methods, i.e. cotton swabs, sprays, and rolling devices, primarily to treat dermatological and gynecological lesions [3]–[6]. After World War II, the commercial availability and low cooling capacity of liquid nitrogen (-196°C) led to its preferred use in cryosurgical applications [7].

Freezing at greater depths (up to 5mm) was achieved by placing liquid nitrogen cooled copper discs on the target area and applying slight pressure [8]. In the late 1930s, the first case of deep-tissue cryosurgery was performed by Temple Fay, a neurosurgeon who used irrigations of refrigerated cold solutions and applications of ice packs to freeze cancers of the breast and uterine cervix. Fay also developed a technique that used implantable metal capsules, joined to an eternal cold irrigation system, capable of delivering cold treatment to deep tissue in the brain [9].

By the mid-1950s, a sundry of studies had been performed using various cryogenic agents, cooling delivery systems and techniques to treat focal lesions and tumors primarily in the brain of animal models and inoperable humans [10]–[13]. These studies were critical in paving the way for future innovations in cryosurgery by demonstrating the efficacy and safety of the procedure. The modern era of cryosurgery came about with the development of the first automated cryotherapy probe system by Cooper and Lee in 1961. The system was comprised of a vacuum-insulated, double channel cannula with an exposed (uninsulated) tip [14]. The system carried liquid nitrogen through the inner cannula to the probe tip, where it cooled the surrounding tissue. The resultant nitrogen gas was then returned through the outer cannula. Cooper used this probe to freeze lesions in the brain to treat Parkinson's disease and other neuromuscular disorders. In the years to follow, cryosurgery techniques were applied in many other medical specialties to freeze tumors of bone, head and neck [15], [16] as well as to treat eye diseases and bronchial and esophageal cancers [17]–[19]. Cryosurgery was also used in the treatment of Meniere's disease, hemangiomas, nasopharyngeal angiofibromas, hemorrhoids, tonsillitis, oral cancer, and rectal cancers [1].

With respect to prostatic diseases, Gonder and Soanes were the first to apply cryoablation to the prostate for the treatment of benign prostatic hyperplasia and prostate cancer. They modified the cryoprobe to facilitate transurethral freezing of the prostate [20]. Post-surgical complications resulting from this approach were severe; freezing of the urethra led to urethral sloughing, rectourethral fistulas and urinary incontinence requiring prolonged post-operative care. Additionally, the lack of control of the freezing front resulted in excessive freezing often extending into the bladder and external sphincter [21]. In 1972, Flocks et al. used an open perineal approach to perform cryosurgery by creating an incision in the perineum to insert the probe [22]. While the open perineal approach allowed for direct visualization of the freezing front, the approach still produced high complication rates. In 1974, Megalli et al. used a closed perineum approach to ablate the prostate, monitoring the freezing via rectal palpation [23]. This technique eliminated complications caused by open incision, however accurate probe placement and monitoring of the freezing front continued to be problematic. Consequently, high morbidity rates associated with cryosurgery led to its abandonment for the treatment of prostate cancer.

During the 1970s and 1980s, clinical research in cryosurgery significantly declined. Although cryosurgery was becoming a standard treatment option for many dermatological and gynecological diseases, the inability to monitor and control the treatment for deep-tissue applications was realized by the medical community. Furthermore, novel technologies including lasers and therapeutic drugs provided superior results for many of the same applications [1].

Advancements in technology in the early 1990s revived interest in cryosurgery as many cryosurgical techniques could be performed with high fidelity. The two primary contributions came from the development of: (i) intraoperative ultrasound, which enabled real-time monitoring of the freezing front and (ii) vacuum-insulated, smaller diameter cryoprobes that use super-cooled liquid nitrogen (-200°C) [24]. A description of these developments in the context of prostate cryosurgery is provided in Section 1.3.

1.2 Mechanism of Tissue Injury

Tissue damage due to freezing can be grouped into two stages, one having an immediate effect and the other having a latent effect [25]. The immediate effect is direct cell injury as a result of ice crystal formation. The latent effect occurs after the tissue thaws and is caused by the progressive failure of microcirculation, ultimately resulting in vascular stasis. When tissue temperature falls in the hypothermic range (-33°C to -0°C), the function and structure of cells are stressed and cell metabolism begins to fail. Once the temperature drops below freezing, water begins to crystallize in the extracellular spaces, creating a hyperosmotic extracellular environment. As a result, water is drawn out from the cells, causing denaturation and electrolyte imbalances. While the resultant effects of cell dehydration and increased solute concentration are harmful, they are not always lethal to the tissue. Intracellular ice, however, is almost always lethal [26]. Intracellular ice begins to form below freezing, achieving heterogeneous nucleation at -15°C and homogenous nucleation at temperatures below -40°C [27]. During thawing, a process called recrystallization occurs, where ice crystals fuse to form large crystals causing further damage to cell membranes [27].

Tissue injury is attributed to three basic features of the cryosurgery technique: rapid freezing, slowing thawing, and multiple freeze-thaw cycles [28]–[30]. Fast cooling rates induce intracellular crystallization and slow thawing rates promote recrystallization, arguably the most deleterious mechanism in cellular destruction [31]. Depending on the application, the procedure may use a single or multiple freeze-thaw cycles. Typically, multiple free-thaw cycles are performed to ablate tumors as they can survive a single freeze-thaw cycle [32], [33].

During the procedure, a cryoprobe is inserted in the target volume and a frozen lesion is created at the onset of cryoprobe operation. The circulation of the cryogen extracts heat from the contacting tissue. Once the tissue reaches the phase transition temperature, direct cell injury initiates and the tissue begins to freeze. As operation continues, more heat is extracted from the tissue and the interface between the frozen and unfrozen tissue begins to propagate outwards from the probe. This freezing front continues to grow until cryoprobe operation is terminated or until the heat from the surrounding unfrozen tissue is equal to the heat that the cryoprobe is able to remove. Successful cryosurgery mandates a close match between the target volume and the lethal isotherm. In the case of prostate cryosurgery, the freezing front is visualized using ultrasound imaging. It is important to note that a temperature gradient exists between the cryoprobe and freezing front and between the freezing front and surrounding tissues—the planning isotherm cannot be directly visualized and must be estimated by the physician. Selection of cryoprobe cooling features and implementation is a critical component in cryosurgery and is discussed in Section 1.4.

1.3 Modern Prostate Cryosurgery

In 2014, the American Cancer Society estimated roughly 233,000 new diagnoses of prostate cancer with approximately 29,480 deaths from prostate cancer in that year [34]. Second only to lung cancer, prostate cancer is the leading cause of cancer death among American men. The prostate is a walnut-sized gland located below the bladder and in front of the rectum, which is responsible for making and storing seminal fluid. The cause of prostate cancer remains unclear, but age, familial history and race play an important role in the likelihood of its occurrence. This section reviews prostate cancer diagnosis measures to provide context for cryosurgery candidacy selection as well as reference for the following chapter. Additionally, advancements in cryosurgery technology and techniques are described followed by an overview of the procedure.

1.3.1 Prostate Cancer Diagnosis

Two common screening methods used for clinical detection of prostate cancer are the prostate-specific antigen (PSA) blood test and digital rectal exam (DRE). PSA is a substance produced by the prostate and in most men, small traces of PSA in the blood are commonly found; however, high levels of PSA (above 4.0ng/mL) can be indicative of abnormal prostate pathology. The DRE screens for tumors that can be palpated on exam by a physician during the rectal exam. Any abnormality cited by the DRE, especially in conjunction with elevated PSA, requires a transrectal needle biopsy to obtain prostatic tissue for histologic examination. If a biopsy reveals malignant cells, the exact stage and tumor grade are then determined. Tumor grade is used to classify cancer cells based on their propensity to grow and spread and also their structure and growth pattern. The Gleason system is the standard classification used to grade tumors, with a score ranging from two to ten. The score is allocated based upon how similar, or dissimilar, cancer cells are compared to a healthy cell. Cancer stage is used to characterize the severity of cancer based on tumor location, size, number of tumors, and lymph node involvement. Both prognostic measures, tumor grade and cancer stage, are used when determining the appropriate course of treatment.

Prostate cancer is most often staged using the TNM classification system [35] which characterizes the severity of cancer based on the extent of the primary tumor (stage T), lymph nodes involvement (stage N), and metastasis (stage M). The T stage is further divided into four sub-stages, summarized in Table 1.1. Cancer is considered to be localized if it is at stage T3 or lower and has not metastasized to local (N0) or distant lymph nodes (M0) [36]–[38].

Table 1.1: TMN classification system is used to stage prostate cancer, where T marks the extent of primary tumor growth, N describes lymph nodes involvement, and M represents metastasis. Localized cancer is defined by tumor growth in stage T1-T3 with no lymph node involvement and metastasis (N0, M0).

Prostate Cancer Stages					
T1	**T2**	**T3**			**T4**
a-c	a-c	a	b	c	a-b
Tumor is confined within the prostate gland		Unilateral ECE	Bilateral ECE	Spread to seminal vesicles	Spread to adjacent tissue

The natural history and clinical significance of localized prostate cancer relates to its pathological stage and grade at diagnosis, but despite this method of categorization it can still behave in a highly variable and therefore unpredictable manner in individual patients [39]. Because early prostate cancers are characterized by slow growth, it is not possible to identify with certainty whether these early tumors will put the patient at a substantial risk for disease progression and metastatic disease. If the risk of disease progression or tumor advancement is low, it may be more advantageous to take no action at all. Therefore several factors, including patient age, life expectancy, risk of treatment related morbidity, health related quality of life are taken into consideration before selecting the optimal treatment for the individual.

Common treatments for localized cancer include radical prostectatomy, radiation therapy and watchful watching. Cryosurgery is a minimally invasive treatment for localized prostate cancer, where the target ablation region can be the entire gland, or a portion of it (known as salvage cryosurgery). Cryosurgery is an ideal treatment for patients with co-morbidities, patients who cannot afford blood loss and are poor candidates for radiation therapy and radical prostectatomy. Cryosurgery can also be performed as a secondary treatment for patients who encountered radiation therapy failures. It is recommended that patients with prostates larger than 40-50cc receive neoadjuvant or concomitant hormonal therapy [36] to reduce the size of the prostate.

1.3.2 Advancements in Prostate Cryosurgery Technology

Cryosurgery tools and techniques have undergone considerable transformation since its first introduction in the late 1960s. This subsection describes key technological and procedural advancements that were paramount in the resurgence of cryosurgery as a means for treatment of prostate cancer.

1. *Image-Guided Technique:* In 1988, Onik et al. integrated transrectal ultrasound (TRUS) imaging into the minimally invasive procedure, allowing for real-time monitoring of the freezing front and also ensuring proper cryoprobe placement [40], [41].

2. *Urethral Warmer:* The introduction of the urethral warmer, a catheter placed in the urethra used to circulate saline solution at body temperature significantly reduced post-surgical complications, urethral sloughing and rectourethral fistulas, by maintaining urethral temperatures at above freezing [42].

3. *Temperature Sensors:* The utilization of thermocouples during the procedure increased control over the freezing process by providing temperature readings at critical neighboring anatomical structures to verify their safety and at locations not visible in imaging used to assess frozen region coverage [43].

4. *Cryoprobe Design:* The use of gas as a cryogen using the Joule-Thomson effect, free expansion of compressed gas, gave rise to the development of small diameter, 3.4mm, cryoprobes. The transition from liquid nitrogen to argon (-185.7°C) further reduced cryoprobe diameter, 1.47mm [37]. As a result, multiple cryoprobes were used to compensate for the lower cooling capacity associated with the smaller diameter. The use of multiple cryoprobes allowed surgeons to sculpt the frozen region, due to sufficient overlap of ice balls, generating a more homogenous frozen region [44]. This obviated the need for skin incisions and tract dilation that were otherwise required for the insertion of larger diameter cryoprobes. Additionally, the thawing process was accelerated by the use of helium gas, which warms as it expands.

5. *<u>Placement Grid:</u>* A brachytherapy-like placement grid (a block containing a matrix of 17-gauge holes, typically spaced 5mm apart) was adapted to the procedure to facilitate transperineal cryoprobe insertion.

1.3.3 Cryosurgery Practices & Additional Considerations

Minimally invasive cryosurgery is performed by strategically placing an array of cryoprobes within a target region in order to maximize internal freezing damage, while minimizing damage to the surrounding tissues. In the case of prostate cryosurgery, the target region for destruction may be all or a preselected portion of the prostate gland [36]. In total gland cryosurgery, the target volume is defined to be the entire prostate, plus a safety margin. Safety margins are selected by the surgeon in order to minimize harm to critical adjacent tissue (bladder, rectum, and urethra) and to ensure destruction of target tissue especially in areas where tumors have a

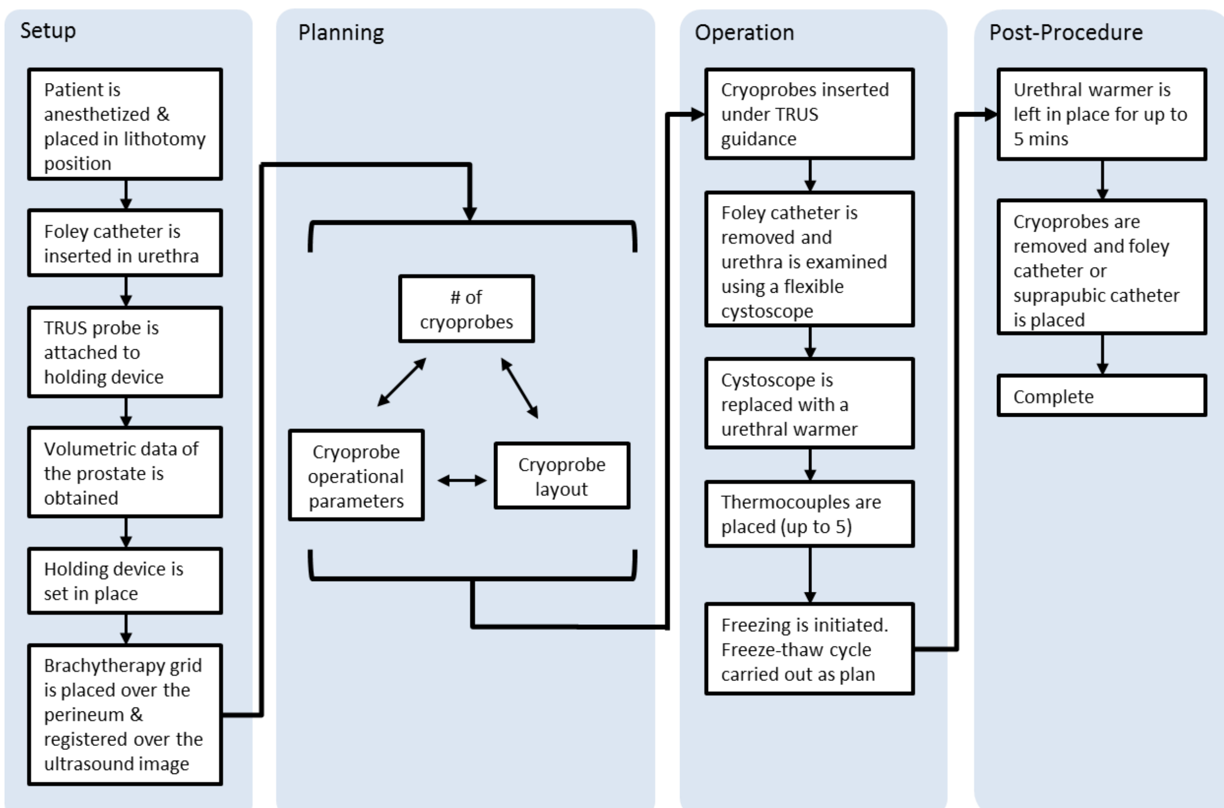

Figure 1.1: Schematic of current prostate cryosurgery practice. Procedure can be divided into four components: setup – patient and operating equipment are primed, planning – optimal cryoprobe plan is determined, operation – probes are inserted and operated under TRUS guidance), post-procedure – appropriate measures are taken to transition patient out of operating room.

propensity to grow. Safety margin selection tends to be highly variable due to the irregular shape of the prostate.

With reference to Figure 1.1, the procedure can be segmented into four stages: setup, planning, operation, and post-procedure. Critical steps within each stage are presented in Fig. 1.1. Most prostate cryosurgery procedures are performed using cryoprobe manufacturers' software (Endocare Inc. and Galil Medical) packages that provide means for synchronization of TRUS imaging, grid placement, along with cryoprobe and thermocouple operation. Figure 1.2 shows patient and cryosurgery system configuration at the setup stage. Prior to planning, patient volumetric data is examined and contours of the prostate, rectal wall, and urethra are identified at multiple cross-sections.

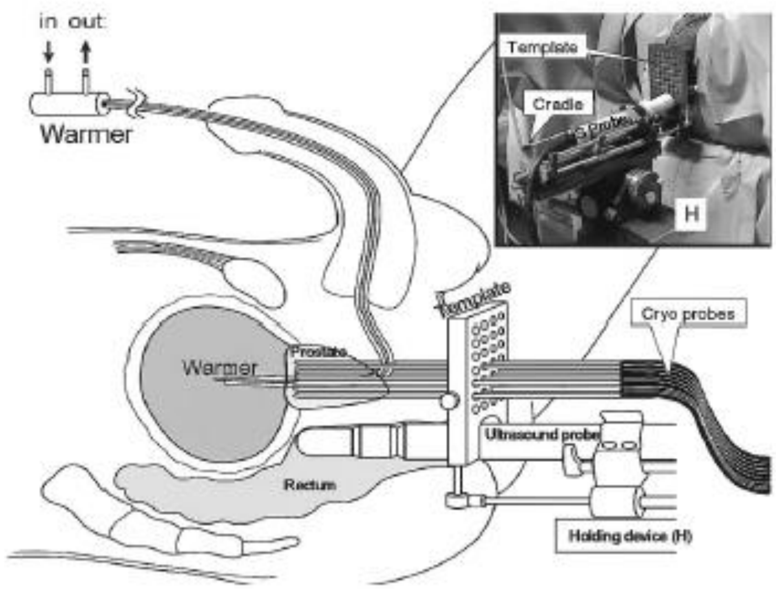

Figure 1.2: Sagittal view of patient and cryoprobe configuration [37].

During the planning stage, the physician must determine the number of probes, their layout and operation. Often the number of probes used is dictated by the prostate volume and dimensions. Planning software may be used to devise a strategy, however, it should be noted that software recommendations are based on three-dimensional assumptions using two-dimensional temperature data of an individual probe.

Cryoprobes are inserted through the perineum under TRUS guidance using the brachytherapy grid. Cryoprobes placement is verified through imaging; probes create a white triangular artifact, displayed in Fig 1.3(a). Once probes and urethral warmer are in place, up to 5 thermocouples are placed at mid gland, level of external sphincter, left and right neurovascular bundles, and the Denonvilliers' fascia.

Typically two freeze-thaw cycles are performed in prostate cryosurgery. The thaw cycle can be either passive, no temperature change induced, or active, heated using helium. The formation of ice prevents ultrasound signals from traveling through the tissue, therefore to maximize ice ball visibility, freezing is initiated at the anterior probes first and guided towards the posterior probes. The change in density of tissue at the freezing front creates a hyperechoic rim with acoustic shadowing, marked by the white line in Fig. 1.3(b) transverse view and (c) sagittal view. For prostates much longer than the effective cooling length of the cryoprobe, a pullback procedure may be performed where one or more probes are moved towards the proximal end of the prostate to freeze along the entirety of the gland.

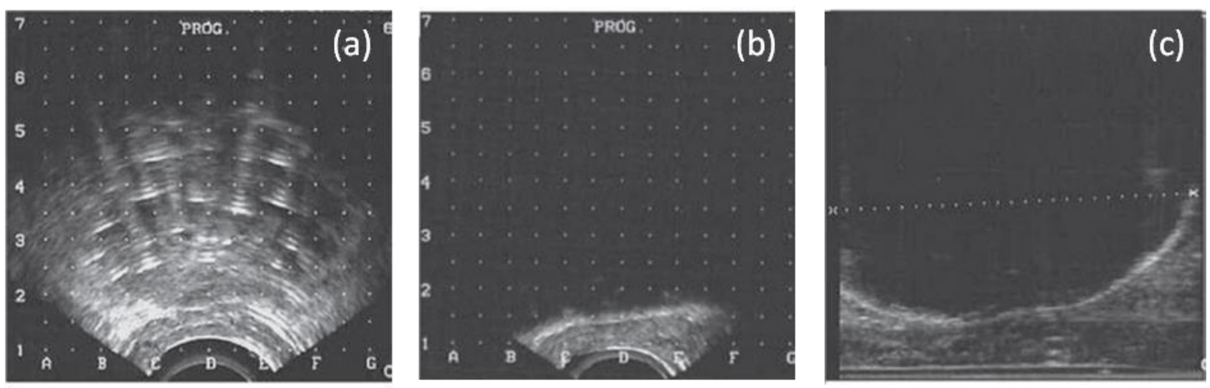

Figure 1.3: Ultrasound image of: (a) the prostate with cryoprobes in situ before freezing; (b) transverse view of the frozen region at the end of the freeze-cycle; (c) sagittal view of the frozen region at the end of the freeze-cycle [45].

The post-procedure frozen lesion contains partially necrotic tissue at the periphery with uniform necrosis at its center [25]. With time, inflammatory cells invade the lesion and the necrotic tissue is replaced by fibroblasts and new collagen formation, resulting in a contracted healed area. The typical operative time averages two hours and patients are generally discharged within one day of operation.

1.4 Computerized Cryosurgery Planning

Cryosurgery planning is an art held by the cryosurgeon, where techniques used are based on the surgeon's own experience, accepted practices, and recommendations made by cryodevices manufacturers. Suboptimal cryoprobe layout may unintentionally leave untreated areas in the target region, lead to cryoinjury in the healthy surrounding tissues, require unnecessarily large numbers of cryoprobes, increase the duration of the surgical procedure, and increase the likelihood of post-cryosurgery complications, all of which affect the quality and cost of the medical treatment [46].

A key to the successful cryosurgery outcome is the optimal selection of the number of cryoprobes, the cryoprobe layout, and cryoprobe thermal history (collectively termed *cryosurgery parameters*) during the planning stage. An ideal cryoprobe plan involves the creation of a three-dimensional (3D) thermal field such that a pre-selected isotherm (the *planning isotherm*) matches perfectly to the outer surface of the target region. The selected isotherm can be: (a) the temperature at the onset of freezing, which is closely related to the visualized frozen region by means of medical imaging; (b) the lethal temperature—a temperature threshold below which maximum destruction is assumed; or, (c) a clinically relevant temperature selected based on the surgeon's own preference [27].

Recent developments in computer hardware and computation techniques are enabling researchers to develop computerized means to aid in the selection of optimal cryosurgery parameters and training of cryosurgery. While early sporadic studies have been presented to optimize the cryoprobe layout [47]–[49], those studies have been based on traditional optimization techniques, where the associated computation cost prohibited reduction to clinical practice. More recently, two alternative optimization techniques have been developed, known as force-field analogy [50] and bubble-packing [51]–[53], which accelerated the optimization process tremendously. Combined with an efficient numerical technique to simulate the bioheat transfer process of tissue freezing [54], computerized planning is closer than ever before to become a clinical reality.

1.5 Computerized Training

1.5.1 Current Cryosurgery Training

Concurrent training in minimally invasive cryosurgery follows the apprenticeship model, wherein a novice physician first reviews a set of guidelines believed to yield cryosurgery success, followed by observing surgical practice by an experienced physician. The surgical case may include computer-assisted planning, provided by the cryosurgery hardware manufacturer. Following the apprenticeship approach and relying on available clinical cases may be constrained by opportunity, availability of patients and instruction time, and may even conflict with clinical operations [55]. Moreover, since cryoprobe placement is not standardized, the applied cryosurgery techniques and the supporting concepts are likely to vary among instructing cryosurgeon. While the apprenticeship approach may provide appropriate training for specific cases and environment of operation, it lacks the exposure to a wide range of cases and also to a wide base of knowledge, which would lead to the development of a broader skillset.

Determining the optimal cryosurgery parameters is an extremely challenging task to which there are many external factors to consider. A competent cryosurgeon must integrate concepts and knowledge from the following areas during surgery planning: patient history and evolution of the disease, geometry of the target region and surrounding tissues, cryosurgery hardware capabilities, knowledge and/or intuition about heat transfer during cryosurgery, and medical imaging interpretation. The work presented in this thesis aims to integrate bubble-packing algorithm and numerical bioheat transfer simulations towards the goal of developing a computerized training system. Such a system is expected to shorten the clinician's learning curve, while providing a wider perspective on thermal effects and clinical practice. Section 1.5 summarizes the use of computerized training in other medical applications.

1.5.2 Computerized Training in Other Medical Applications

Computer-based training can potentially overcome some of the limitations inherent to traditional education methods, while offering a variety of potential benefits, such as reduced risk, increased cost-effectiveness, increased opportunities for demonstration and practice/exercise, improved means to assess knowledge and competences, and mitigation of ethical issues associated with training on patients [56]. Computer-based training tools can be grouped into two categories: part-task trainers and screen-based systems. A part-task trainer includes a part- or a full-body mannequin capable of replicating normal patho-physiological vital signs. Screen-based training tools consist of multi-media applications and virtual-reality simulators, often paired with part-task trainers. A virtual reality system recreates the operating environment with high-fidelity and is typically accompanied by one or more haptic systems that replicate the kinesthetic and tactile perception of the task being trained [57]. Virtual reality systems are widely used to train physicians on vascular access, endoscopic, arthroscopic and laparoscopic surgical techniques [58]–[60]. Multi-media applications provide computer-assisted instruction (CAI) that may complement lectures or provide case-based instructions to hone decision-making and diagnostics skills [61]–[64].

Intelligent tutoring systems (ITSs) represent a subset of CAI. An ITS integrates explicit programming of domain knowledge and pedagogic expertise, in order to provide individualized instruction and feedback throughout the student problem-solving process. The ITS presents a set of problems, each strategically broken down into multiple steps, allowing the system to intervene at every step as needed. By contrast, a traditional tutoring system does not intervene; it only provides feedback to the student based on the final solution. In essence, the ITS aims at emulating the teaching approach—much like one-on-one teacher-student interaction [65].

ITS design is heavily influenced by the intrinsic nature of the domain (i.e., cryosurgery) and the transferability of its pedagogic strategy into computerized instruction. The two most common types of ITS are known as *cognitive* and *constraint-based*, differentiated by the specific learning theory used to model the domain. Cognitive modeling is based on Anderson's ACT-R theory, which states that there are two types of knowledge: declarative and procedural. Initially declarative knowledge (i.e., fact-based knowledge) is learned, which is later translated into more efficient procedural knowledge (i.e., skills) [66]. Here, the domain is modeled using procedural knowledge, represented in the form of rules. In general, cognitive tutors are considered superior for linear domains, where rules may be constructed in a way that force students to take a specific path to reach an established solution. Constraint-based modeling is rooted in Olsson's theory of learning from performance errors, where mistakes result from declarative knowledge that has not been internalized in one's procedural knowledge [67]. Here, the domain is modeled using declarative knowledge represented in the form constraints. Constraint-based tutors allow students to reach a solution, or a solution-space through a somewhat self-selected path. These domain modeling techniques have been successfully applied to develop tutoring systems for subjects such as mathematics, science and computer programming [68]–[70]—all demonstrating to be highly effective when compared to human tutoring. The implementation of such techniques to develop tutoring systems for medical applications becomes more complicated, as most medical applications are not as linear as the aforementioned domains. Chapter 3 discusses the challenges faced in modeling cryosurgery in a way that is appropriate for computerized instruction.

The earliest attempt to develop an ITS for medical applications was known as the GUIDON project in the early 1980s, which focused on the treatment of infectious meningitis, bacteremia, and causative organisms based upon individual patient presentation [71]. In the mid-1990s, Elliot and co-workers developed the Cardiac Tutor [72], to teach resuscitation management of patients undergoing cardiac arrest. The Cardiac tutor integrated simulations of physiological and functional cardiac arrhythmias in response to various medications and interventions. In the late 1990s, parallel efforts focused on the development of two ITS prototypes to interpret and diagnose abnormalities in mammograms and neuroradiology imaging, termed the RadTutor and the MR Tutor, respectively [17,18]. At about the same time, Crowley and co-workers developed the SlideTutor, an ITS prototype that teaches medical residents how to interpret pathology slides for diagnostic inference [75]. In the following years, Evens developed the CIRCSIM, a cardiovascular physiology tutor emphasizing the causal relationships in circulatory physiology [76]. Among the prototypes listed above, only the Cardiac Tutor [72] integrated the domain subject with simulation. The ITS approach for computer-based medical education presents a new and unique opportunity with fast growing potential, associated with rapid advancement in computation techniques, computer platforms, and communication technology.

1.6 Research Objectives

The primary objective of this research is to develop computational tools for cryosurgery training in order to shorten the clinician's learning curve. Towards that goal, the following contributions have been made:

1. Tumor growth patterns for prostate cryosurgery candidates, typically at stage T3 cancer, were characterized based on available information from the literature. Results of this

characterization were used to provide guidelines on how to develop a prostate model database for training, which is representative of the patient population undergoing cryosurgery (Chapter 2).

2. A computational technique was developed for generating geometric prostate models, utilizing an extended free-form deformation (EFFD) (Chapter 2).

3. A proof-of-concept of a simulation-based cryosurgery ITS was built, using the simplified case of uniform insertion depth planning as a model. The ITS targets the acquisition of knowledge and the development of intuition necessary to create an optimal match between the frozen region and the target region (Chapter 3).

4. A formative evaluation was performed to determine the effectiveness of the ITS by measuring the performance of surgery residents during training (Chapter 3).

5. A proof-of-concept for an advanced-level tutoring system was built with the goal of variable cryoprobes insertion depth, a concept which is rarely applied due to the complexity of planning (Chapter 4).

6. A formative evaluation was performed on the advance-level tutoring system by measuring learning gains of surgery residents after training (Chapter 4).

7. Experimental design for advanced investigation of computerized cryosurgery training system was developed (Chapter 6).

Chapter 2. Generating Prostate Models by Geometric Deformation

Beyond adequate computer resources, computerized training necessitates three key elements: (i) a simulator of the procedure, (ii) a tutor to provide feedback on specific simulated cases, and (iii) a database to store case-specific information. The mainstay of the above key elements is the availability of high-quality organ models of candidates for cryosurgery—the objective of this current study. The long-term goal in this line of study is to develop a database representative of the patient population undergoing cryosurgery. Specifically, developing a computerized training system for prostate cryosurgery relies on having realistic prostate geometries to study the effects of prostate cancer and its implications as it relates to cryosurgery. One approach to represent an abnormal growth of a prostate due to cancer tumors is by selecting a normal prostate model—a template—and deforming it to correspond with the progression of the disease. The challenges associated with generating a prostate model from a template originate from the intrinsic asymmetry of the organ, and the variability in growth patterns exhibited in the population of prostate cancer patients.

In this chapter, a computational technique is presented for deforming a template model using extended free-form deformation (EFFD), while proposing a systematic approach for generating a database that is reflective of the prostate cryosurgery patient population. Additionally, this chapter provides an overview of prostate cancer and its effects on the overall shape of the prostate in efforts to characterize growth patterns. The subject matter of this chapter has been published in Proceedings of the American Society of Mechanical Engineers (ASME) 2011 Summer Bioengineering Conference, Biomedical Engineering Society (BMES) Annual Meeting 2012, and International Journal of Computer Assisted Radiology and Surgery [77]–[79].

2.1 Prostate Cancer and Tumor Growth

The approach proposed in this study for determining critical tumor characteristics is based on surface changes caused by cancer penetrating through the prostatic capsule. Nevertheless, cancer confined within the capsule has the potential to alter prostate geometry, and even in the early stages of cancer as T1 and T2. Tumors typically grow by invading adjacent tissue, which can replace glandular tissue, displace glandular tissue, or a combination of both [80], where glandular tissue displacement may also affect the prostate shape. Furthermore, prostate cancer can be multifocal, which presents a challenge in analyzing cancer-related prostate contour changes, as the overall shape of the organ may be affected by different deformation mechanisms at various locations.

Tumor size and location are the primary considerations for prognosis and subsequent selection of treatment. However, little attention has been paid to determining the relationship between tumor growth type and prostate shape changes. To the best of our knowledge, since prostate cancer treatments are mostly focused on excision, resection, or destruction of the tissue in situ, the effects of cancer growth type on the prostate shape have never been studied before. In a multifocal cancer, the primary tumor (i.e., the largest tumor) is most frequently used to define the cancer stage. About 80% of non-primary tumors are of small volume (defined as less than 0.5 cc) and low grade (cells poorly resemble cancer cells according to the Gleason score), indicating that most of the non-primary tumors may not call for clinical intervention [81]. Relative to the average volume of the candidate prostate for cryosurgery (about 35 cc), those tumors would have negligible effects on the prostate shape.

It is noted that describing prostate geometry changes solely based on cancer growth is challenging as prostate cancer is often diagnosed in older men, with two-thirds of the cases above 65 years old [34]. This may further complicate the analysis of prostate-shape changes since the prostate tends to enlarge with age naturally, but may also enlarge as it becomes more susceptible to other prostatic diseases such as benign hyperplasia [82]. In the current study, characterization of critical geometric features that affect a T3-stage prostate is based upon the assumption that only the primary tumor experiences extra-capsular extension (ECE). Here, the T3-stage cancer can be further classified as unilateral ECE, bilateral ECE, or spread into the seminal vesicles [83]. Only unilateral ECE and bilateral ECE are considered in the current study, since cryosurgery is routinely performed on prostates in which cancer is confined to the gland.

It has been observed that 68% of cancer tumors are found in the peripheral zone of the prostate [84], which correlates with about 70% of the prostate total volume [85]. Since the majority of tumors are found in the peripheral zone, clinical data used in the current study is restricted to cancer originating from this area, whereas follow-on studies are planned to address the remainder of the prostate. With reference to Fig. 2.1, peripheral-zone cancers typically spread laterally (x-y plane) along the nerve branches towards the posterolateral capsule, and vertically (z-direction) towards the superior pedicle along the base [86]. Therefore, shape changes in the current study are further restricted to the posterior mid-region and the base.

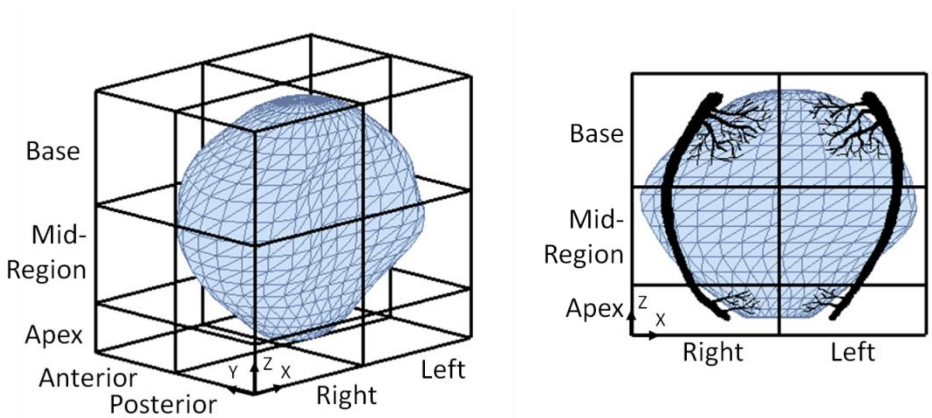

(a) (b)

Figure 2.1: Sectioned prostate template used in the current study to identify areas of cancer growth: (a) an isometric view, (b) top view showing the neurovascular bundle and superior and inferior pedicle. The notation on the x axis refers to the patient's left and right, as it would be viewed by the clinician.

McNeal and Haillot [87] investigated 571 prostates removed during radical prostatectomy to evaluate cancer growth patterns relative to cancer volume. Each prostate was dyed, preserved (fixed in formaldehyde), and then cut into 3 mm-thick slices along the transverse plane. Each slice was examined by means of microscopy to trace tumor and relevant prostate boundaries. Tumors were sorted by zone of origin and by tumor volume. Measurements related to tumor location (sub-capsular invasion) within the transverse plane, percent of prostate base and apex replaced by cancer, extent of tumor capsular penetration, and tumor volume were calculated using computer planimetry. Each measurement was taken on the transverse plane.

The results presented by McNeal and Halliot [87] do not fully describe the geometric effects of cancer on the prostate surface but provide the key parameter values listed above, as cancer tumors may take arbitrary shapes. Sub-capsular invasion relative to tumor volume are summarized separately from tumor extension at the prostate base relative to tumor volume. However, the combined effects of tumor sub-capsular invasion and tumor extension at the base relative to the tumor volume have not been specified. Based on that study, it follows that one may predict the percentage of tumors of a specific volume that occur at a specific location, but may not know the likelihood of all possible tumor volumes occurring at the same location. Additionally, the location of tumor extension on the transverse plane has not been clearly assessed.

Figure 2.2 displays the statistical distribution of extra-capsular extension (ECE) based on tumor volume and tumor location, as compiled in the current work from the study of McNeal and Halliot [87], while integrating the topographical anatomy of periprostatic and capsular nerves, as

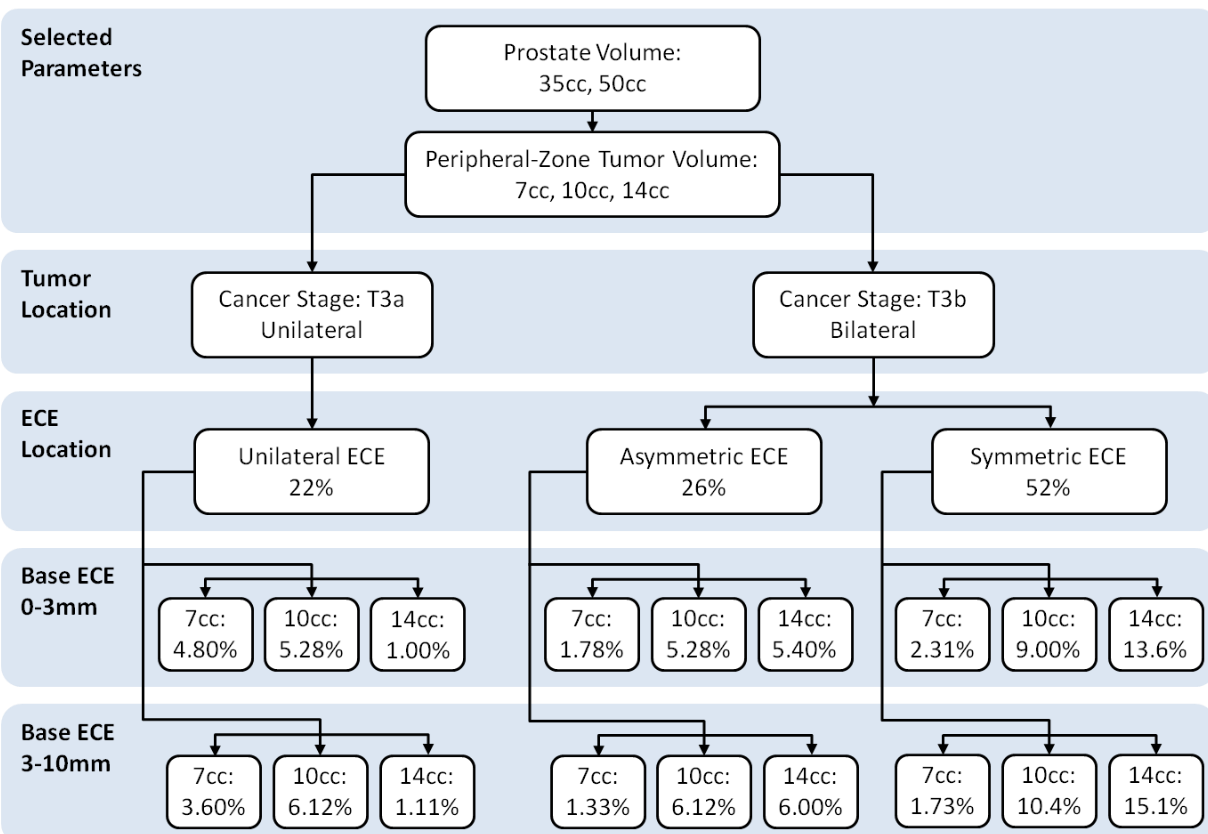

Figure 2.2: Statistical distribution of extra-capsular extension (ECE) based on tumor volume and tumor location selected in the current study for database generation; data was compiled from [87], [88].

quantified by Ganzer and co-workers [88]. The compiled data presented in Fig. 2.2 serves as the mainstay in developing a strategy to construct a database for candidate prostates for cryosurgery (up to T3-stage cancer). Model parameters selection for demonstration purposes in the current study is presented below, whereas database construction is a task left to be performed in concert with the tutoring code development [89], [90].

For demonstration purposes, two healthy prostate templates are used in the current study that represent the average and the maximum prostate volume of cryosurgery patients, 35 cc and 50 cc, respectively. McNeal and Haillot [87] found that ECE was more prevalent in tumors larger than 4 cc, therefore this study assumes that a prostate at T3 stage cancer is likely to have tumors larger than 4 cc. For those tumors, ECE was observed primarily at the base of the prostate and was most frequently associated with cancer spread extensively along extra-prostatic nerves of the superior pedicle (see Fig. 2.1b). Consistent with the specific volume information presented in [87], three representative tumor volumes are selected in the current study: 7 cc, 10 cc, and 14 cc. The relative distribution of each of those representative tumor volumes in the stage T3 cancer patient population is unknown, as there is no direct correlation between tumor volume and cancer staging. In the absence of more specific information, the model presented in this study does not assume higher likelihood of finding any particular tumor volume in stage T3 cancer. Furthermore, the primary concern in constructing a prostate model for cryosurgery planning is capturing surface changes that result from the tumor extension and, therefore, the actual tumor volume is of lower importance since majority of the tumor lies within the prostate.

Location and extent of prostatic capsular extension are further attributed to each representative tumor volume, as displayed in Fig. 2.2. Tumor location is determined by its subcapsular invasion, which can be either unilateral or bilateral. Unilateral tumors are characterized by tumor sub-capsular invasion extending to and slightly beyond the midline. For these tumors, ECE remains on the lobe of origin. Bilateral tumors are further divided into two groups of asymmetric ECE and symmetric ECE. Asymmetric ECE extends past the mid-line, but is primarily on the lobe of origin. Symmetric ECE is defined by tumor extension beyond the prostatic capsule on both lobes. For each tumor volume, 22%, 26%, and 52% of occurrences were found to have unilateral ECE, bilateral-asymmetric ECE, and bilateral-symmetric ECE, respectively [87], [88]. Both sub-capsular invasion and extra-prostatic nerve distribution were used to tabulate the ECE location percentages because cancer tends to spread along the extra-prostatic nerves.

For peripheral zone cancer, three base ECE configurations are possible: (1) left or right unilateral, (2) left or right bilateral-asymmetric, or (3) bilateral symmetric. Tumors are equally likely to originate from the left or the right lobe [91]. Each ECE configuration at each location is associated with a transverse span along the prostate perimeter, based on extra-prostatic nerve distribution. Ganzer and co-workers [88] took transverse slices of prostate specimens, which were removed during non-nerve-sparing radical prostatectomy, and dissected them into 12 evenly spaced sections in order to determine the extent of extra-prostatic nerve surface area within each section. The same sectioning scheme has been adopted in the current study to match each ECE configuration with a transverse span. Each span is composed of a set of sections that encompass the prostate perimeter with respect to the tumor location, where extra-prostatic nerves are likely to be found. It follows that for each ECE configuration, the corresponding transverse span defines the area along the prostate surface where ECE is likely to be found.

Figure 2.3 displays a transverse cross-section (x-y plane) of the prostate template divided into 12 sections. The transverse span coupled with left unilateral and bilateral-asymmetric ECE configuration are associated with section numbers 2–6 and 2–8, respectively; right unilateral and

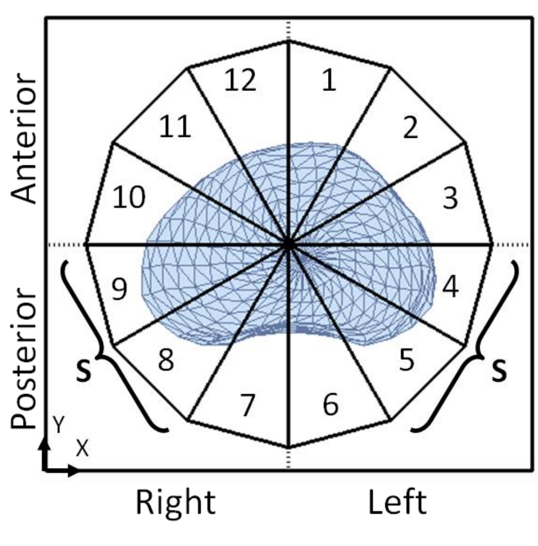

Figure 2.3: Transverse sectioning of the prostate, where S represents regions along prostate base with highest extra-prostatic nerve density, found in the posterolateral ends of the prostate as displayed in Fig. 2.1.

bilateral-asymmetric ECE configuration are associated with section numbers 7–11 and 5–11, respectively. Sections 2–11 are associated with the transverse span of bilateral symmetric ECE configurations. The section pair labeled with S represents the region with the highest concentration of nerves to surface area, which correlates with 84.1% of the total extra-prostatic nerve surface area [88]. Based on the ECE location, tumors are likely to penetrate the capsule wall along the transverse span with maximum extension in region S.

For each ECE location, the likelihood that a tumor will extend beyond the prostate capsule are 48% and 52% for extensions of 0–3 mm and 3–10 mm, respectively [87]. The percentage of 7 cc, 10 cc, and 14 cc tumors calculated to extend 0–3 mm and 3–10 mm beyond the prostate capsule for each ECE location is presented in Fig. 2.2. Based on the data summarized above, critical tumor features—ECE location and ECE length—were selected for the development of a prostate-model database for cryosurgery candidates.

2.2 Computational Technique

This study applies extended free-form deformation (EFFD) on a 3D prostate template, using a modified computational technique [92]. The EFFD method is an extension of Sederburg's free-form deformation (FFD) method [93], where the deformation is applied to the space in which an object is embedded, rather than directly to the object.

Numerous studies have developed computational methods that apply FFD to a template object, to create patient-specific 3D anatomical models based on a set of 2D medical images such as those obtained from CT, MRI, SPECT, and X-ray [94]–[97]. In these studies, FFD is applied through an optimization process to minimize either the distance or the cross-sectional area difference between contours found on the 2D images and the deformed model contour. Little attention has been paid to integrating clinical data into modeling of the prostate in order to model the exact shape of the cancerous prostate. In the current study, we attempt to generate realistic geometric models that are likely to be encountered by clinicians in typical cases of prostate cryosurgery. The current study uses EFFD and can be viewed as an extension of our pervious exploratory study [89], which employed the basic FFD method. Furthermore, our previous study [89] did not incorporate ECE nerve distribution to determine the likelihood of lateral tumor ECE location, nor did it include criteria for successful deformation.

The FFD method is presented here in brief, for the completeness of presentation. With reference to Fig. 2.4(a), a local coordinate system is imposed on a parallelepiped region which can be used to describe any point *X* in the unit volume by:

$$X = X_0 + sS + tT + uU \tag{1}$$

where X_0 is the origin of the local coordinate system, *S*, *T*, *U* are unit vectors of the local coordinate system, and *s*, *t*, and *u* are given by:

$$(s,t,u) = \left(\frac{T \times U \cdot (X - X_0)}{T \times U \cdot S}, \frac{S \times U \cdot (X - X_0)}{S \times U \cdot T}, \frac{S \times T \cdot (X - X_0)}{S \times T \cdot U}\right) \tag{2}$$

where *s*, *t*, and *u* are in the range of 0 and 1. A set of control points, $P_{i,j,k}$, are imposed on the parallelepiped region, where *l*, *m*, and *n* are the number of subdivisions along each of the unit vectors *S*, *T*, and *U*, respectively:

$$P_{ijk} = X_0 + \frac{i}{l}S + \frac{j}{m}T + \frac{k}{n}U \tag{3}$$

The control points are moved, and the displaced object vertices are determined using the trivariate Bézier function:

$$X_{ffd}(s,t,u) = \sum_{i=0}^{n}\sum_{j=0}^{m}\sum_{k=0}^{l} p_{ijk} B_i^n(s) B_j^m(t) B_k^l(u) \tag{4}$$

where $B_i^n(s)$ is the Bernstein polynomial given by:

$$B_i^n(s) = \binom{n}{i} s^i (1-s)^{n-i} \tag{5}$$

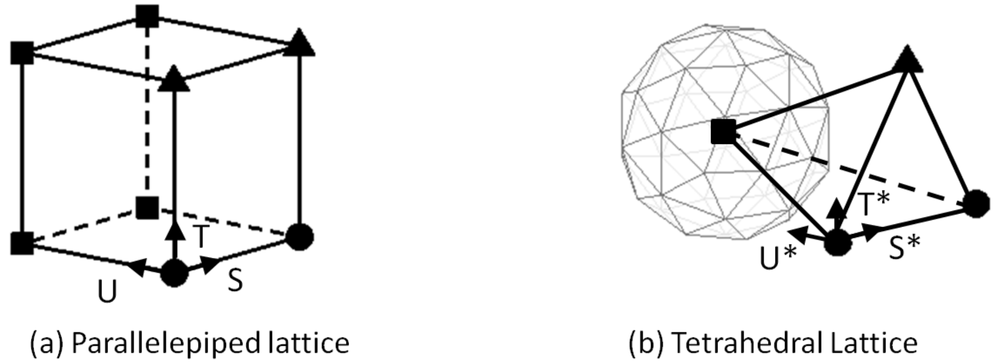

Figure 2.4: Tetrahedral lattice is formed by merging two sets of points of on the parallelepiped lattice. ● is an unchanged control point. ■ and ▲ control points are merged.

Although FFD is a powerful modeling technique, its main disadvantage is that the types of deformation that can be created are restricted by the parallelepiped shape of the lattice. The FFD method discussed in this paper refers to the case where the entire object is embedded in a single control grid and the FFD deforms the object globally; here one control point movement affects the entire surface of the object. By contrast, EFFD allows the user to create localized deformations of an arbitrary shape on the object surface [95]. Non-parallelepiped lattices can be designed specifically for the deformation desired. The EFFD lattice is comprised of multiple FFD lattice structures. The object is embedded in the EFFD lattice and deformation is passed only onto the object surface that lies within the individual FFD lattices associated with the displaced control point.

A spherical EFFD lattice composed of tetrahedral lattices was selected to deform the prostate model template. A tetrahedral lattice is obtained by merging two sets of points of a parallelepiped lattice, as shown in Fig. 2.4. The primary challenge with implementing EFFD is calculating the parameterized coordinates (s, t, u) of the object in a non-parallelepiped space. Coquillart used a Newton approximation to calculate the coordinate [98]. MacCracken and Joy presented a FFD technique, which uses arbitrary lattices, namely, Catmull-Clack subdivision volumes [99]; but the lattice space definition is time consuming and difficult, requiring a great deal of CPU time and memory. Xiao used a projection technique to calculate the parameterized coordinates in a cylindrical space [100]. The projection method has been modified in the current to calculate the (s*, t*, u*) coordinates in a tetrahedral lattice, an intermediate step in obtaining the (s, t, u) coordinates. The coordinate mapping process in the current study follows the following steps:

1. Determine the center-point of the triangle (tetrahedron face) that lies on the S*T* plane.

2. The line that connects the center-point to the tetrahedron corner point in the center of the spherical EFFD lattice can be defined. The point can be projected onto this line. Calculate u from the ratio between the entire line length and the length obtained by the projected point.

3. Determine the triangle parallel to the S*T* plane, formed at the u coordinate of the point. Define the base and height of the triangle to be parallel to S* and T* axes, respectively.

4. Determine the width of the triangle at the point. Calculate s from the ratio between the width and the length obtained by projecting the point onto the width.

5. Project the point onto the triangle height. Calculate t from the ratio between the length of the height and the length obtained by the projected point.

Using the projection method, the object vertices (s*, t*, u*) encompassed by the tetrahedron are mapped onto a rectangular solid, forming one-half of the parallelepiped lattice. The (s, t, u) coordinates are obtained by calculating the parameterized coordinates with respect to the entire parallelepiped lattice. Each control point moved is translated onto the parallelepiped lattice. The Bézier function can then be applied to determine the displaced object vertices in the parallelepiped space. The final deformed object vertices are obtained by mapping the displaced object vertices, calculated in the parallelepiped space, back onto the tetrahedron.

The spherical lattice is composed of 80 tetrahedrons and has 42 control points. Each tetrahedron is defined by 64 points, however only three of the four corner control points are used to manipulate the object surface. The EFFD lattice is formed by merging the matching control points on neighboring tetrahedrons. Each control point moved on the EFFD lattice displaces adjacent control points within the corresponding lattice, as shown in Fig. 2.5. This maintains a smooth contour between surface deformations made from neighboring control points of the EFFD lattice.

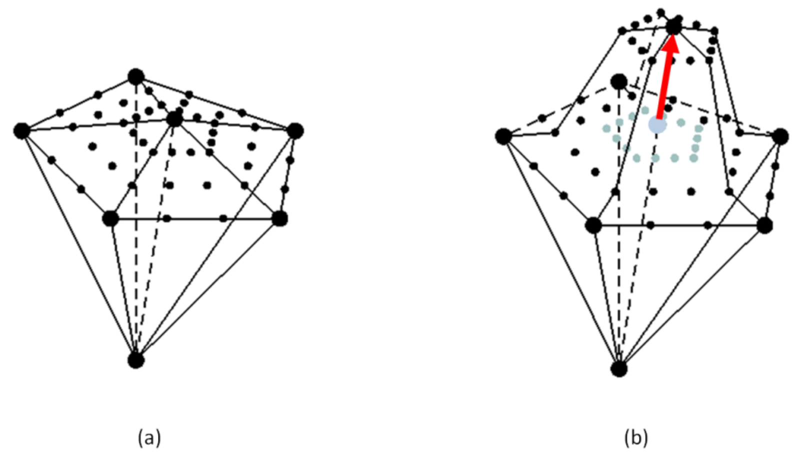

Figure 2.5: Control point movement within each tetrahedral lattice. (a) A section of the spherical extended free-form deformation (EFFD) lattice with surface control points. Large black dots represent the control points available for manipulation and small black dots represent the remaining control points within each tetrahedral lattice. (b) EFFD is carried out for each control point movement, by displacing the neighboring control points (gray dots) an equal amount within each tetrahedral lattice.

The template 3D prostate shape is represented as a closed shell of a polygonal mesh, consisting of a set of vertices and a set of triangular faces. It is important that there be no gap or overlap between faces. Any gap or overlap will make is impossible to create a quality mesh for finite element based cryosurgery simulations. Also, the resolution of the template prostate should be sufficiently fine so that small features of its shape will still be visible after the template prostate geometry is deformed. The current template polygonal model consists of 581 vertices and 1158 triangular polygons.

Deformations are carried out on a GUI, allowing the user to manually displace control points and instantaneously view the applied deformation on the template model. Figure 2.6 displays the basic framework of the code used to generate deformed prostate models along with the required user inputs. Deformation criteria used to generate prostate models are consistent with Fig. 2.2. Deformation is restricted to the posterior base and mid-region, therefore only control points normal to these regions are moved. Starting from the distal end of the prostate template, the apex is defined to be 9-mm thick, mid-region is 18-mm thick, and the remaining volume is the base [87]. Both templates of 35cc and 50cc are sectioned in the same manner. For each deformed model, the volume, maximum ECE – length and location are calculated. The ECE length is defined as the distance between the transverse template contour and deformed model contour.

Given the iterative process of correlating linear movements of control point with volume deformation, successful deformation is considered when the deformed model meets the criteria listed in Fig. 2.6.

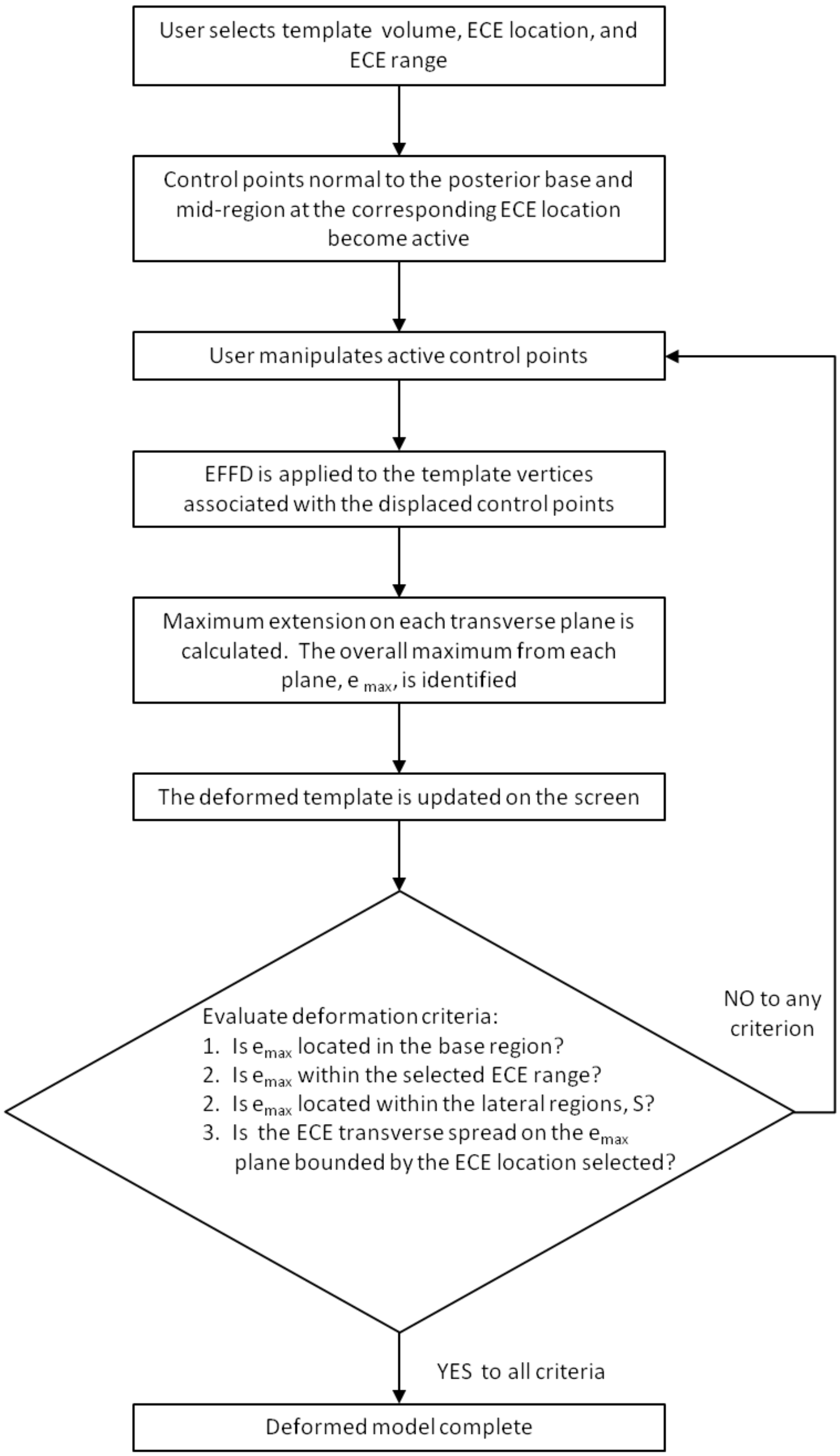

Figure 2.6: A flow chart for the process of creating a prostate model from a prostate template.

2.3 Results and Discussion

The study of key parameters of ECE presented by McNeal and Haillot [87] is unique and comprehensive, but provides only key geometrical features relevant to the current study: the location of the maximum extension, its magnitude, and the plane on which its maximum extension was measured (always in the transverse direction). This information is extremely significant for prostate cryosurgery, as the trans-rectal ultrasound (TRUS) transducer, commonly used to monitor prostate cryosurgery, provides raw imaging information on the same plane. Further qualitative information by McNeal and Haillot [87] suggests that the pattern of tumor growth correlates very well with the neural system of the gland. The topographical anatomy of periprostatic and capsular nerves have been thoroughly studied by Ganzer and co-workers [88], which enables us to link the tumor growth patterns with specific areas of the prostate, as summarized in Fig. 2.2.

When presenting a computational technique for geometrical representation of an organ, a comparison of results with a "ground truth" model would be highly commendable. Unfortunately, the actual shape of prostate tumors is not available in the literature. Not surprisingly, the actual shape of the extra-capsular portion of the tumor is not reported in the literature, where typical to cancer growth, the tumor contour may take virtually an infinite number of shapes. Hence, a "ground truth" model for the deformed ECE is non-existent. Accordingly, one of the modeling objectives in the current study is to meet the experimental pathology parameters measured by McNeal and Haillot [87], while taking into account the likelihood of finding a tumor in specific areas of the prostate (Fig. 2.2). The credibility of the captured ECE in the deformed models can be evaluated by consultation with imaging experts, urologists, pathologists, or oncology experts, as routinely done by the current research team. More discussion on the topic is included at the end of the current section, along with an outlook on how the developed model may be integrated with cryosurgery training.

As described in the Prostate Cancer and Tumor Growth section, two deformed models are presented in this section to demonstrate the application of the mathematical model, using a graphical user interface created with Matlab. The template for deformation has been developed in a previous study focusing on computerized planning of cryosurgery [51]; these templates have been created from 3D ultrasound data. Figure 2.7 displays a deformed model with right unilateral ECE. A 35cc template model was deformed to a volume of 36.8 cc. The selected ECE range for

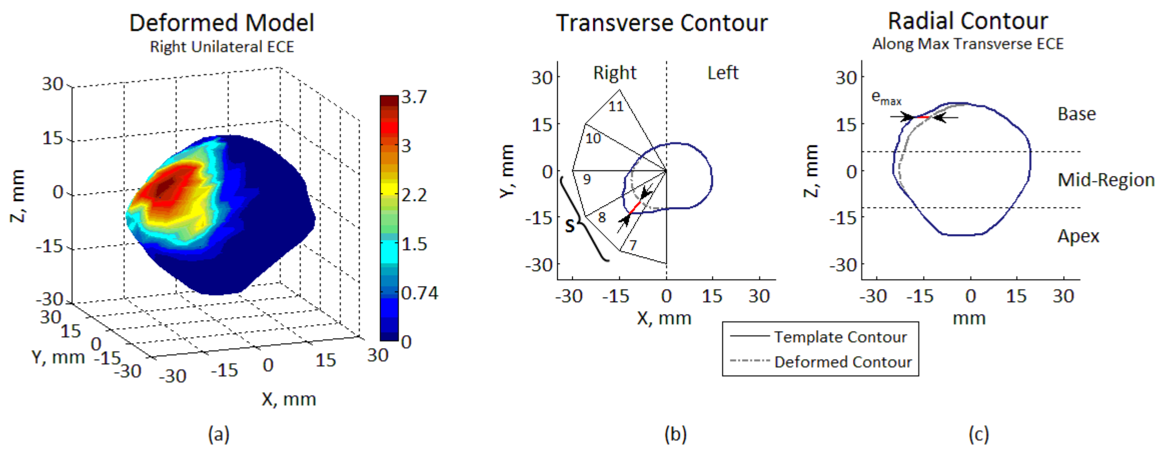

Figure 2.7: An example of a prostate model created by the Tutor, following the flow chart illustrated in Fig. 2.6: (a) 3D view of right unilateral ECE, (b) transverse contour on a cross-section at a depth of 17 mm, and (c) radial contour defined as the cross-section perpendicular to the transverse plane along the maximum ECE.

this deformation was in the range of 3–10mm (Fig. 2.2), where e_{max}, defined as the maximum distance between deformed contour and template contour on any transverse plane, received a value of 5.3mm. Figure 2.7(b) displays the transverse cross-section of the prostate at e_{max}. The highlighted region represents the maximum transverse span for the selected tumor location. The total ECE is confined to the transverse span specified for right unilateral ECE, with e_{max} located in the lateral region. Figure 2.7(c) shows that e_{max} is located at the base of the prostate model, at z=17mm.

Figure 2.8 displays a deformed model with symmetric ECE for the selected base ECE range of 0–3mm. A 35cc template model was deformed to a volume of 36.9 cc. Figure 2.8(c) confirms that e_{max}, 2.5 mm, is located at the base, at z=11 mm. The total ECE is located within the maximum transverse span for the tumor location selected and e_{max} is stationed in the lateral regions, as shown in Fig. 2.8(b).

Figure 2.9 displays three examples of deformed models representing worst-case scenarios for prostate cryosurgery, having maximum ECE, e_{max}, of 10 mm (Fig. 2.2). In general, the overall complexity of the prostate geometry increases with the extension size, making the cryosurgery procedure more challenging. The models in Figs. 2.9(a) and 2.9(c) exhibit left unilateral ECE and right bilateral-asymmetric ECE, respectively. Both were created using an initial template volume of 50 cc, eventually leading to deformed volumes of 51.9 cc and 52.2 cc,

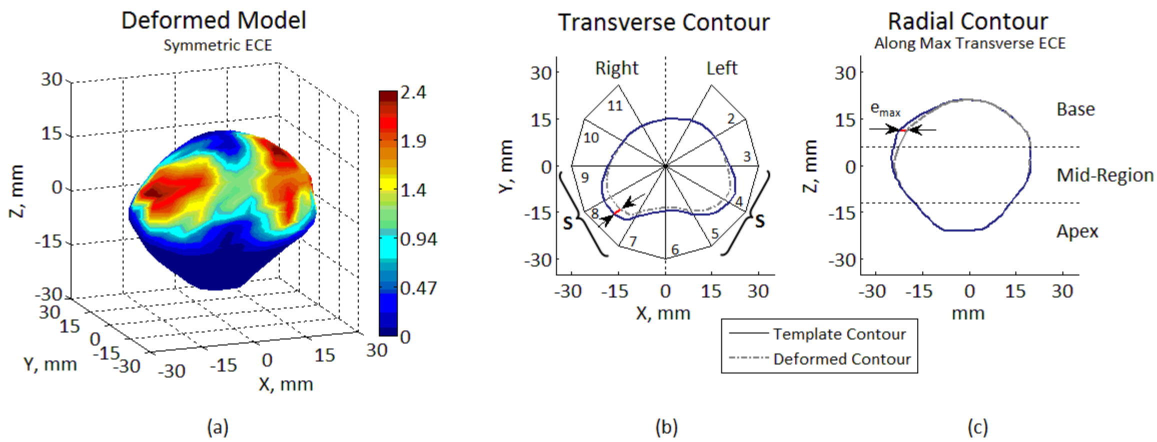

Figure 2.8: An example of a prostate model created by the Tutor: (a) 3D view of symmetric ECE (b) transverse contour on a cross-section at a depth of 11mm, and (c) radial contour defined as the cross-section perpendicular to the transverse plane along the maximum ECE.

respectively. The model displayed in Fig. 2.9(e) was created from a 35cc template, eventually resulting in a volume of 38cc, after demonstrating a bilateral-symmetric ECE.

Selected case study results. Case I represents a deformed 50cc prostate template to create a left-unilateral ECE model: (a) top view, and (b) corresponding transverse cross-section at maximum ECE. Case II represents a deformed 50cc prostate template to create a right-bilateral asymmetric ECE model: (c) top view, and (d) corresponding transverse cross-section at maximum ECE. Case III represents a deformed 35cc prostate template to create a symmetric bilateral asymmetric ECE model: (e) top view, and (f) corresponding transverse cross-section at maximum ECE.

.

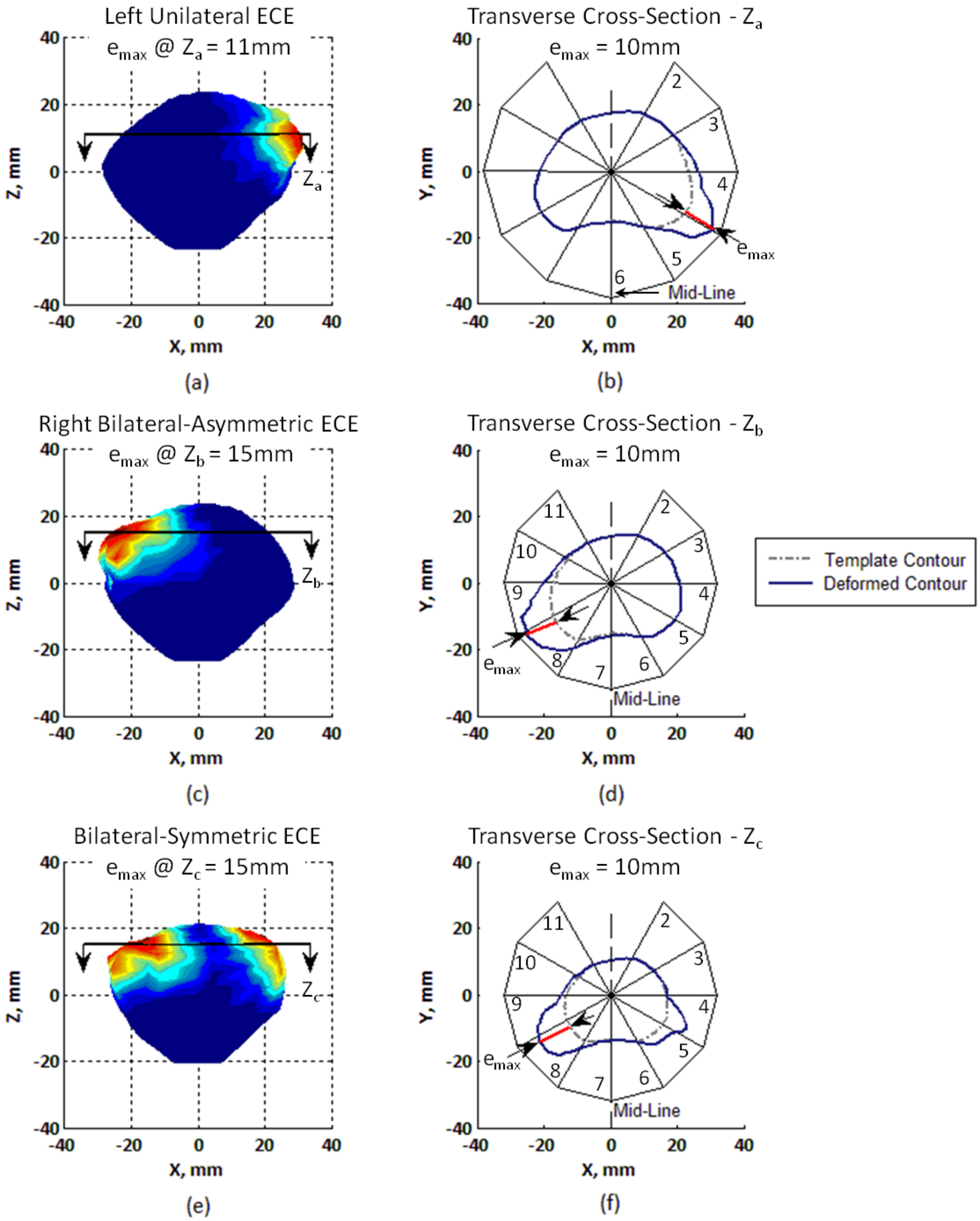

Figure 2.9: Selected case study results. Case I represents a deformed 50cc prostate template to create a left-unilateral ECE model: (a) top view, and (b) corresponding transverse cross-section at maximum ECE. Case II represents a deformed 50cc prostate template to create a right-bilateral asymmetric ECE model: (c) top view, and (d) corresponding transverse cross-section at maximum ECE. Case III represents a deformed 35cc prostate template to create a symmetric bilateral asymmetric ECE model: (e) top view, and (f) corresponding transverse cross-section at maximum ECE.

These models were generated by first selecting the desired deformation parameters - base ECE range and ECE location- and then manipulating the lattice control points until the deformed prostate model ECE length and transverse span fell within the selected range. It is noted that the selected criteria for deformation does not lead to a unique deformed body. Interestingly, different cancer growth histories may also lead to a similar outcome of a specific size but different local features. Hence, a random deformation approach is selected to guide database construction, which is consistent with that of tumor growth. Randomized parameters are: e_{max}, transverse span and of the deformed region, and contour of the deformed region.

While the general technique used to deform the template model is well established, an original contribution in this research is in integration of prostate geometry with prostate cancer growth pattern, and tailoring the deformation technique to generate the specific prostate models. The objective in the current study is to replicate the experimental results, with an emphasis on tumors at T3-stage cancer, by using the computational technique outlined above in the particular plane that the experimental data was measured. As discussed in the previous section, similar computational techniques [94]–[97] have been developed to generate 3D models of anatomical structures, using datasets composed of multiple 2D medical images containing cross-sections of the target structure. In these studies, deformation is guided by an optimization process that aims at minimizing the distance or cross-sectional area difference between the 2D image contour and the model contour at the corresponding plane. In the current study, such detailed information is not available and, therefore, optimization is not integrated into the current modeling process. In the current study, the problem is under-constrained and there is an infinite number of deformation patterns that could give the same distance or cross-sectional area difference. Hence, there is no guarantee that any other method from the literature will produce superior results for the purpose of quantitative comparison.

Lastly, an outlook on the integration of the proposed method with thermal surgery training is briefly discussed. A key difficulty in cryosurgery simulations and training is the lack of a credible target region to be destroyed by freezing [101]. This difficulty is not unique to cryosurgery simulations and training, but common in the training of other minimally invasive energy-based therapies, such as Brachytherapy (local radiation therapy using radiation seeds), local hyperthermia by means of laser probes, thermal ablation by means of high-frequency ultrasound (HIFU), and the emerging application of hyperthermia using nanoparticles in an alternating magnetic field.

While the development of a training software is a major challenge, far extending the scope of the current study, three relevant key issues are inherent to the minimally invasive energy-based therapies listed above: (i) identifying the guiding principles to treat a typical target region (the prostate base case in the current study), (ii) exploring how the target region may evolve with the progression of the disease, and (iii) evaluating how changes in the target region shape with the progression of the disease may affect the practice of the specific minimally invasive procedure.

While many criteria affect the success of minimally invasive cryosurgery, it is typically associated with matching some planning isotherm with the target region shape, such as the onset of freezing, completion of freezing, or the so-called lethal temperature—a temperature threshold below which maximum destruction is achieved. In Brachytherapy, a radiation dose region is typically matched with the target region shape. Similarly, a thermal dose region is typically matched with the target region shape in hyperthermic applications. Surgical planning of all of the above applications relies on computer simulations.

The computational method proposed in the current study can be integrated into computerized training in three primary ways: (i) to enable a "walk-through" demonstration of changes in the gland with the progression of the disease, (ii) to enable demonstration of how changes in the target-region shape affect changes in the energy sources layout (cryoprobes in the case of cryosurgery for example), and (iii) to create a database of prostate models having the same statistical distribution of candidates for the particular thermal surgery. For the latter application, automation can be employed in creating template deformations. For the latter two applications, computer generated surgical planning [50]–[54], [77], [89], [90], [101], [102] can be compared with interactive trainee operation, where the differences are automatically quantified, while the entire process is monitored by an experienced clinician. Either way, medical training is not perceived as an independent study, and the presence of an experienced surgeon should provide additional feedback on the virtual operation, including the credibility of the computer generated shapes.

Chapter 3. Cryosurgery Intelligent Tutoring System (ITS) Prototype

Computerized training necessitates three key elements: (i) a simulator of the procedure, (ii) a tutor to provide feedback on specific simulated cases, and (iii) a database to store case-specific information. This chapter focuses on the development of the tutor component, specifically the training methodology and proof-of-concept of a cryosurgery ITS. The subject matter of this chapter has been published in the 50th Annual Meeting of the Society for Cryobiology, 2014 Annual Meeting of the American College of Cryosurgery, and Advances in Health Sciences Education—submitted [103], [104].

Table 3.1: Proposed instructional modes of cryosurgery tutoring system.

Investigated Parameters	Mode 1	Mode 2	Mode 3
# of cryoprobes	Given	User-selected	User-selected
Cryoprobe layout	User-selected	Given	User-selected
Operation	Given	Given	Given

The pedagogic approach selected to teach cryosurgery planning divides each cryosurgery parameter into an instructional mode, displayed in Table 3.1. Cryosurgery operational parameters (i.e. cryoprobe geometry, cooling rate, duration of freezing, thawing rate, and repetition of freeze-thaw cycles) are not included in this thesis, as current planning algorithms do not have the means to determine individual cryoprobe operation; optimization and integration of cryoprobe operational parameters in training will be addressed in follow-on studies. Mode 1 focuses on teaching how to create an optimal cryoprobe layout, given the number of cryoprobes. In this mode, all investigated parameters are given and held constant, except for the cryoprobe layout.

Similarly, Mode 2 focuses on selecting the appropriate number of cryoprobes for a particular prostate geometry. Lastly, Mode 3 combines the selecting of the number of cryoprobes and their layout within the given geometry. For all three modes, the cryoprobes are operated in unison and powered off once a minimum defect value is reached, with defect defined as a region exterior to the prostate that is below the lethal temperature and any interior region of the prostate that is above the lethal temperature. The defect value, G, is calculated by [51]:

$$G = \int_V w \, dV \qquad w = \begin{cases} 1, & T_c < T \quad \textit{interior to the target region} \\ 0, & T \leq T_c \quad \textit{interior to the target region} \\ 1, & T \leq T_c \quad \textit{exterior to the target region} \\ 0, & T_c < T \quad \textit{exterior to the target region} \end{cases} \tag{6}$$

where V is the volume of the domain under consideration, w is a spatial weight function determined by the local temperature distribution, T is the local temperature, and T_c is the lethal temperature. At the beginning of the simulated procedure the entire unfrozen target region is defect. The overall defect value decreases with the progression of freezing, as an increasing portion of the target region falls below the isotherm threshold for planning. Eventually, an excessive frozen volume develops outside of the target region (external defect), which leads to a gradual increase of the overall defect size. Between the trends of decrease in internal defect region and subsequent increase in external defect, there is a point of minimum overall defect value—which is unique to the analyzed case. It is the point of minimum defect, where the simulated procedure is terminated and its quality is analyzed.

The ITS proof-of-concept presented in this chapter contains Mode 1 instruction, where the goal is to determine optimal layout given the number of cryoprobes. The ITS targets the acquisition of knowledge and the development of intuition necessary to create an optimal match between the frozen and the target regions. The tutoring system lists geometrical constraints of cryoprobes placement, simulates cryoprobe insertion, displays a rendered shape of the prostate, enables distance measurements, simulates the corresponding thermal history, and evaluates the mismatch between the target region shape and a pre-selected planning isotherm. The quality of trainee planning is measured in comparison with a computer-generated planning, created for each case study by previously developed planning algorithms [105]. Two versions of the tutoring system have been tested in the current study: (i) an unguided version, where the trainee can practice cases in unstructured sessions, and (ii) an intelligent tutoring system (ITS), which forces the trainee to follow specific steps, believed by the authors to potentially shorten the learning curve. While the tutoring level in this study aims only at geometrical constraints on cryoprobe placement and the resulting thermal histories, it creates a unique opportunity to gain insight into the process outside of the operation room.

In this chapter, methods used to construct the cryosurgery ITS prototype are briefly reviewed, followed by presentation of a formative evaluation to determine the effectiveness of the ITS by measuring performance displayed by surgery residents. A reduced version of the simulator was used for control in this study, representing less intelligent training as a benchmark. This study represents the first attempt to develop a cryosurgery ITS and the first attempt to evaluate a computerized tutoring system for cryosurgery.

3.1 Cryosurgery ITS Development – Methodology & Framework

In this section, the challenges in translating cryosurgery planning into computerized instruction are discussed, followed by the ITS learning objectives, description of tutoring system architecture and interface.

3.1.1 Challenges

In most computerized medical tutoring systems, the case-based teaching approach, focusing on students' successful integration of domain knowledge to solve a particular problem, is frequently employed. Material presented in such tutors typically comes from an extensive database of annotated cases, in fields with fairly well-established, standardized practices. This allows the developer to represent the domain by a set of rules, consistent with linearity of standardized practice and problem-solving strategies demonstrated in the annotations. In cryosurgery however, where accepted practices and criteria for surgical success may vary among clinicians and practicing institutions, the selection of optimal cryosurgery parameters may be equivocal. Instead of having a single path to a unique cryosurgery solution, several acceptable solutions may be created, with each solution developed in a non-sequential iterative fashion. This observation calls for a problem-solving process that accommodates multiple solutions and strategies. Furthermore, many intuitive steps may be involved in cryosurgery practice, which are difficult to formalize into verbal instruction targeted towards learning. For example, a competent cryosurgeon must integrate concepts and knowledge from the following areas during surgery planning: patient history and evolution of the disease, geometry of the target region and surrounding tissues, cryosurgery hardware capabilities, knowledge and/or intuition about heat transfer during cryosurgery, and medical imaging interpretation.

The cryosurgeon must possess the ability to process the resulting data streams in order to create mentally reconstructed, three-dimensional images of the target region and the frozen region. The cryosurgeon must plan and operate the specific procedure with the goal of minimizing the mismatch between the above reconstructed images. The solution to this minimization process may come about by varying the cryosurgery parameters and by selecting the appropriate comparison metrics, which are often dictated by clinical and individual patient data. Some of the related surgeon's abilities are intrinsic while others can only be developed by training. Either way, they can all improve with experience, whether in the operation room or by using a virtual tool such as the one developed in the current study.

The ITS development in the current study focuses on planning of the cryoprobe layout for a cryosurgical procedure, while placing an emphasis on thermal and geometrical considerations. For the current phase of development, it is assumed that the patient is a good candidate for the cryosurgery treatment, and that the trainee is competent with the relevant medical imaging method. Even with these assumptions in mind, it is quite challenging to encode some of the highly intuitive concepts listed earlier into computerized instruction for an ITS. The approach taken in this study combines trial-and-error interaction with customized ITS feedback. Hence, this paper presents a hybrid modeling approach, using both rules and constraints to represent the cryosurgery planning domain.

3.1.2 ITS Learning Objective

The learning objective in the current study is to develop or improve the ability to create an acceptable cryoprobe layout for cryosurgery. A necessary but not sufficient condition for achieving this objective is that each and every cryoprobe of the array satisfies a set of preselected procedural constraints. With this condition in mind, the learning objective is met if the trainee generates a similar or better-quality cryoprobe layout in comparison with a fully automated computer-generated layout, based on previously developed planning algorithms. The quality of planning is calculated as the overall volume mismatch between the planning isotherm and the target region contour.

Derived from common prostate-cryosurgery practices, specific criteria used in the current study, are: (1) any probe must not be closer than 3 mm from the prostate capsule, (2) any probe must not be closer than 3mm from urethra, and (3) the active cooling surface of a probe must be included within the target region. A tolerance of 1 mm is used as an acceptable match between the trainee probe placement and the computer-generated probe location, which is comparable with the certainty in distance measurements based on high-quality ultrasound imaging for prostate cryosurgery. The above criteria have been encoded in the form of constraints (geometric conditions) and rules (overall layout adequacy) that are used to evaluate the trainee solution. Note that the above rules and constraints do not define a planning solution or a strategy, where it is possible to find multiple cryoprobe layouts that fulfill all the above criteria. Furthermore, the computerized solution created by the trainer is not merely a correct solution but also a computer-optimized solution, generated by planning algorithms discussed in the ITS Architecture section below. Thus, it is used as a form of an expert solution in the current study. The learning objectives have been evaluated using typical thermal histories and cooling capabilities to Joule-Thomson based devices, as discussed in detail in [54]. A representative prostate model volume of 35 ml was applied in all case studies.

3.1.3 ITS Architecture

With reference to Fig. 3.1, the cryosurgery trainer comprises of two components: ITS and computerized cryosurgery tools (CCT). The CCT is comprised of the cryosurgery simulator and the cryoprobe-layout planner. The simulator takes a specific cryoprobe layout as input and uses an efficient numerical technique to simulate the resulting bioheat transfer process in the treated tissue [54]. The simulator's output are: (i) the three-dimensional temperature field at the end of the simulated procedure, and (ii) the mismatch between the planning isotherm and target region shape, also defined as the *defect value* [50]. The cryoprobe layout planner is based on the bubble-packing method [102], [105], and is applied on the specific geometry of the target region (i.e., the prostate and the urethra) for a given number of cryoprobes. The ITS is comprised of three components: a domain module, a student module, and a tutor. The domain module contains a set of rules and constraints that govern the cryosurgery planning process, combined with means to

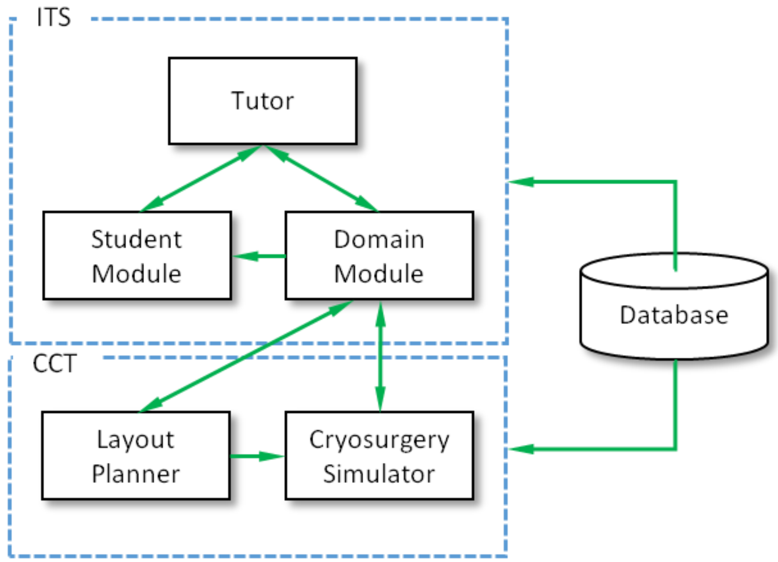

Figure 3.1: Schematic illustration of the computerized cryosurgery trainer architecture.

evaluate the trainee solution against the computer generated solution. The student module records the trainee actions throughout the problem solving process, including possible violations of rules and constraints. The tutor can be viewed as the administrative portion of a physical instructor, as it presents the student with a problem, asks relevant questions, passes the trainee-input to the domain module for evaluation, and returns feedback to the student based on the evaluator output. The database holds all case-related information, including organ geometries, previously solved cases, and student track record.

With reference to Fig. 3.2, the trainee-ITS interaction within each ITS case is comprised of five phases: (0) initial setup, (1) plan layout, (2) verify constraints, (3) cryosurgery simulation, and (4) case evaluation. The trainee can progress from one phase to the next only if all the rules and constraints are met. Otherwise, feedback containing the appropriate instructions are provided, to help correct the process. Phase 2 is the only phase where constraint violations do not impact the trainee's ability to move on to the next phase. Here, the trainee is given direct feedback regarding probe-constraint violation and the trainee may move affected probes as desired. During phase 3, a defect minimization search is conducted using an optimization technique previously developed [54]. The graphical user interface (GUI), shown in Fig. 3.3 and Fig. 3.4, provides the trainee with an interactive problem-solving environment. Prostate cryosurgery is typically performed under ultrasound guidance. In the current study, the added

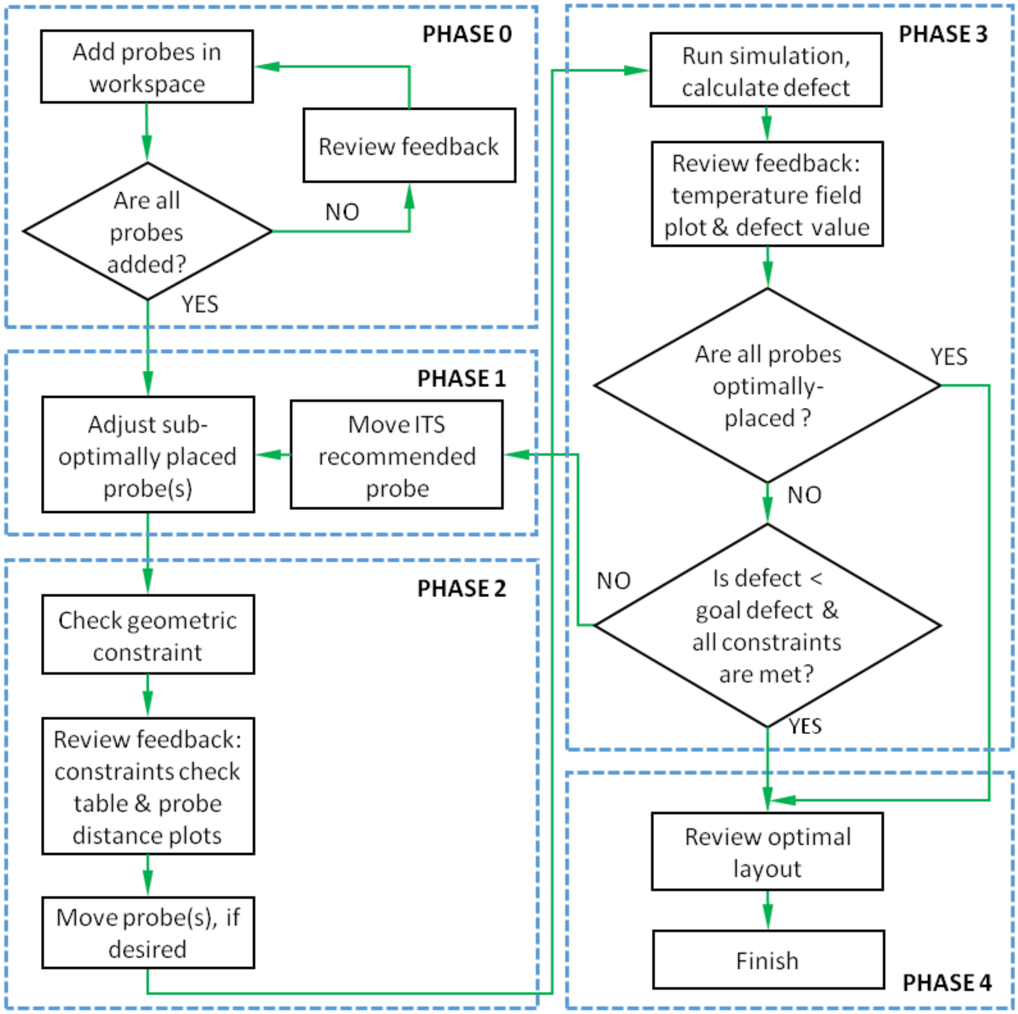

Figure 3.2: Schematic illustration if the sequence of operations during trainee-ITS interaction.

challenges associated with imaging analysis have not been integrated into the educational experience. Concurrent effort is now being devoted to integrate medical imaging analysis to cryosurgery education [106].

Figure 3.3: A representative screen of the cryosurgery ITS used to evaluate cryoprobe layout: (A) instructions panel; (B) geometrical presentation of the prostate to be treated, where (1) is the prostate capsule, (2) is the urethra warmer, and (3) is a cryoprobe; (C) color-coded scheme for probes at various stages of placement; (D) a transverse cross section of the prostate and urethra, with an sliding bar (E) for sagittal location; (F) a sagittal cross section of the prostate, with adjustable transverse location with the sliding bar below; (G) a button to request the trainer for a constraints-violation check; (H) table summarizing all probe violations; (I) probe-selection list for detailed analysis; (J) and (K) are distance tools, where the red line represents the distance constraint, blue line represents measured distance by the training software, green corresponds to the portion of the active surface of the cryoprobe which does not violate any constraints, yellow bar corresponds to a constraint-violating portion of the probe; (L) a button to request the trainer for a bioheat simulation of the current layout; (M) table displaying the total defect value results; and (N) is an area to for the trainer to provide comments and hints after an execution of a simulation. The viewing direction with trans-rectal ultrasound transducer during an actual prostate cryosurgery case can be switched between D and F.

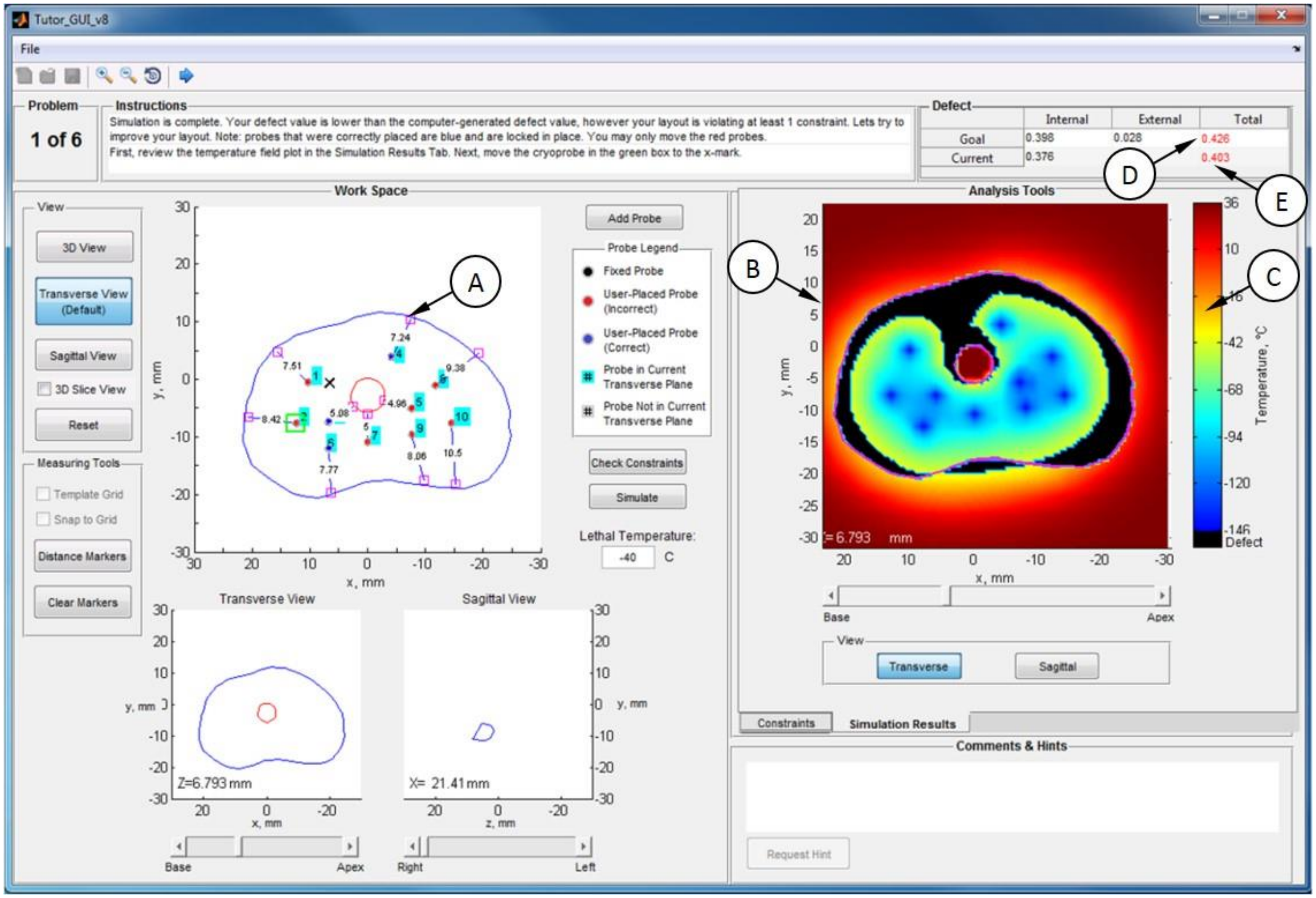

Figure 3.4: A representative screen of the cryosurgery ITS to evaluate cryoprobe layout: (A) prostate contour with user-selected distance measurements; (B) temperature map presented at the end of a cryosurgery simulation, where pink represents the prostate contour, black represents defect region, and the red-blue spectrum is correlated with temperature according to color scale (C); (D) goal defect, which is equal to the defect value of the optimized, computer-generated cryoprobe layout; and, (E) total defect value of the most recent trainee planning.

3.2 Study Design and Evaluation Methods

It is reemphasized that the current study is not aimed at a comprehensive educational experience on how to perform cryosurgery, nor is it aimed at verifying simulation results with follow-up clinical procedures; those broader aims are left for follow-up investigations and extend well beyond a single report. The objective in the current study is to develop a proof-of-concept for a cryosurgery ITS trainer, to explore its effectiveness, and identify possible pathways for its future development.

It is quite difficult to study the effectiveness of the computerized training concept, as comparable data from current training methods (i.e., non-computerized) is virtually nonexistent. Therefore, the current study presents a novel benchmarking concept where the ITS system performance is compared against the performance of a second but simplified computerized training system, containing no ITS components. The non-ITS trainer is essentially a reduced version of the same training code, where all functionalities are identical except for the features that provide feedback, guidance, and force the trainee to go through a sequence of instructional steps. In the non-ITS tutor, the trainee can study the 3D shape of the prostate, place cryoprobes, measure distances, run a bioheat simulation of the cryoprocedure, inspect the resulting 3D temperature field, and evaluate defect results relative to the computer-generated expert solution. While the non-ITS trainer provides the temperature field and defect value for a generated layout, it does not provide instructions on how to improve the layout using the resulting simulation data. Furthermore, the non-ITS tutor does not provide feedback on geometric constraints violations. In a sense, the non-ITS trainer facilitates intuition development in an unstructured manner.

The human subject study was approved by the Allegheny Singer Research Institute, Allegheny Health Network (AHN), Pittsburgh, PA (IRB Protocol #14-006). This study was performed at the Simulation, Teaching and Academic Research (STAR) Center of AHN. Twenty three subjects were recruited from the AHN surgical residency programs, where 15 and 8 subjects participated in the ITS tutor and non-ITS evaluation, respectively. Of the 23 residents, 16 (70%) were male, 7 (30%) were female, not by choice but due to the current demographics of the surgical residency program at AHN. Five residents reported previous experience with medical software and 17 residents reported previous video gaming experience at variable level of competence.

For both the ITS and non-ITS groups, trainees were given a brief introduction to prostate cryosurgery and planning guidelines, followed by a demonstration on how to use the computer code. For both groups, each session combined six cases for training and three cases for post-training test. For each case, the trainee was presented with a prostate and urethra model and asked to use ten cryoprobes to plan a layout. Each case used a different geometrical model of the prostate and the urethra, which was generated by means of geometrical deformation, based on ultrasound-reconstructed organs [79]. All cases were limited to a uniform insertion-depth for cryoprobes [51], where the trainee can only select the x and y coordinates for each probe (follow-on studies are planned to address multi-depth configurations, which presents a higher level of planning complexity in 3D).

During training, the ITS trainees had to follow instructions provided by the system, resulting in a finite number of attempts until evaluation criteria was met. The non-ITS trainees could have as many attempts as they wish. During the post-training test, all trainees regardless of the group had only one attempt to solve each case. During these tests, all trainees had access to the distance-measuring tool but no additional means of feedback. After each planning case, the trainees were able to see the resulting defect values and bioheat simulation results. Trainees concluded the session by filling out a short questionnaire about their medical background, computation skills, and their thoughts about the tutor.

3.3 Results

All statistical analyses were performed using Statistical Package for the Social Sciences (SPSS), IBM Co. Comparison between the two tutor groups was performed using the Mann-Whitney U-test, a non-parametric alternative for the unpaired t-test. Evaluation of the effectiveness of specific tutor features was performed using logistic regression and correlation between two variables was determined using Spearman's rho correlation coefficient.

For both tutor groups, the training session and posttest lasted on average 60 and 30 minutes, respectively. Figure 3.5 displays the mean time spent and number of attempts made on each case during the training portion of the session. Overall, the time required to complete a case tends to decrease with increasing number of cases solved (displayed in Fig. 3.5), with little difference between the two groups ($U=50$, $p=0.52$). The mean number of attempts per case remains in the

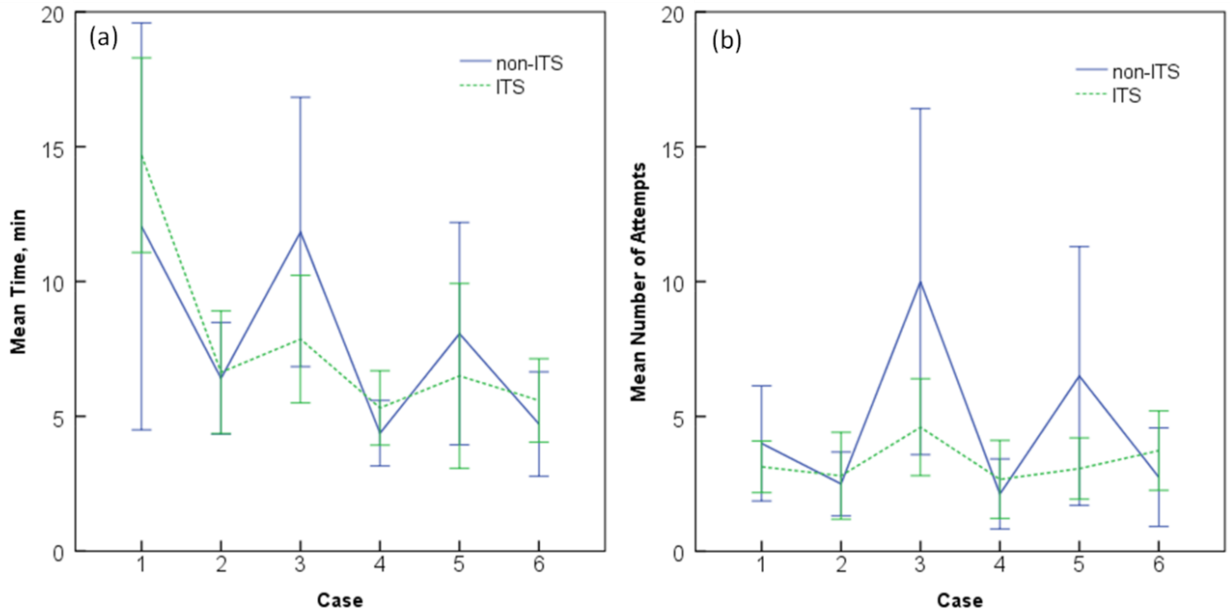

Figure 3.5: (a) Mean time and (b) mean number of attempts per case number for ITS and non-ITS groups. Error bars represent standard error at 95% confidence interval.

same range throughout the training session for the ITS group, but varied considerably for the non-ITS group, with statistically significant difference between the groups (U=24.5, p=0.02).

For the ITS group, all cases are structured such that the solution must meet both defect and constraints criteria, resulting in solutions that are free of constraint violations. For the non-ITS group, the solution must only meet the defect criterion, although the trainee has the option (and was verbally encouraged during the introductory portion of the session) to continue modifying the layout as deemed necessary in order to meet all rules and constraints. Since no computerized mechanism prohibits the solution for a non-ITS case to be free of constraint violations, the trainee can use the distance measurements tool and must use their own judgment. In the lack of constraint violation enforcement, the number of solutions submitted by the non-ITS group that met the constraint criteria was remarkably low. The best performance in this group was 5 out of 6 cases that met the criteria, achieved only by one trainee. Due to technical problems, data was lost for the first case for one trainee; this trainee submitted 3 out of 5 passing cases. Out of the six cases, one trainee submitted a total of 2 passing cases, three trainees submitted only 1 passing case, and the remaining two trainees completed the training session with 0 cases that met the constraint criteria.

Both tutors had unlimited access to the distance measurement tool. Twelve out of 15 and 6 out of 7 trainees in the ITS and non-ITS groups, respectively, measured probe distances using the measurement tool in the first training case. The same measurement tool was used only once by five trainees (ITS: 1, non-ITS: 4) in one of their remaining five cases.

The effectiveness of the probe distance plots (labeled J on Fig. 3.3)—a feature only available for the ITS group—was evaluated using logistic regression. In this plot (labeled J), the red line represents the constraint, the blue line represents the actual distance between the probe and the respective organ contour along the active surface of the cryoprobe, the green bar represents a safe region, and a yellow bar represents the portion of the cryoprobe which violates the distance constraint. The constraints check table (labeled H on Fig. 3.3) is continuously displayed for review by the trainee. It is assumed for the current analysis that if the trainee did not use the probe distance plots (based on recorded keystrokes), the trainee must have used the constraints check table. Improvement in meeting the constraints criteria is defined as the reduction in number of probes violating a constraint during an attempt. A scenario in which the trainee had no constraint violation before and after using the same distance tool is also classified as an improvement, since it demonstrates that the trainee understands the geometric concepts while the operation is counted as a positive step towards meeting all constraints. Only a scenario in which the trainee moved a probe after checking constraints and before running a simulation were included in this analysis (n=101). Among the ITS group, no significant difference is observed between trainees who used the probe distance plots and those that did not (B= -0.816, SE=0.517, p=0.12).

The effectiveness of the temperature field plots was evaluated for the non-ITS tutor only, where the trainees could relocate probes with no restrictions. With reference to Fig. 3.4, label B points to the organ contour, label C points to the temperature-to-color scale bar, and black displays a defect region. Improvement is defined as decrease in the total defect value between two consecutive attempts, where the possible scenarios are listed in Table 3.2 (n=159). Logistic regression revealed that improvement in defect was not statistically significant with the use of temperature field plots (B=0.187, SE=0.357, p=0.60).

Table 3.2: Defect evaluation scheme to determine improvement between attempts in cryoprobe layout, where D is the trainee planning defect, i is the planning attempt counter, and G is the computer-generated planning defect.

Defect Results	Improvement
$D_{i-1} > D_i > G$ $D_{i-1} > G > D_i$ $G > D_{i-1}$ and $G > D_i$	Yes
$D_i > D_{i-1} > G$ $D_i > G > D_{i-1}$	No

To examine the tutors' learning effect, the probe violation rate was calculated for each case as the ratio of the number of probes violating a constraint to the number of probes available to be moved at same stage, with the median error rate displayed in Fig. 3.6. Expectedly, each of the ITS cases eventually reaches a solution free of violations. By contrast, the non-ITS group displays no definitive pattern. The defect ratio (trainee defect value divided by the computer-generated defect value) and probe constraint violations after the first attempt for each case are plotted in Fig 3.7.

Post-training test results are displayed in Fig. 3.8. A defect ratio smaller than one indicates a superior trainee solution compared with the computer-generated solution. Results of Case 7 (the first posttest case) indicate an average trainee defect value close to the optimized computer-generated defect. Posttest results for the next two cases (#8 and #9) indicate trainee planning superior to computer generated planning, when constraint violations are not accounted for. In terms of the mean defect ratio alone (U=49, p=0.48) or in terms of the mean number of probes violations alone (U=52, p=0.60), there is no statistically significant difference between the ITS and the non-ITS groups. Bivariate correlation analysis was performed between trainees' background, including self-rated computational skills (1 to 5 scale), years of video gaming experience, and year of residency and trainee's posttest performance in terms of number of probes violating a constraint and defect ratio, but no statistically significant correlation was found.

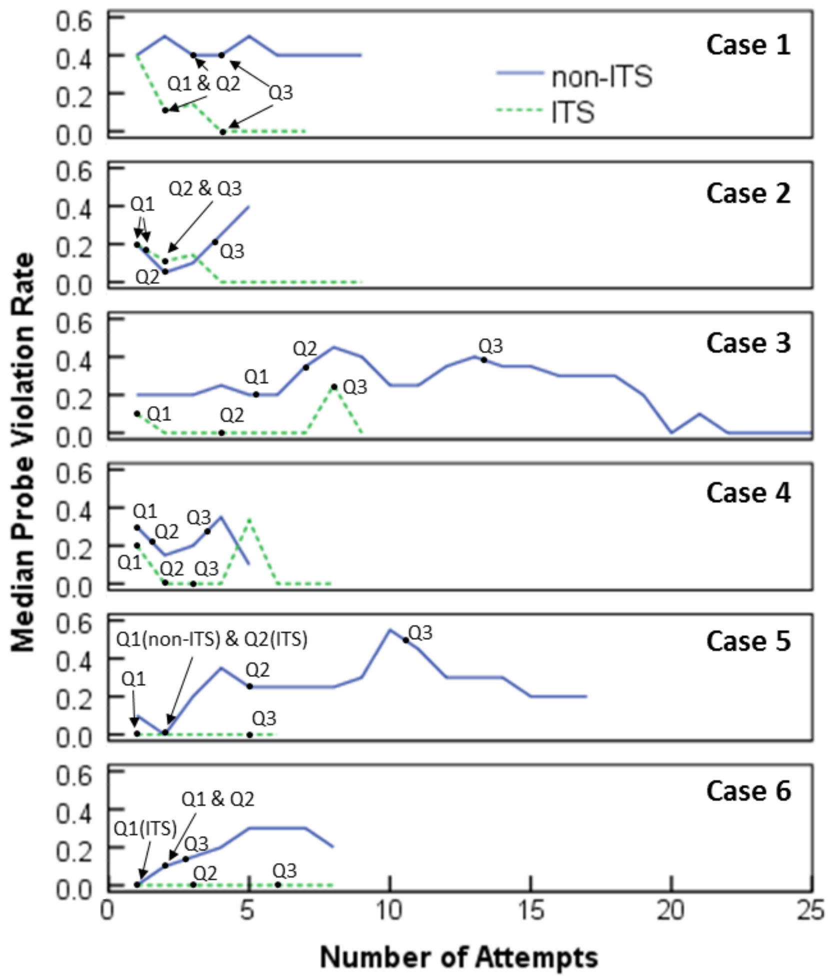

Figure 3.6: Median probe violation rate versus number of attempts, where Q1, Q2, and Q3 indicate quartiles of the total number of attempts by all trainees to complete the case. Non-ITS group demonstrates marginal improvement, if any, with increased attempts.

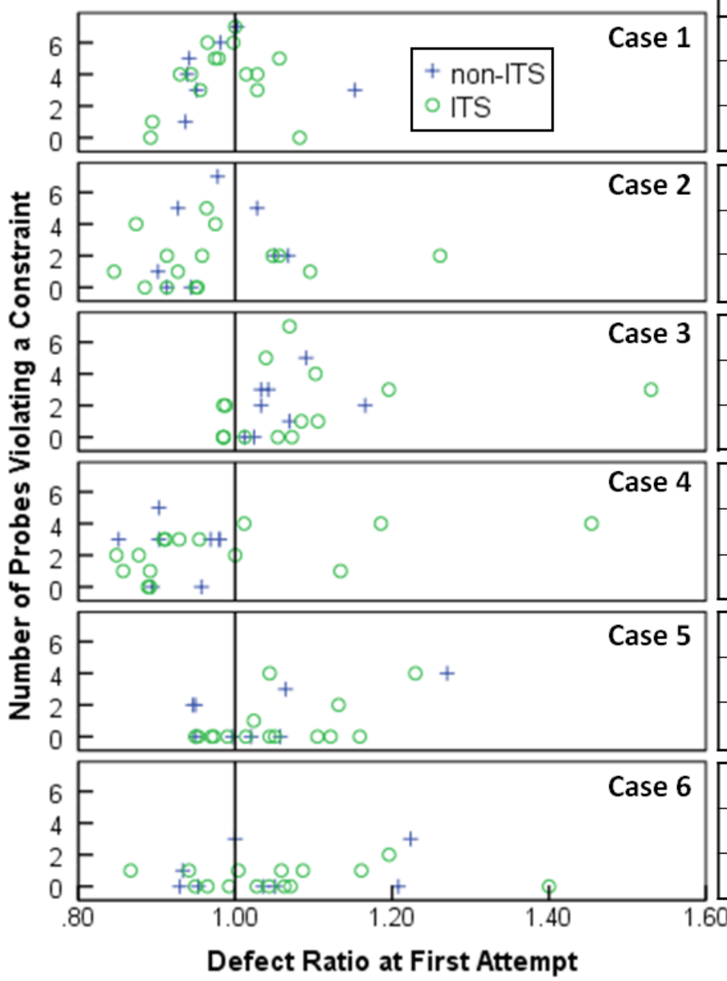

	ITS	non-ITS
C	.13	.00
D	.60	.71
A	.07	.00
C	.27	.25
D	.73	.63
A	.27	.25
C	.40	.25
D	.33	.00
A	.20	.00
C	.13	.25
D	.67	1.00
A	.13	.25
C	.73	.50
D	.33	.50
A	.33	.25
C	.53	.63
D	.40	.50
A	.20	.25

Figure 3.7: The number of probes violating at least one constraint in the first planning attempt versus the defect ratio, defined as the ratio of trainee-planning defect to the computer-generated planning defect (optimized solution). Tabulated values display ratio of trainees who met: (C) constraints criteria, (D) defect criteria, and (A) all-constraints and defect criteria.

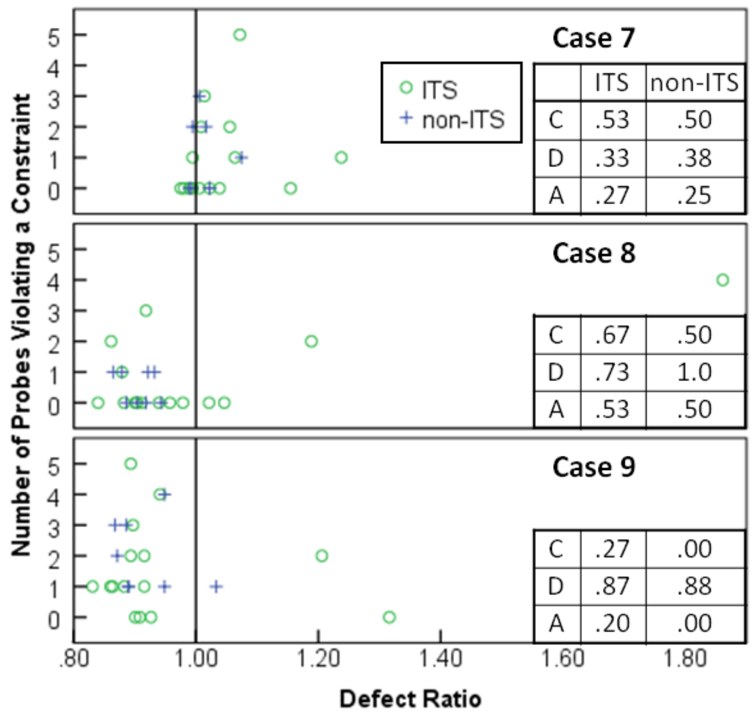

Figure 3.8: The number of probes violating at least one constraint in the posttest versus the defect ratio, defined as the ratio of trainee-planning defect to the computer-generated planning (optimized solution) defect. A defect ratio smaller than one indicates a superior trainee solution compared with the computer-generated solution. Tabulated values display ratio of trainees who met: (C) constraints criteria, (D) defect criteria, and (A) all-constraints and defect criteria. On average, ITS group is better able to meet the combine evaluation criteria than non-ITS group in each posttest case.

3.4 Discussion

Inherent differences between trainees and varying complexity between prostate shapes are two major confounding effects in the current study. Given the total number of available trainees (medical residents) and volunteering time (up to two hours) for this proof-of-concept study, constructing a more elaborate study to filter trainee variability effects is deemed unwarranted. Additionally, given the typical volume and the variable shape of candidate prostate for cryosurgery, creating a larger selection of cases (nine cases used in the current study) may be warranted in future studies, where more flexible cryoprobe placement strategy will be tested (such as multi-depth insertion). Following this approach, further tools will have to be developed to control for the geometrical variations of the target region, an effort which extends beyond the proof-of-concept level of the current study.

Within the ITS group, using the probe distance plots (versus constraints check table) did not lead to statistically significant improvement in terms of probe placement violations. The frequency with which trainees used the distance plots decreased with increasing number of cases solved, which were used 47%, 44%, and 22% of the time during cases 1&2, 3&4, and 5&6, respectively. A plausible explanation for this behavior is that the trainee's intuition about the layout quality may have increased, which is also consistent with the decreasing number of attempts as more cases are completed. It may also be that generating a higher incentive to use this tool may improve the training outcome.

The usage of the temperature-field plots also displayed a similar trend of deceased use as training progressed. In the ITS group, trainees used the plots 58% of the time in the first case and then their usage fluctuated between 12.5-38% (mean 25%) in the subsequent cases. The non-ITS group used temperature field plots over 70% of the time in the first two cases, which declined to the range of 37% to 58% of the time in subsequent cases. The feedback provided by the temperature-field plot is essential to layout-quality planning, but its interpretation requires analytical reasoning for which further step-by-step instructions may need to be integrated. Difficulties with this tool may be associated with scrolling through two-dimensional plot in order to create a mental image of a three-dimensional field. It appears that this difficulty can be overcome by at least one of the two alternatives: (i) pre-training in bioheat transfer effects, or (ii) integrating a tutor-generated three-dimensional illustration of the temperature field following (see [105] as an example). The latter alternative is more consistent with the approach presented in the current study, while the prior alternative may be more appropriate if training of the principles of cryosurgery is needed for cryosurgery hardware developers.

The ITS provides two additional forms of feedback during Phases 3 and 1. In Phase 3, if the layout has yet to meet the defect target, any probe that is placed within a predefined tolerance of its optimal location (according to the computer-generated optimized layout), is locked in place. With this hint, the trainee will then return to Phase 1 and continue the session while focusing only on the remaining probes that are sub-optimally placed. In addition, the ITS will reveal the optimal location for an additional probe at the beginning of revisited Phase 1—suggesting the least intuitive probe displacement for the trainee (i.e., the farthest required probe displacement).

Once the trainee follows this move, the trainee has the freedom to keep moving the remaining probes in an attempt to improve the overall layout. With this scheme in mind, the training process will converge, where the maximum attempts for a cryoprobe layout is bounded by the number of cryoprobes. Average results displayed in Fig. 3.8 support this reasoning, indicating that indeed the ITS group displays superior performance in the posttest. Analysis of results distribution suggests that this scheme does not have a major impact on the trainee's performance in terms of overall posttest results alone (Fig. 3.8). It may well be that this instruction scheme will yield a better return with a larger number of training cases or a longer time of ITS operation. However, this outcome calls for developing alternative and more efficient ITS schemes.

Regardless of the minimization process of the defect region, the ITS provides a unique opportunity to decrease constraint violations, as can be seen from Fig. 3.6, which is related to geometrical relationships rather than the thermal effects. In the first two cases in Fig. 3.6, the median probe violation rate is the same for both tutor groups during the first attempt. In the next three cases, the median rate for ITS is 0.1 below the non-ITS rate and in the last case, the median probe rate is 0 for both tutors. While the differences between the two tutors are small, both tutors appear to be effective in increasing the trainees' understanding of geometric conditions. On the other hand, the shape of the overall curve of each tutor in Fig. 3.6 differs significantly. While the non-ITS curve displays marginal improvement with the increasing number of attempts, the ITS curve displays a significant effect on the quality of learning.

Figure 3.7 displays results of the first attempt for all the training cases, with the objective of evaluating the learning-curve trend during the training session. In terms of constraints violations, both tutors display improvement with increasing case number. In terms of overall performance, the ITS group performed better in 4 out of 6 cases than the non-ITS group. Nonetheless, compared with the first case, there is an improvement performance trend with increasing case number for both groups. With these observations in mind, it should be noted that six cases may be considered a small training set for trend evaluation as the geometric complexity of the prostate models may vary significantly.

While the data analysis relates primarily to how well the trainees followed the rules defined for training, some trainees had difficulties in reconciling those rules and their own clinical judgment about planning. These subjects were well aware of critical neighboring anatomical structures around the prostate and felt that, in some instances, it would be better to increase the local defect in favor of reducing risk of harming those structures. This led them to disagree with some of the tutor recommendations, which could have prolonged their session and led to increased error as interpreted by the tutor. With this observation in mind, no trainee had prior experience in cryosurgery, and it was well articulated that the current study is about how well the trainee can learn the computerized trainer rules. Ultimately, integrating individual clinical judgment will strengthen the educational experience. This goal will be achieved by live expert (human) mentorship present in the background and also, independently, by contextualizing the planning algorithms.

Chapter 4. Cryosurgery Trainer − Variable Insertion-Depth Planning

The study presented in Chapter 3 provides important insights regarding the effectiveness of the tutoring system prototype and the learning behaviors of surgery residents, which resembles the target population for the cryosurgery trainer. These observations have led to the development of an advanced-level version of the cryosurgery tutoring system. The current study builds upon the presentation in Chapter 3, where the only changes to the system design are highlighted. The current prototype advances planning form two-dimensions (single insertion-depth) to three-dimensions (variable insertion-depth), where the trainee must determine the x and y location for cryoprobe insertion and its depth. The objective of the tutoring system remains essentially the same—to develop a cryoprobe layout for a given number of cryoprobes, in order to maximize the match between the resulting frozen region and the target region (the prostate minus the urethra). While many similarities are evident between the contexts of Chapter 3 and 4, duplicated explanations have been kept to minimum. Nevertheless, some repeated information is included in Chapter 4 for simplicity in presentation.

4.1 Trainer Objective

The objective of the trainer is to develop or improve the ability to create an acceptable cryoprobe layout for cryosurgery. A necessary but not sufficient condition for achieving this objective is that each and every cryoprobe of the array satisfies a set of preselected procedural constraints. With this condition in mind, the learning objective is met when the trainee generates a similar or better-quality cryoprobe layout in comparison with a fully automated computer-generated layout, based on previously developed planning algorithms [105]. The quality of planning is calculated as the overall volume mismatch between the planning isotherm and the target region contour, also known as the *defect region*, Eq. (6).

Two sets of criteria are used to evaluate the trainee layout, one based on geometric constraints and the other based on the match between target region and resulting frozen region. Geometric constraints are derived from common prostate-cryosurgery practices and include: (i) any probe must not be closer than 3 mm from the prostate capsule, (ii) any probe must not be closer than 3mm from urethra, and (iii) the active cooling surface of a probe must be included within the target region. The defect criterion compares the defect value of the trainee layout with the computer-generated layout. Defect, in the current study is defined as the percent of tissue external to the target region below the planning isotherm and tissue internal to the target region that is above the planning isotherm. Note that the above criterion does not define a planning solution or a strategy, where it is possible to find multiple cryoprobe layouts that fulfill all the above constraints. Furthermore, the solution created by the computerized trainer is not merely a correct solution but also a computer-optimized solution. Thus, it is used as a form of an expert solution in the current study against which the trainee layout is evaluated. The learning objectives have been evaluated using typical thermal histories and cooling capabilities to Joule-Thomson based devices, as discussed in detail in [54]. A representative prostate model volume of 35 ml was applied in all case studies.

4.2 Trainer Design

The architecture of the trainer remains largely the same as presented in Chapter 3 with reference to Fig. 3.1, the trainer is comprised of two main components: cryosurgery computational tools and the tutoring system. Cryosurgery computational tools (planning algorithms [102], [105] and numerical bioheat transfer simulator [54]) are used to generate an expert solution and evaluate trainee layout. The tutoring system is comprised of a tutor, student module, and domain module. The domain module contains the probe layout planning criteria and is used to compare the trainee solution with that of the computer-generated solution. The student module keeps track of student performance throughout the training session. Lastly, the tutor components acts as the administrative portion of a physical tutor, as it presents the student with a problem, asks relevant questions, passes the trainee-input to the domain module for evaluation, and returns feedback to the student based on the evaluator output. Both the tutoring system and cryosurgery computational tools have access to a database, which holds all case-related information, including organ geometries, previously solved cases, and student track record.

Figures 4.1 and 4.2 present the graphical user interface (GUI) of the current prototype, where design changes from the previous version of the system are marked by (*) next to the annotation. In the current study, design changes made in the second prototype are driven by two main factors: (i) to correct trainee behavior so they are in line with good cryosurgery problem-solving practices and (ii) to redesign or improve features to maximize their impact during the planning process. Four modifications have been implemented in the current prototype: variable insertion-depth (label E in Fig. 4.1), trainer feedback (labels I and J in Fig. 4.1), automated simulation display (label C in Fig. 4.2), and assessment metrics (labels D-F in Fig. 4.2).

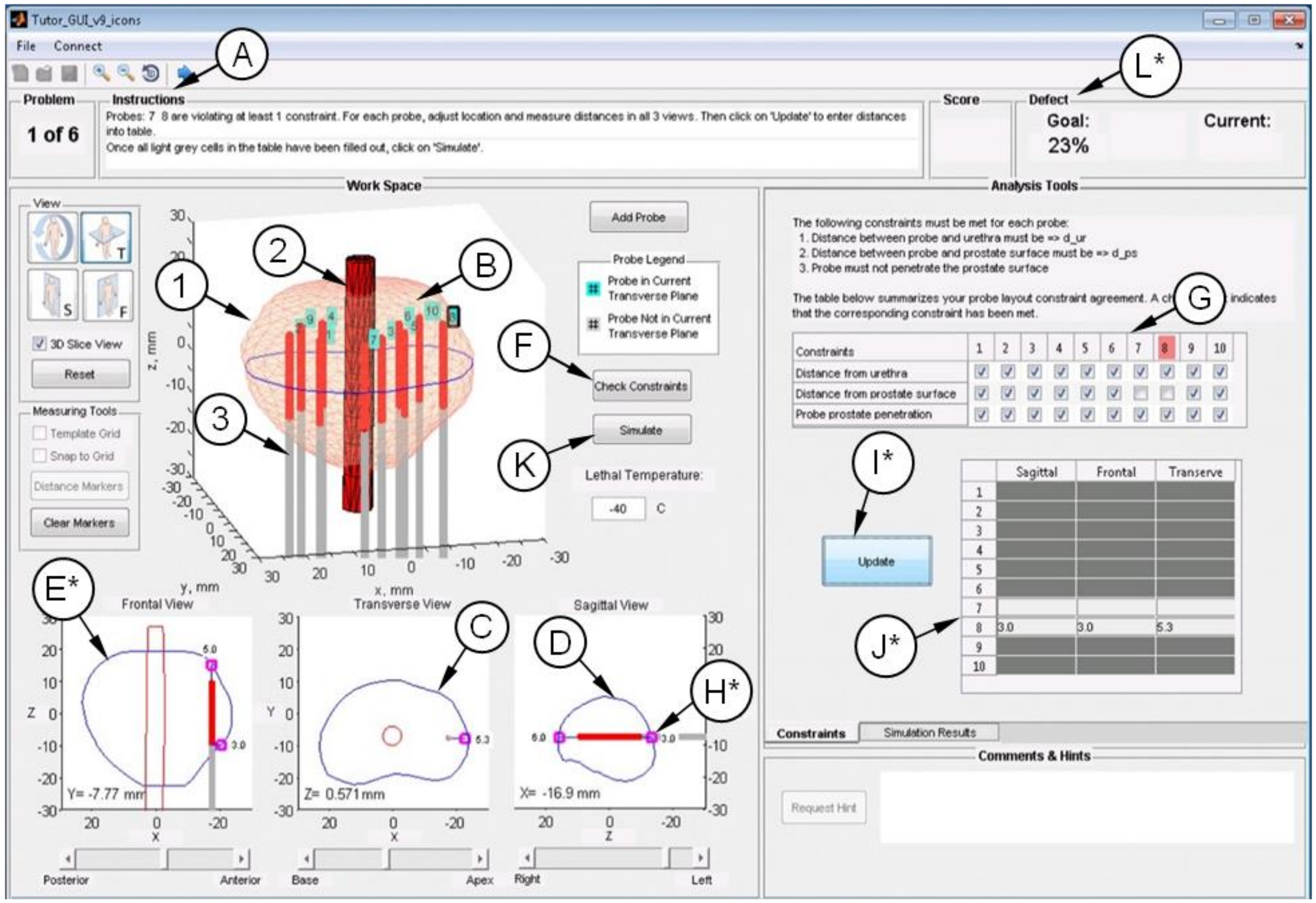

Figure 4.1: A representative screen of the cryosurgery trainer, where (*) marks features that were changed from the previous version of the trainer: (A) instructions panel; (B) geometrical presentation of the prostate to be treated, where (1) is the prostate capsule, (2) is the urethral warmer, and (3) is a cryoprobe; (C) a transverse cross section of the prostate and urethra, with an sliding bar for sagittal location; (D) a sagittal cross section of the prostate, with adjustable transverse location with the sliding bar below; (E) a frontal cross section of the prostate, with adjustable sagittal location with the sliding bar below; (F) a button to request the trainer for a constraints-violation check; (G) table summarizing all probe violations; (H) distance markers to measure relevant distances (I) probe-distance update button for constraint violating probes; (J) table with measured distance values for violating probes only; (K) a button to request the trainer for a bioheat simulation of the current layout; and (L) panel displaying the total defect percentage.

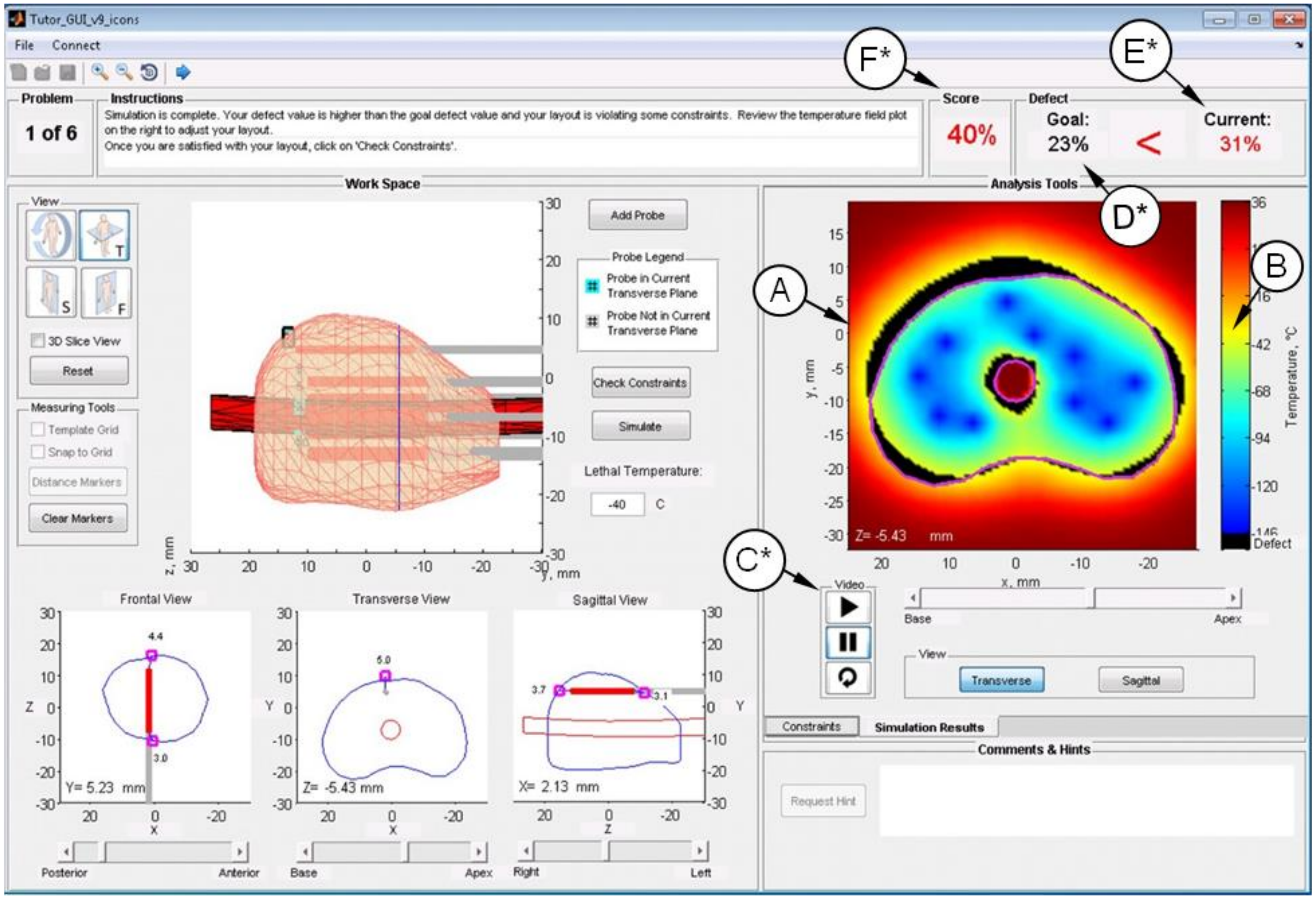

Figure 4.2: A representative screen of the cryosurgery trainer, where (*) marks features that were changed from the previous version of the trainer: (A) temperature map presented at the end of a cryosurgery simulation, where pink represents the prostate contour, black represents defect region, and the red-blue spectrum is correlated with temperature according to color scale (B); (C) video panel for automated viewing of the temperature map (D) goal defect, which is equal to the defect percentage of the optimized, computer-generated cryoprobe layout; and, (E) defect percentage of the most recent trainee planning; (F) score based on the combined constraint and defect criteria of the most recent trainee planning attempt.

4.2.1 Variable Insertion-Depth

Depending on the target geometry, a surgeon may choose to insert all probes at the same depth (termed uniform insertion-depth planning), or stagger probes within the target geometry as seen fit (termed variable insertion-depth). In terms of planning, variable insertion-depth is more complex, as it adds another degree of freedom (z-coordinate) to the planning process. The quality of the variable insertion-depth plan is typically higher as the resulting frozen region is better able to match an arbitrary shape, especially in the case of the prostate. Additionally, uniform insertion-depth presents a three-dimensional problem with two-dimensional constraints. In terms of the clinical setting, where the surgeon must mentally reconstruct the three-dimensional target region from ultrasound imaging and the resulting frozen region from the proposed layout, uniform insertion-depth planning may be less intuitive and therefore increase the difficulty of the task. Matching a three-dimensional problem with three-dimensional constraints is believed to be more intuitive and thus easier to learn. The trainer prototype presented in this study uses a modified bubble-packing algorithm [46], capable of generating a variable depth cryoprobe layout.

In order to facilitate three-dimensional planning, an additional cross-section (frontal view - label E in Fig. 4.1) was added to complete 3D representation of the prostate model. It should be noted that in practice, only transverse and sagittal TRUS images are accessible. Adding the third cross-section removes some of the inherent difficulty in visualizing the target area. In the current study, the trainee is able to move cryoprobes in the x and y directions using a mouse and in the z direction using a keyboard.

4.2.2 Trainer Feedback

In the previous version of the trainer (Chapter 3), two features were integrated to identify which probe was violating a constraint (constraint check table) and the location of the violation (probe distance plots). These features were found to be equally as effective in reducing probe-constraint violations, thus the latter was removed from the current version of the trainer. Additionally, the use of the distance measurement tool—a tool that requires the trainee to manually measure distances from the probe to relevant surfaces—was voluntary. Trainees were strongly encouraged to take distance measurements as it helps verify probe-constraint agreement

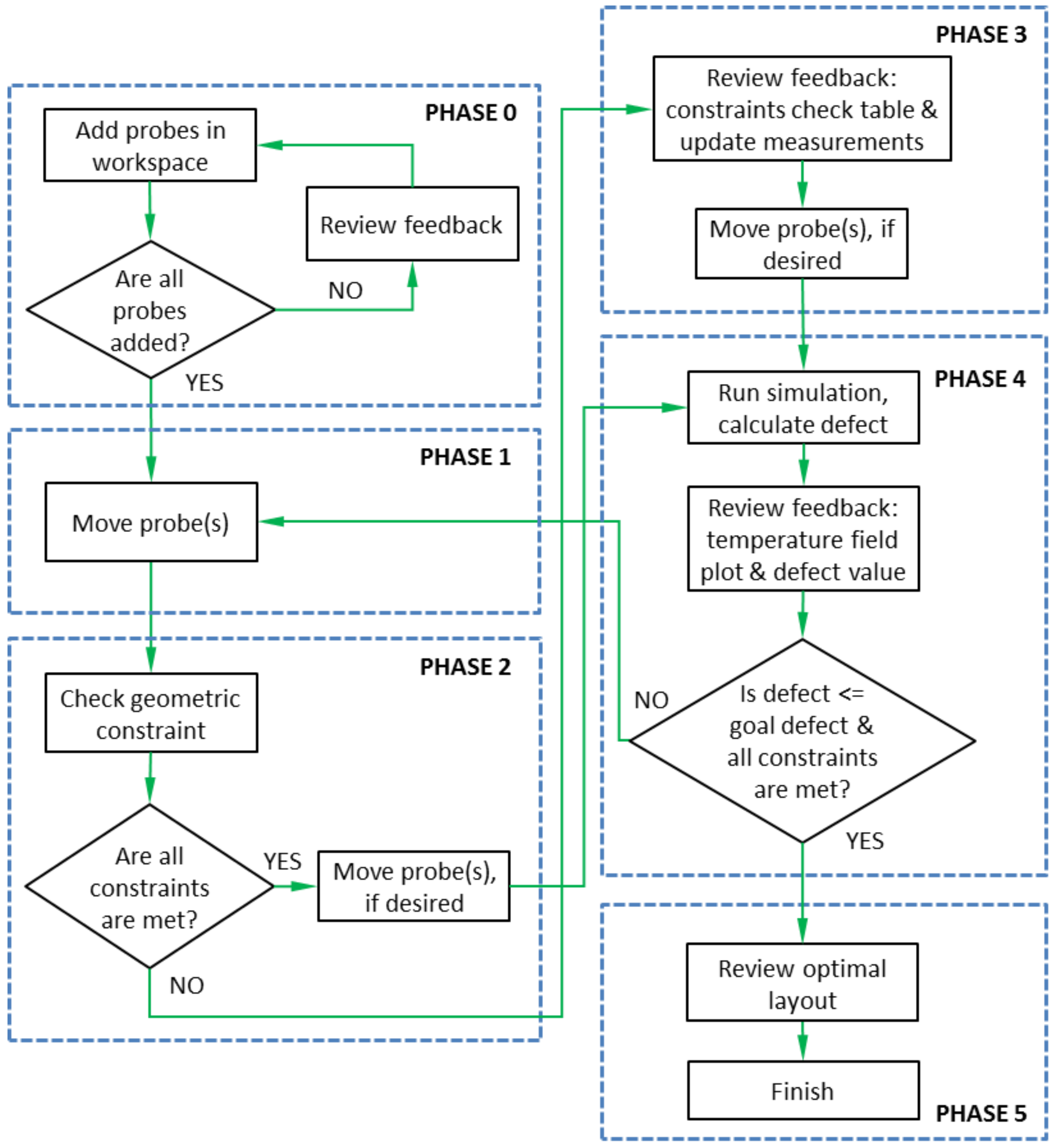

Figure 4.3: Schematic illustration of the sequence of operations during trainee-tutor interaction. Compared with the previous case structure, Fig. 3.2, Phases 1, 2, and 4 have been simplified and Phase 3—required measurement of probes that are violating at least one constraint—has been added.

and it is consistent with current clinical practice. Despite this instruction, the vast majority of cases were solved without the use of this tool. This observation led to a redesign of the training case structure. With reference to Fig. 4.3, Phases 1 (plan layout), 2 (verify constraints) and 4 (cryosurgery simulation) were simplified and Phase 3 (required probe distance measurement) was added to the case structure, where if a probe-violation exists, the trainee must measure distances from the probe to relevant surfaces in each of the cross-sectional views (labels C-E in Fig. 4.1). To ensure this action takes place, after measurement, the trainee must update the table labeled J in Fig. 4.1. Only after all violating probes have been measured and corrected, can the trainee move onto the simulation phase of the case.

The previous trainer study compared the quality of layout planning after training on the cryosurgery ITS with that of a reduced version of the trainer which provided limited feedback. After each layout attempt, the ITS locked any probes that were placed within 1mm of an optimal probe location and revealed the optimal location of an additional probe, such that the trainee only had to focus on the sub-optimally placed probes in the following layout attempt. The ITS trainees had fewer attempts on average during the training session, however, the quality of planning during the posttest remained comparable. Thus, the feedback in the current version of the trainer had been scaled back; it does not compare the physical location of the trainee layout with that of the computer-generated layout.

4.2.3 Automated Simulation Display

In the study presented in Chapter 3, it was found that the simulation temperature field plots were reviewed in the first few cases solved, but their use decreased substantially in the second half of the case set. Furthermore, giving trainees the autonomy to scroll through the temperature field using the slider bar may have negatively impacted their performance as they may have scrolled through only a portion of the entire temperature field. As a result, the presentation of the temperature field has been automated in the current version, such that once the bioheat transfer simulation is complete, a video of the resulting temperature field runs uninterrupted. After the first viewing, the trainee can replay the video (label C in Fig. 4.2), and start and stop at selected cross-sections.

4.2.4 Assessment Metrics

In the current version, an overall score combining the constraint and defect criteria is given after each planning attempt (label F in Fig. 4.2). The goal of scoring each attempt is to provide trainees with the means to assess the quality of their layout based on the combined effects of geometric constraints and resulting defect. The defect presentation has been changed from a decimal value to an overall percentage (labels D and E in Fig. 4.2) to simplify interpretation.

4.3 Study Design and Evaluation Methods

It is reemphasized that the current study is not aimed at a comprehensive educational experience on how to perform cryosurgery, nor is it aimed at verifying simulation results with follow-up clinical procedures; those broader aims are left for follow-up investigations. The objective in the current study is to measure the effectiveness of the second version of the cryosurgery trainer and identify possible pathways for its future development.

The human subject study was approved by the Allegheny Singer Research Institute, Allegheny Health Network (AHN), Pittsburgh, PA (IRB Protocol #14-006). This study was performed at the Simulation, Teaching and Academic Research (STAR) Center of AHN. Eighteen subjects were recruited from the AHN surgical residency programs. Of the 18 residents, 13 (72%) were male, 5 (28%) were female, not by choice but due to the current demographics of the surgical residency program at AHN.

Table 4.1: Trainer study outline.

Study	Cases	Time (min)
Introduction	-	10
Interactive Demo	1	20
Pretest	3	15
Training	up to 6	50
Posttest	3	15

With reference to Table 4.1, three sessions of six students were held, each lasting roughly two hours. In each session, a brief introduction to cryosurgery was presented along with the long-term goals of this line of research. The introduction was followed by an interactive demonstration of the training software, where trainees were asked to follow along with the presenter, while working through one attempt of a planning case at their computer station. The interactive demonstration reviewed how to use each tool provided in the trainer, including verification of probe-constraint criteria and interpretation of the resulting temperature field.

Prior to training, a pretest was administered where all trainees had only one attempt to solve each of the three cases. During this test, all trainees had access to the distance-measuring tool, but no additional means of feedback. In each case, the trainee was presented with a unique prostate and urethra model and asked to use ten cryoprobes to plan a layout by selecting x, y, and z coordinates of each probe. Models were generated by geometrically deforming base prostate shapes, reconstructed from preclinical ultrasound scanning [79].

During the training session, trainees had 50 minutes to complete as many cases as possible (up to 6). A case was successfully completed when a score of 100% was reached, meaning both defect and geometric constraint criteria were met. Trainees were given unlimited number of attempts to reach a score of 100%. The study session concluded with a posttest, in which the trainee solved the same three cases as the pretest.

4.4 Results and Discussion

All statistical analyses were performed using Statistical Package for the Social Sciences (SPSS), IBM Co. Comparison between the pretest and posttest results was performed using the Wilcoxon signed rank sum test and correlation between two variables was determined using Spearman's rho correlation coefficient.

Figure 4.4 displays the mean number of attempts made by all trainees for the respective case during the training session. The training analysis in the current study used data from 17 out of 18

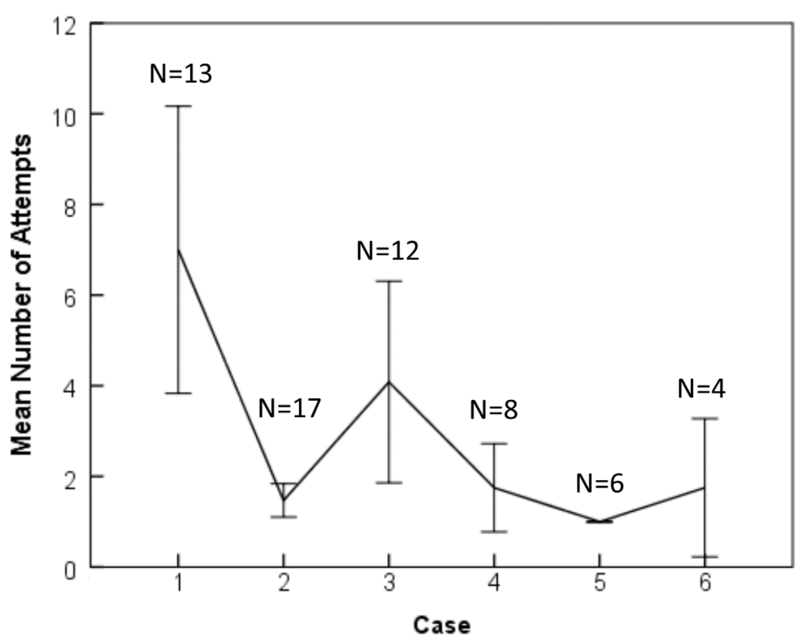

Figure 4.4: Mean attempts per case. Error bars represents standard error at 95% confidence interval.

trainees; one trainee's data was removed entirely because this trainee was unaware that the probes could be moved in the z-direction and did not complete any cases during the training session. Out of the 17 trainees, case 1 data for four trainees was omitted—three trainees' data was lost due to technical problems and one trainee was unaware that probes could be moved in the z-direction, an error that was corrected in their subsequent cases. Overall, the number of attempts required decreases with increasing cases solved. Within the allotted time, all trainees completed at least two cases, with only four completing all six case exercises.

Pre- and posttest performance was evaluated by determining the percentage of cases where trainees met the defect, constraints, and the combined defect and constraints criteria. Table 4.2 presents the mean pre- and posttest performance in terms of defect ratio (trainee defect over goal defect), constraints, and both criteria, along with the Wilcoxon signed-rank test for each of these parameters. The Wilcoxon signed-rank test is the non-parametric alternative for the paired t-test used to compare pre- and posttest scores from each trainee. The defect ratio is evaluated at three values, when defect ratio is: (i) less than or equal to one, (ii) less than or equal to 1.05 (trainee defect was at least within 5% of the goal defect), and (iii) less than or equal to 1.1 (trainee defect was at least within 10% of the goal defect). The Wilcoxon signed rank sum test revealed that there was a statistically significant difference between the pre- and posttest results in terms of defect ratio (≤ 1 and ≤ 1.05) and in terms of the combined criteria using a defect ratio of one or less. Bivariate correlation analysis was performed between the trainee's posttest performance in terms of number of probes violating a constraint and defect ratio, and the number of cases solved and the total number of attempts made during the training session—correlation between these parameters was not statistically significant.

In order to assess the effectiveness of the trainer, it is important to evaluate trainee performance by using the pass/fail criteria as detailed above, and also by measuring the incremental change in performance exhibited by the trainee from pre- to posttest. In performing such an analysis, any change in performance towards the goal criteria is considered to be a success. Out of 17 trainees, two trainees' pre- and posttest data was removed because these trainees did not change cryoprobe depth during their pretest. The pre- versus posttest defect ratios have been plotted in Fig. 4.5 for each of the three planning cases. Data is further segmented by the change in number of probe-constraint violations from pre- to posttest. With reference to the legend in Fig. 4.5, all green data points mark improvement in probe-constraint agreement. There were three observed scenarios of improvement: (i) trainees who met the constraint criteria in the pre- and posttest—zero probe-constraint violations, (ii) trainees who did not meet the constraint criteria in either test, but there was an overall reduction in the number of probe-constraint violations from pre- to posttest, and (iii) trainees who reduced the number of probe-constraint violations and met the constraints criteria in the posttest. No improvement, displayed in red, was classified using two observed scenarios: (i) trainees who increased the number of probe-constraint violations and (ii) trainees whose probe-constraint violations did not change across the two tests. Roughly 80% of trainees in case 1 and 67% of trainees in cases 2 and 3 demonstrated improvement in terms of the number of probe-constraint violations. While the Wilcoxon test revealed no statistically significant difference between the pre- and posttest with respect to the constraint parameter, the actual percentage of trainees who were able to demonstrate an improvement over the course of their training is quite significant.

The dashed horizontal line marks the posttest goal defect for each case. The solid diagonal line has a slope of one; trainee data below this line signify a reduction in defect from pre- to posttest and trainee data above this line signify an increase in defect from pre- to posttest. Out of 15 trainees, 13, 9, and 12 trainees were able to further reduce their pretest defect in cases 1-3, respectively. Looking at defect alone, 9 and 8 trainees met the posttest defect criteria in cases 1 and 2, respectively, and only 3 trainees were able to meet the defect criteria in case 3. Additionally, the number of trainees that met both constraints and defect criteria in cases 1-3 are 7, 5, and 2 trainees, respectively. The variation between the number of trainees able to meet the planning criteria may be due to the inherent complexity of the case; the prostate geometry used in case 3 appears to be the most difficult of the three. Incidentally, as follow-on work, a pilot study may be conducted to determine prostate geometry complexity in terms of layout planning by measuring how many in a group are able to achieve or approach the computer-generated solution. Results may be used to present problems in order of increasing difficulty, consistent with many educational strategies prior to future formal evaluations of the trainer.

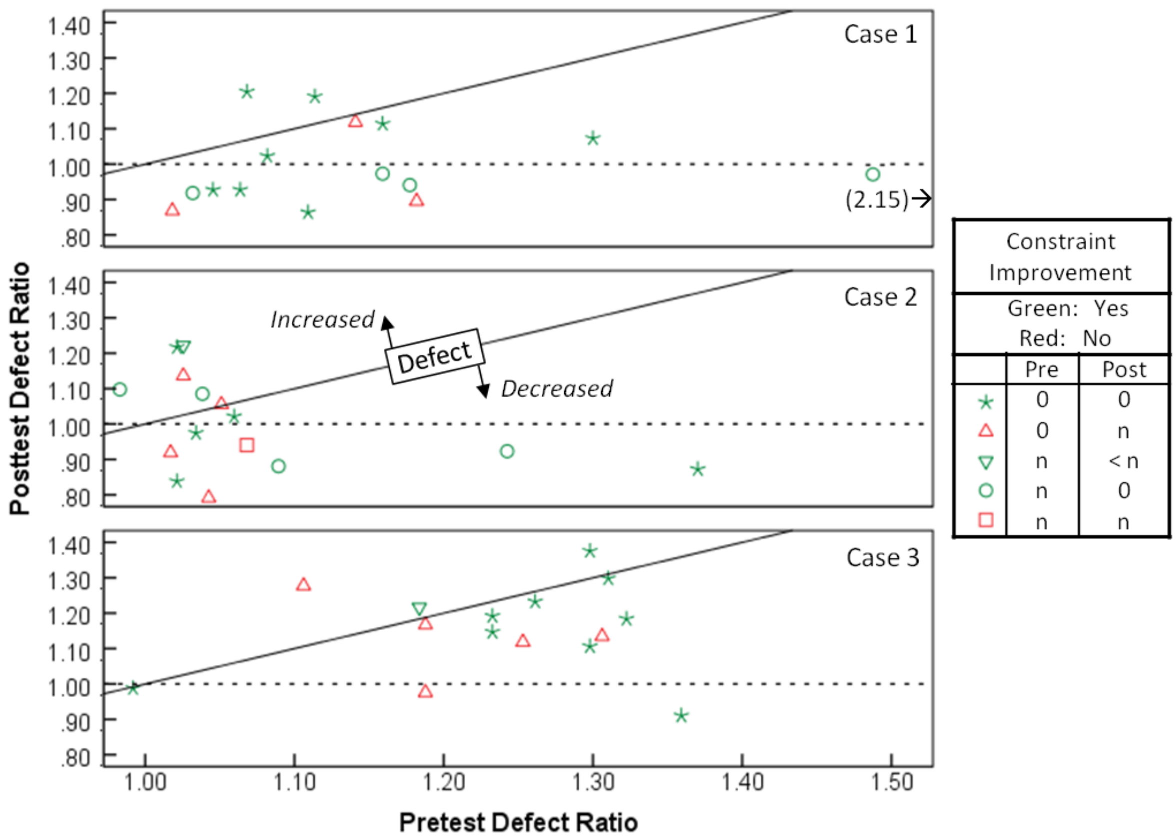

Figure 4.5: Trainee pretest versus posttest defect ratio, where green symbols represent an improvement in terms of constraint violations from pre- to posttest, red points represent no improvement. Symbol type correspond to type of improvement with n representing number of probes violating a constraint. Dashed horizontal line marks goal posttest defect and points to the right of the diagonal line signify improvement in defect from pre- to posttest.

The number of trainees able to satisfy both planning criteria is quite low. While minimizing defect is a complicated task requiring a multitude of concepts and skills, planning a layout free of constraint violations is highly procedural. With unlimited time and access to adequate measuring tools, creating a layout that meets the constraint criteria is a relatively stress-free, simple task. In total, probe distance measurements were taken in less than half of the cases completed during the pretest (20 out of 45) and during the posttest, probe distances were measured in only 7 of the 45 cases. Trainees either felt they did not need to measure, they were confident with their ability to eye-ball distances, or they were simply too sluggish to measure. Although the training case structure in the current trainer was redesigned to force probe-surface distance measurement—a necessary task, consistent with current clinical practice—trainee behavior remained uncorrected.

This observation suggests that additional measures be taken to correct trainee behavior such as imposing a greater penalty for unmeasured probe-violations during training or force distance measurements during pre- and posttest evaluations. It should be noted that these training sessions were held at 8AM and while many residents arrived on-time, alert, and ready to learn, an equal amount arrived late, post overnight call, and less than eager to complete the training exercises. This is likely to have an effect on their performance and their general ability to follow recommended practices. Nevertheless, variances in the data collected due to external factors such as those described above are representative of the target clinician population.

Although training and study parameters differed between the current study and previous proof-of-concept tutoring system evaluation presented in Chapter 3, the objective and key concepts remain the same. A greater majority of trainees were able to satisfy thermal planning criteria using variable insertion-depth planning than with the uniform insertion-depth planning approach. This finding suggests that variable insertion-depth planning—an approach rarely used in practice, but believed to yield layouts of a higher quality—may be easier to learn, and thus more intuitive in terms of thermal effects. Furthermore, the number of planning exercises or strategic intervention while planning maybe less critical during training. In the previous tutoring system evaluation, all trainees were required to complete six cases during the training session and the system intervened after every layout attempt, guiding the trainee towards a correct solution. The current study demonstrates that mere exposure to the training tool may be adequate in improving the trainees' planning performance.

Chapter 5. Summary and Conclusions

As part of an ongoing effort to develop computerized training tools for cryosurgery, this thesis presents work that is focused on the medical training and education of cryosurgery. At present, advanced computational techniques developed by the Biothermal Technology Laboratory and Computational Engineering and Robotics Laboratory allow for optimal cryoprobe layout planning [105], simulation of the resulting bioheat transfer process through efficient numerical schemes and generation of synthetic ultrasound imaging including recreation of the physical effects of frozen tissue and metallic objects in ultrasound imaging [106]. The long-term goal of this line of research is to develop a cryosurgery training software that facilitates a virtual cryosurgery setup, where a trainee can practice creating an optimal 3D thermal field to conform to a particular organ shape at various stages of cancer. Such a tool may enable case studies of "what-if" scenarios and even reevaluation of past clinical procedures. A computerized training tool is expected to shorten the clinician's learning curve, while providing a wider perspective on thermal effects and clinical practice.

Computerized training necessitates three key elements: (i) a simulator of the procedure, (ii) a tutor to provide feedback on specific simulated cases, and (iii) a database to store case-specific information. In developing the latter two elements, effective computerized cryosurgery training requires a database of realistic three-dimensional prostate models that reflect the cryosurgery patient population and a training framework to enable virtual cryosurgery planning. Towards that goal, this chapter summarizes the development of (i) a computational technique to geometrically deform a three-dimensional organ template in efforts to generate a database of prostate models representative of the cryosurgery patient population and (ii) a proof-of-concept computerized cryosurgery tutoring system for uniform and variable insertion-depth planning. The tools developed have been presented in the context of the prostate, however, they may be applied more broadly to any minimally-invasive cryosurgery procedure.

5.1 Geometric Model Deformation

Critical geometric variations found in prostates at T3-stage cancer, representative of the cryosurgery candidate population, were characterized to determine the effects of tumor growth on the prostate surface. Analysis was restricted to the primary tumor originating from the peripheral zone at the base of the prostate. The statistical distribution of key tumor features—ECE location and ECE length—based on a given tumor volume likely to be found in T3-stage cancers, was compiled using cancer growth patterns tabulated by McNeal and Halliot [87], while also integrating topographical anatomy of periprostatic and capsular nerves, as quantified by Ganzer and colleagues [88]. Combinations of tumor ECE parameters were systematically selected to serve as basic guidelines for deforming a prostate template in order to develop clinically relevant 3D prostate models.

A computational technique was developed to apply the extended free-form deformation (EFFD) method on a three-dimensional organ template in order to create localized surface changes that resemble extra-capsular tumor growth. The technique used a spherical EFFD lattice composed of 80 tetrahedrons and 42 control points and was applied by first selecting the desired deformation parameters—base ECE range and ECE location—and then manipulating the lattice control points normal to the target template surface until the deformed prostate model ECE length and transverse span fell within the selected range. The technique was demonstrated on two prostate models, representing the average and maximum prostate volume of cryosurgery patients, 35cc and 50cc, respectively. Three cases studies were conducted to generate models with the maximum observed ECE of 10mm, representing worst-case scenarios for prostate cryosurgery.

The model generation approach presented focuses on key geometrical features relevant to the extension of cancer tumors through the prostate capsule: the location of the maximum extension, its magnitude, the spread of the tumor on the prostate surface, and the plane on which its maximum extension was measured. This information is extremely significant for prostate cryosurgery, as the TRUS transducer commonly used in prostate cryosurgery provides raw imaging information on the same plane. It is noted that the selected criteria for deformation may not lead to a unique deformed body. Interestingly, different cancer growth histories may also lead to similar measured key parameters but different local features. Hence, a random deformation approach was selected to guide database construction, which is consistent with actual tumor growth. Demonstrations were based on two prostate templates, where more templates are planned to be included in the actual process of database construction.

The computational method proposed in the current study can be integrated into computerized training in three primary ways: (i) to enable a "walk-through" demonstration of changes in the gland with the progression of the disease, (ii) to enable demonstration of how changes in the target-region shape affect changes in the cryoprobe layout, and (iii) to create a database of prostate models having the same statistical distribution of candidates for the particular thermal surgery. For the latter application, automation can be employed in creating template deformations. For the latter two applications, computer-generated surgical planning can be compared with interactive trainee operation, where the differences are automatically quantified, while the entire process is monitored by an experienced clinician.

5.2 Computerized Cryosurgery Tutoring System

A proof-of-concept computerized cryosurgery tutoring system was developed for the simplified case of uniform insertion-depth (2D) and the advanced case of variable insertion-depth (3D) cryoprobe layout planning. The objective of the tutoring system is to determine optimal probe layout in order to minimize the mismatch between the target region and the resulting frozen region. The tutoring system lists geometrical constraints of cryoprobes placement, simulates cryoprobe insertion, displays a rendered shape of the prostate, enables distance measurements, simulates the corresponding thermal history, and evaluate the mismatch, termed defect, between the target region shape and a pre-selected planning isotherm. The quality of trainee planning is measured in comparison with computer-generated planning, created for each case study by previously developed planning algorithms. It is noted that the computer-generated solution is not unique, and alternative solutions can be found of similar quality; this observation was taken into account in the tutoring system feedback and data analysis.

5.2.1 Uniform Insertion-Depth Planning – ITS Benchmarking

In uniform insertion-depth planning, all probes are inserted at the same depth with the goal of creating a probe layout that minimizes the mismatch between the target region and the resulting frozen region. A proof-of-concept for a computerized cryosurgery tutoring system was developed where the insertion depth was fixed; trainees only had to determine the x and y coordinates of each probe. A formative evaluation was performed by testing two versions of the tutoring system on surgical residents: (i) an unguided version, where the trainee can practice cases in unstructured sessions, and (ii) the ITS, where the system forces the trainee to follow specific steps, believed to potentially shorten the learning curve. In total, 23 residents participated in the study, where 15 and 8 subjects participated in the ITS tutor and non-ITS evaluation, respectively. Participants completed six layout planning exercises during the training session, followed by a posttest to evaluate planning performance.

Posttest results indicate that the ITS system maybe more beneficial than the non-ITS system, but the proof-of-concept was demonstrated with either system. While the tutoring level in this study aims only at geometrical constraints on cryoprobe placement and the resulting thermal histories, it creates a unique opportunity to gain insight into the process outside of the operation room. It appears that the computerized trainer effectively illustrates several basic concepts: the geometry of the target region, how cryoprobe placement affects the resulting defect region, and how using two-dimensional cross-sections in cryoprobe placement (such as those created by the rectal ultrasound transducer during prostate cryosurgery) requires special attention to prevent damage in the third dimension.

5.2.2 Variable Insertion-Depth Planning – Learning Gains Measurement

A proof-of-concept for an advanced-level tutoring system was built, based on the previous prototype architecture, for cryoprobe layout planning at variable insertion-depths. In this tutor, trainees had to determine an optimal layout by adjusting the x and y coordinates, as well as the depth of each probe. The following tutor design modifications were implemented: means to change probe depth (variable-depth planning), improved trainer feedback, automated viewing of simulation thermal history, and improved trainee assessment metrics. Guided by observations made in the previous ITS study, modifications were designed to align trainee behavior with good cryosurgery planning practices and improve tutor features in order to maximize their impact during layout planning.

A formative evaluation was performed to measure the effectiveness of the tutoring system using 18 surgical residents. Participants were given a pretest, followed by a fixed time interval to complete as many planning exercises as possible using the trainer. The study concluded with a posttest. The tutor proved to be very effective in improving trainee cryoprobe planning performance. Comparison between pre- and posttest revealed a significant improvement in terms of minimizing defect and also in terms of satisfying both, probe geometric constraints and defect planning criteria.

These findings suggest that variable insertion depth planning—an approach rarely used in practice, but believed to yield layouts of a higher quality—may be more intuitive, and thus easier to learn in terms of thermal effects. Although training parameters differed between the two proof-of-concept tutoring systems, the objective and key concepts remain the same. A greater majority of trainees were able to satisfy defect criteria using variable insertion-depth planning than the uniform insertion-depth planning approach. Furthermore, the number of planning exercises or strategic intervention while planning maybe less critical during training—mere exposure to the training tool was found be adequate in reducing the trainees' learning curve.

The work presented in this thesis champions the development of a prostate model database and provides the training framework for tutor construction—essential in creating a well-grounded, clinically relevant computerized training software for cryosurgery. Combined with the computational tools developed by Biothermal Technology Laboratory and Computational Engineering and Robotics Laboratory, the presented work contributes towards the long-term goal of the research team, to build a computerized cryosurgery training system that facilitates virtual cryosurgery practice in efforts to reduce cryosurgeons' learning curve.

Chapter 6. Experimental Design for Advanced Studies – Future Work

This chapter presents areas that require further investigation in efforts to achieve the long-term goal of this line of research—developing a computerized training software for cryosurgery. At present, cryosurgery practice has yet to be standardized; common practice is left to the interpretation of the practicing clinician. Beyond adequate resources i.e., time and manpower, disparities in cryosurgery practices and difficulties in clinical knowledge and decision-making representations present a major challenge in developing cryosurgery tools apt for computerized instruction. One can imagine in the absence of such constraints, the combined knowledge and skills of the physician and heat transfer/computation experts can give rise to an ideal cryoprobe planning approach where a plan is systematically generated to maximize the effectiveness of the surgery.

With reference to Fig. 6.1, in an ideal planning scheme, patient geometry, clinical context, and procedure constraints, combined with the surgeon's clinical judgment, are used to select optimal cryosurgery parameters—a function of probe number, layout, and individual probe operation. Clinical context includes geometric constraints that limit the distance between cryoprobe placement and critical tissues, safety margin selection around the target tissue to ensure adequate destruction, a planning isotherm as a function of location, and other—presented here for completeness, as there may be factors that vary between physicians. Procedure constraints are comprised of cryoprobe dimensions and cooling capacity, imaging modality available, placement grid dimensions, type of insertion depth (uniform or variable), principles of heat transfer and again for completeness, other factors.

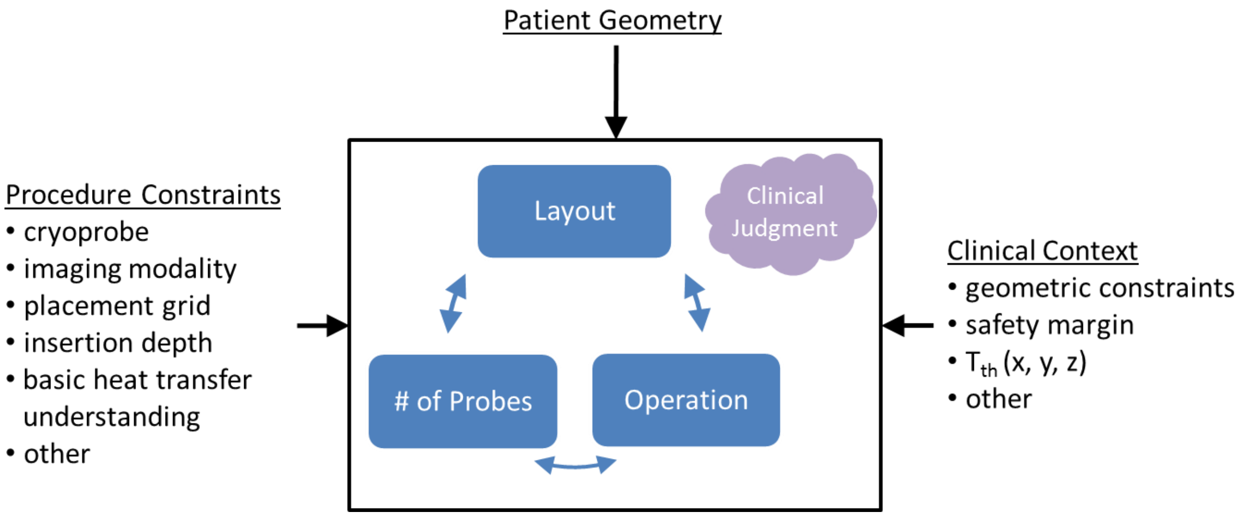

Figure 6.1: Schematic of ideal cryosurgery planning components.

The computerization of such a scheme would necessitate that all components presented in Fig. 6.1 be integrated in a flexible, adaptive manner such that recommendations made are able to fit any and all cryosurgical cases—the number of possibilities is virtually endless. Additionally, not all variables can be accounted for or optimized—some are rigid constraints, i.e. equipment available to physicians Hence, a practical approach to developing a computerized cryosurgery training tool is to prioritize the integration of clinical variables and address the more significant elements first. A tool with this capacity provides the surgeon with the freedom to modify selected input-variables and their values, while providing optimized cryosurgery parameters and the means to evaluate said parameters at and across every iteration. The surgeon may then integrate their clinical judgment and carefully determine, or modify, the plan that best fits the individual patient presentation. It is believed that a training tool that provides planning guidance at the level proposed will facilitate the surgeon's decision-making process by reducing their current cognitive load, while improving the quality of planning as the computer recommendations are based on the true bioheat transfer processes that take place.

In order to build such a tool, it is critical to correlate the planning process employed under the following methods: ideal cryosurgery planning, current computational tools, and clinical practice. With reference to Fig. 6.2, the planning process and corresponding planning components for ideal, computational, and in-practice methods are briefly discussed here to provide context for the subsequent sections.

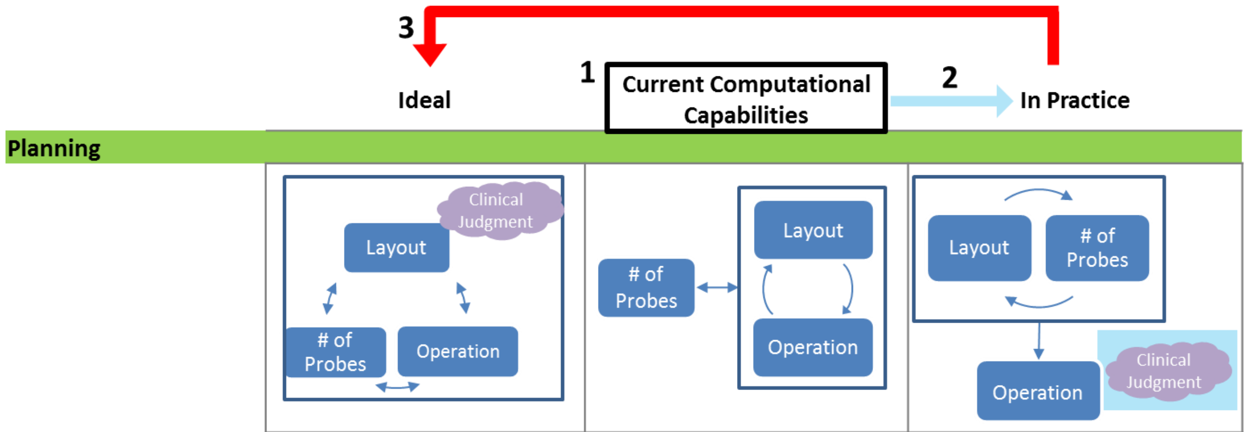

	Ideal	Current Computational Capabilities	In Practice
Main Components			
# of probes		Pre-selected	Based on prostate dim
layout			
operation	f (probe, T, t, image)	f(defect(T, geometry))	f(probe, 5-Tsensors, t, image)
Procedure Constraints			
cryoprobe	x	x	x
imaging modality			x
placement grid	x	x	x
insertion depth		x	x
basic HT understanding	x	x	~
other			
Clinical Context			
geometric constraints	x	x	x
select safety margin	x		x
T_{th} (x, y, z)	x		x
other			

Figure 6.2: Components of ideal, computational tools, and in practice cryosurgery planning.

Current computational methods use a pre-selected number of cryoprobes, and link layout planning and cryoprobe operation. Planning algorithms [105] determine an optimal layout and probes are operated in unison until a minimum defect value is reached, Eq. (6). By holding operation constant (operating to minimum defect), current computational tools can be extended to optimize the number of cryoprobes through successive probe layout simulations using a range of probe numbers with the objective of minimizing overall defect. Additionally, these algorithms are able to account for various size and cooling capacity of probes, placement grid constraints, variable depth insertion, and geometric probe constraints all the while integrating principles of heat transfer.

In practice, the cryosurgeon uses patient prostate volume and maximum dimensions to make an initial estimate of the number of cryoprobes to use; the number may be adjusted as seen fit during placement. After placement, probes are individually operated under TRUS and temperature sensor guidance. Knowledge of individual probe ice-ball geometry as it relates to operation time is provided by the manufacturer, and is typically factored into the planning process by the surgeon, during operation.

In efforts to develop a cryosurgery computerized training tool, the following approach is proposed: (1) complete development and validation of current computational tools, (2) contextualize training tools by identifying and integrating key elements used in a clinical setting, and (3) disseminate training tool in order to help inform and advance clinical practice, ultimately to improve clinical outcome. The remaining chapter presents methods that may be used to accomplish steps 1 and 2 in the approach outlined above.

6.1 Validate Current Computational Tools

Computerized training necessitates three key elements: (i) a simulator of the procedure, (ii) a tutor to provide feedback on specific simulated cases, and (iii) a database to store case-specific information. Significant efforts have been made to develop each of the key elements. This section provides the current status and paths for future investigation within each trainer element.

6.1.1 Tutor − Evaluation of Training Framework

Chapter 3 & 4 presented a fully-functioning prototype of the cryosurgery tutoring system. The training focused on instructional Mode 1, see Table. 3.1, developing necessary intuition to plan a cryoprobe layout given the number of probes and their operation. The remaining modes of instruction (Mode 2- varying number of cryoprobes and Mode 3- combined effects of cryoprobes used and their layout) need to be developed and formally evaluated. Table 6.1 displays the formal evaluation strategy most frequently employed in validating computerized tutoring systems [65], as well as the corresponding cryosurgery trainer instructional mode status. Generally, it is good practice to conduct pilot studies during the development phase to ensure basic usability of the system. Formative evaluations aim to verify that the system has been authored correctly and the educational objectives of the system are met. The last step is a summative evaluation where the effectiveness of the computerized tutoring system is compared with that of current training practices. This presents a major challenge as standardized training of

Table 6.1: Evaluation methods for computerized tutoring system and evaluation status of proposed trainer instructional modes.

Study	Purpose	Mode 1 Probe Layout	Mode 2 # of Probes	Mode 3 Combined
Pilot Study	Basic usability	x		
Formative Evaluation	Verify objective is met & content encoded	x		
Summative Evaluation	Tutoring system vs. real environment			

cryosurgery, let alone standardized practices, do not exist. An alternative path that may be taken is to focus evaluation on how well the tutoring system facilitates cryosurgery training, consistent with the overall development objective of the trainer—which serves as a training tool to be used under the guidance of an experienced cryosurgeon. The summative evaluation may be implemented as a series of studies using expert cryosurgeons, with the aim of measuring the surgeon’s ability to perform a virtual cryosurgery procedure while also using the tool for demonstration purposes. It is recommended that the summative evaluation be performed on Mode 3 only, as current training practices do not separate each cryosurgery parameter.

Beyond a well-grounded and robust training software, successful computerized training also requires complementary framework to maximize trainee engagement and learning. It is essential to address factors that contribute to the quality of trainee learning, e.g. motivation, early on during the research and development phase, as system evaluations performed at this time measure benefits of the tutoring system as a function of trainee performance.

From the medical education perspective, motivation as it relates to learning can be broken down into intrinsic factors such as desire to learn, interest in the subject matter, desire to do well and extrinsic factors including deadlines, threats, and social pressures like competition [107], [108]. Traditionally medical educators followed the learning theories laid out by Knowles, who proposed that as a person matures, the driving factors for motivation shift from extrinsic to intrinsic [109]. Today, motivation is not viewed so simplistically; it is widely-accepted that motivation in learning is a multi-faceted concept [110], [111].

With these observations in mind, the computerized training tool is targeted towards those who have an interest or a need to develop/hone their cryosurgery planning skills. In such cases, where trainees exhibit intrinsic motivation, developing complementary framework may not be as critical. Unfortunately, gaining access to future cryosurgeons during the research and development phase is quite challenging; any available medical subject is viewed as good fortune. Out of 41 surgical residents recruited for the trainer evaluation studies presented in this thesis, only one resident reported that cryosurgery would be a routine procedure in the future. It is therefore recommended that extrinsic motivational factors be integrated into the training framework to maximize learning, regardless of user background.

Motivation can be increased by creating a competitive environment and providing a monetary reward (light refreshments, gift cards, etc.) for the participant's time. For example, during a group training session, real-time data about the problem-solving status of each trainee can be transmitted to a central GUI and projected onto a screen in the front of the computer lab. The GUI may be used to stimulate competition during a training session, where the goal would be to complete as many problems as possible with the least number of attempts within the allotted time.

6.1.2 Simulator – Validation of Synthetic TRUS Imaging

The simulator component of computerized training is aimed at creating a virtual cryosurgery setup, where the physical effects of the procedure are to be replicated with high fidelity. This requires rapid bioheat transfer numerical simulations, cryoprobe layout planning algorithms, and recreation of the physical effects of frozen tissue and metallic objects in ultrasound imaging—the latter being the focus of this section. Concurrent efforts have been devoted to developing a scheme capable of simulating ultrasound imaging that include the generation of synthetic ultrasound imaging using a prostate geometry and integrate imaging effects of artifacts ranging from signal distortion to complete shadowing [106]. The scheme must be experimentally validated using a physical phantom model to match simulated freezing effects with that of the real effects. Additional instructional modes may be required to teach how to interpret TRUS imaging and frozen tissue effects in imaging.

6.1.3 Database − Develop Prostate Shapes

Key to effective computerized training is a database of realistic 3D prostate models that reflect the cryosurgery candidate population. The current database of prostate shapes must be widened to provide sufficient variability in computerized training of cryosurgery. The approach used to generate prostate models for the studies conducted in Chapters 3 & 4 was to first create a new prostate shape by deforming a base template globally using free form deformation (FFD). The EFFD computational scheme was then applied to the new shape to replicate localized geometric features of cancer on the model surface. Localized deformation criteria was systematically selected using the statistical distribution of T3-stage tumor surface features, compiled in Chapter 2, to create numerous deformed models that are clinically relevant and exhibit appropriate geometric variability. This technique can be used to further broaden the template database.

6.2 Contextualize Training Tool

The first step in contextualizing the training tool is to identify differences between the computerized trainer and current cryosurgery practices. Since standardized cryosurgery practices do not exist, the suggested approach is to code varying planning elements as input parameters, where the tutor can recommend optimal cryosurgery parameters while accommodating to the practices of the individual cryosurgeon. This section presents a strategy to identify and integrate key clinical parameters.

6.2.1 Identification of Differences

With reference to Fig. 6.2, the blue highlighted areas indicate planning components that are included in clinical practice in some form, but are not accounted for in the current computational schemes. Safety margin selection, planning isotherm as a function of position, layout creation, and any other unknowns must be identified.

In order to identify these differences, one approach is to perform a cognitive task analysis, where a ‘talk-aloud’ study is performed with an experienced cryosurgeon. Cognitive task analysis enables understanding of cognitive aspects of the task that are not accessible through direct observation [112]. In this study, the surgeon is asked to verbally think out loud through a given task, i.e. perform cryosurgery, at every step. The goal of the task analysis is identify each step of the procedure and the underlying reason for each action. This process is especially helpful in identifying intuitive steps that are difficult to formalize into verbal instruction. Figure 6.3

presents a flowchart of the proposed study, beginning with the surgeon identifying initial planning parameters including safety margin and planning isotherm selection. Next, the surgeon is presented with a prostate geometry and asked to talk out loud through the cryosurgery planning procedure. Ideally, an audio or video recording is taken of the study for future data analysis. During this time, current planning algorithms are used to determine a layout for each case using the surgeon-selected planning parameters. Next, the surgeon is asked to operate both, their plan and computer-generated plan as they would in a real cryosurgery procedure. This mode of operation requires numerical bioheat transfer and ultrasound imaging simulations. Alternatively, layouts from the surgeon and the computer-generated layout can be operated to minimum defect. Following simulation, the surgeon is asked to perform a blind evaluation, where the source of the layout is hidden, and the resulting simulated temperature field and ultrasound imaging is presented in random order. The surgeon is then asked to verbally evaluate each simulated case with the objective of capturing knowledge that contributes to their clinical judgment. Performing a blind evaluation is critical as it minimizes biases that the surgeon may have towards his or her own cryoprobe plan. Results from this study would ideally reveal differences that should be integrated into current computational tools and also provides means for context-based evaluation of a cryoprobe layout that may be incorporated into the training framework.

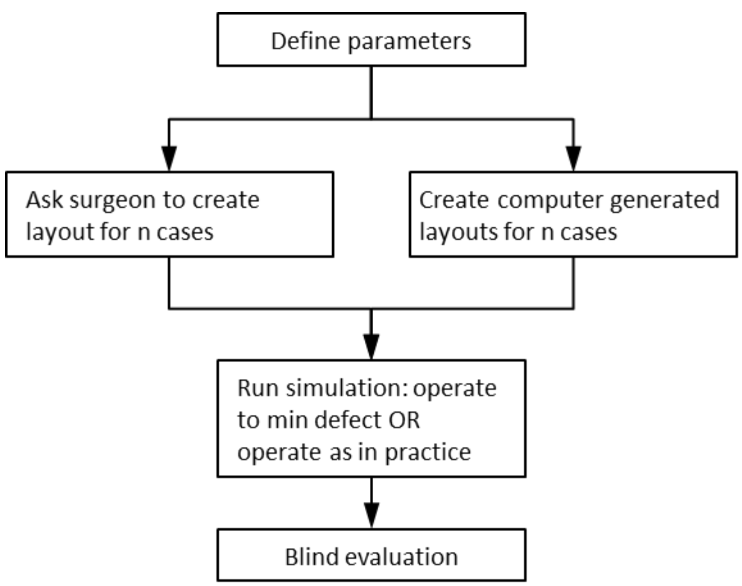

Figure 6.3: Flowchart of planning evaluation.

This study should be performed using multiple surgeons to gain a balanced perspective. Key to implementing such a study is development of a GUI that provides the user with the means to virtually carry out each cryosurgery planning task. It is recommended that a GUI be built that is capable of presenting a target geometry, manipulating cryoprobes, visualizing the workspace as seen in the clinical setting (through ultrasound imaging), and presenting ultrasound and bioheat transfer simulations for latter review.

6.2.2 *Integration of Differences*

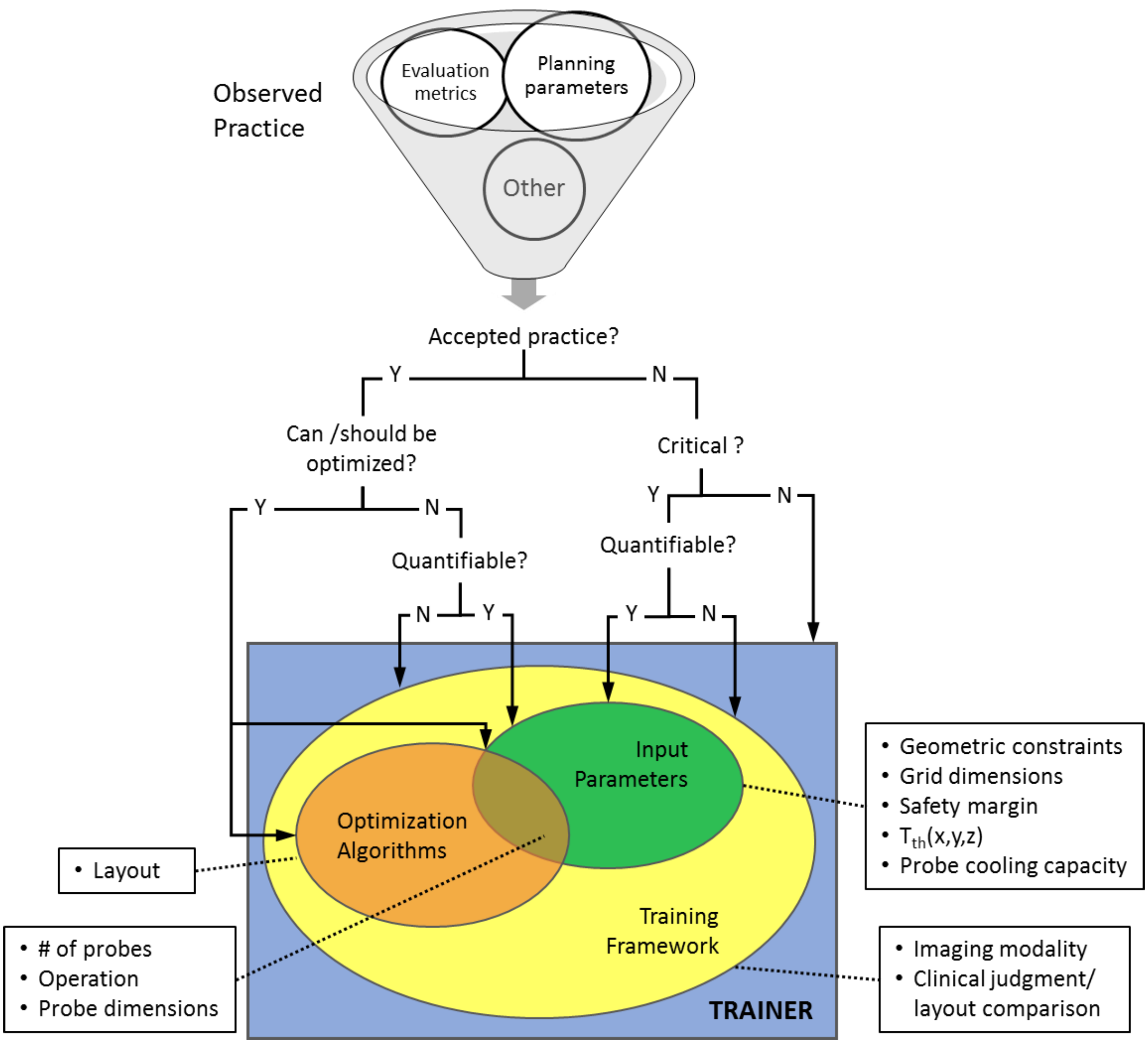

Figure 6.4: Proposed observed planning parameter-selection method for cryosurgery trainer integration. White boxes contain planning parameters that are currently and/or may be encoded into the trainer.

This section presents a systemic approach that may be used to synthesize and integrate data collected from the cryosurgery task-analysis into the cryosurgery training system. With reference to Fig. 6.4, once the cryosurgery task-analysis has been performed, all observed data should be sorted by accepted practice, i.e. if multiple cryosurgeons use the parameter. Accepted parameters should be further segmented in order to determine whether the parameter is optimization-worthy, quantifiable, or qualitative. Similarly, non-accepted parameters that are critical to planning should be segmented into qualitative and quantitative parameters. The remaining non-accepted parameters may be included in the overall trainer as a note to the trainee. Based on this scheme, three scenarios can occur: quantitative parameters may be integrated as (i) optimization algorithms or (ii) input parameters, and qualitative parameters maybe used within the (iii) training framework. A brief description of each component is provided, along with examples of representative parameters.

i. *Optimization Algorithms:* Cryoprobe layout planning algorithms may be further developed to optimize cryoprobe dimensions, as several manufacturers offer cryoprobes with an adjustable effective cooling length. The current set of computational tools can be expanded to include algorithms that optimize individual probe operation using the same defect scheme, see Eq. (6). Lastly, the defect scheme can be updated to account for the effects of over or under freezing critical tissue by assigning location-specific weights and location-specific target temperature (more than one planning isotherm). At present, the defect function assigns equal weight to tissue frozen below the planning isotherm outside of the target region and tissue above the planning isotherm inside of the target region—penalizing all defect equally. In reality, there are areas around the prostate where cryoinjury is more detrimental than others, for instance freezing near the bladder or rectal wall is considered worse than freezing near the neurovascular bundle. The same scenario applies to regions inside the prostate where tumors are more likely to grow.

ii. *Input Parameters:* Currently, the training system accepts cryoprobe geometry and cooling capacity, distances for geometric probe constraints, and a target lethal temperature as planning inputs. The tools can be further extended to incorporate: placement grid dimensions, safety margins, and additional metrics for evaluation.

iii. *Training Framework:* At present, the training framework relies on computing the defect value of a given layout to evaluate its quality. Defect is a concept developed by the Biothermal Technology Laboratory to allow for comparison and determine the point of termination of cryoprobe operation. While this concept is very useful, and currently the only metric available, to the best of the authors knowledge, to quantify layout quality—it is based on temperature and target region geometry only. For a comprehensive layout evaluation, further investigation is required to determine and codify clinical judgment. Additionally, the computerized trainer serves two purposes, enable virtual cryosurgery practice and facilitate teaching via virtual demonstrations performed by experienced cryosurgeon. Examples of demonstration-supporting tools that may be included are: geometric models of neighboring tissue/organs such as bladder, rectal wall, and neurovascular bundles, parallel visualization and monitoring of freezing of neighboring tissue/organs, advanced metrics for layout comparisons (localized vs global effects), and means to analyze multiple layouts simultaneously.

List of Publications

1. Sehrawat A, Shimada K, Rabin Y. Geometric deformation of three-dimensional prostate model with applications to computerized training of cryosurgery. Proc ASME Summer Bioeng Conf, Farmington, PA. 2011; 751–2.

2. Shimada K., Furuhata T, Song I, Sehrawat A, Rabin Y. Generation of 3d prostate models for computerized cryosurgical trainer. CRYO2011-the 48th Annual Meeting of the Society for Cryobiology, Corvallis, OR. Cryobiology. 2011; 63(3):315-316

3. Sehrawat A, Shimada K, Rabin Y. Geometric deformation models for application to the computerized training of cryosurgery. Biomedical Engineering Society (BMES) Annual Meeting, Atlanta, GA. 2012.

4. Sehrawat A, Shimada K, Rabin Y. Generating prostate models by means of geometric deformation with application to computerized training of cryosurgery. Int J Comput Assist Radiol Surg. 2013 Mar;8(2):301–12.

5. Sehrawat A, Shimada K, Rabin Y. Development of an Intelligent Tutoring System for Prostate Cryosurgery. CRYO2013-the 50th Annual Meeting of the Society for Cryobiology, N. Bethesda, DC. Cryobiology. 2013; 67(3):425-426.

6. Sehrawat A, Keelan R, Shimada K, Rabin Y. Interactive tutoring on a prostate model and prototype development. Annual Meeting of the American College of Cryosurgery, Key Largo, FL. Cryobiology. 2014 Aug;69(1):187.

7. Rabin Y, Shimada K, Keelan R, Sehrawat A, Zhang H. Computerized training objectives and prototyping, ACCryo 2014 – Annual Meeting of the American College of Cryosurgery and the Society for Cryobiology, Key Largo, FL. 2014.

8. Rabin Y, Shimada K, Keelan R, Sehrawat A, Zhang H. Computerized training tools for cryosurgery, STM 2014 – Annual Meeting of The Society for Thermal Medicine, Minneapolis, MN. 2014.

9. Sehrawat A, Keelan R, Shimada K, Wilfong DM, McCormick JT, Rabin Y. Simulation-Based Cryosurgery Intelligent Tutoring System (ITS) Prototype. Technology in Cancer Research & Treatment. 2015—*submitted*.

References

1. Gage AA. History of cryosurgery. Semin Surg Oncol. 1998 Mar 1;14(2):99–109.

2. Arnott J. Practical illustrations of the remedial efficacy of a very low or anaesthetic temperature. Lancet. 1850;2:257–9.

3. White A. Possibilities of liquid air to the physician. JAMA. 1901;36:426–9.

4. Whitehouse H. Liquid air in dermatology: its indications and limitations. JAMA. 1907;(49):371–7.

5. Pusey W. The use of carbon dioxide snow in the treatment of nevi and other lesions of the skin: a preliminary report. JAMA. 1907;49:1354–6.

6. Irvine H, Turnacliff D. Liquid oxygen in dermatology. Arch Dermatol Syphilol. 1929 Feb 1;19(2):270–80.

7. Allington H. Liquid nitrogen in the treatment of skin diseases. Calif Med. 1950;(72):153–5.

8. Zacarian SA, Adham MI. Cryotherapy of cutaneous malignancy. Cryobiology. 1966 Jan;2(4):212–8.

9. Fay T. Early experiences with local and generalized refrigeration of the human brain. J Neurosurg. 1959 May;16(3):239–59.

10. Hass G, Taylor C. A quantitative hypothermal method for production of local injury to tissue. Fed Proc. 1947;6(1):393.

11. Rowbotham GF, Haigh AL, Leslie WG. Cooling cannula for use in the treatment of cerebral neoplasms. Lancet. 1959 Jan 3;1(7062):12–5.

12. Rosomoff H, Clasen R, Hartstock R. Brain reaction to experimental injury after hypothermia. Arch Neurol. 1965 Oct 1;13(4):337–45.

13. Clasen R, Brown D, Leavitt S, Hass G. The production by liquid nitrogen of acute closed lesions. Surg Gynecol Obstet. 1953;96:605–16.

14. Copper IS. Cryogenic surgery: a new method of destruction or extirpation of benign or malignant tissues. N Engl J Med. 1963 Apr 4;268:743–9.

15. Gage A, Erickson R. Cryotherapy and curettage for bone tumors. J Cryother. 1968;1:60-6.

16. Miller D, Metzner D. Cryosurgery for tumors of the head and neck. Trans Am Acad Ophthalmol Otolaryngol. 1969;73:300–9.

17. Lincoff H, McLean J, Long R. Cryosurgical treatment of intraocular tumors. Am J Ophthalmol. 1967;63:389–99.

18. DeRoeth A. Cryosurgery for the treatment of glaucoma. Trans Am Ophthalmol Soc. Trans Am Acad Ophthalmol Soc. 1965;63:189–202.

19. Grana L, Kidd J, Swenson O. Cryogenic techniques within the tracheobronchial tree. J Cryosurg. 1969;2:62–7.

20. Gonder MJ, Soanes WA, Smith V. Experimental prostate cryosurgery. Invest Urol. 1964 May;1:610–9.

21. Addonizio JC. Another look at cryoprostatectomy. Cryobiology. 1982 Jun;19(3):223–7.

22. Flocks R, Nelson C, Boatman D. Perineal cryosurgery for prostatic carcinoma. J Urol. 1972;108:933–5.

23. Megalli M, Gursel E, Veenema R. Closed perineal cryosurgery in prostate cancer. New probe and technique. Urology. 1974;4:220–2.

24. Baust J, Chang Z. Underlying mechanisms of damage and new concepts in cryosurgical instrumentation. In: Baust J, Chang Z, editors. Cryosurgery: Mechanism and Applications. Paris, France: Institut international de froid; 1995. p. 21–36.

25. Baust JG, Gage AA. The molecular basis of cryosurgery. BJU Int. 2005 Jun;95(9):1187–91.

26. Mazur P. Freezing of living cells: mechanisms and implications. Am J Physiol. 1984 Sep;247(3 Pt 1):C125–42.

27. Gage AA, Baust J. Mechanisms of Tissue Injury in Cryosurgery. Cryobiology. 1998 Nov;37(3):171–86.

28. Cahan W. Cryosurgery of malignant and benign tumors. Fed Proc. 1965;24:S241–8.

29. Cooper I. Cryogenic surgery for cancer. Fed Proc. 1965;24:S237–40.

30. Gage A, Koepf S, Wehrle D, Emmings F. Cryotherapy for cancer of the lip and oral cavity. Cancer. 1965;18:1646–51.

31. Gage AA, Guest K, Montes M, Caruana JA, Whalen DA. Effect of varying freezing and thawing rates in experimental cryosurgery. Cryobiology. 1985 Apr;22(2):175–82.

32. Zacarian SA. The observation of freeze thaw cycles upon cancer-cell suspensions. J Dermatol Surg Oncol. 1977;3:173–4.

33. Neel H, Ketcham A, Hammond W. Requisites for successful cryogenic surgery of cancer. Arch Surg. 1971;102:45–8.

34. American Cancer Society. What are the key statistics about prostate cancer? [Internet]. Available from: http://www.cancer.org/cancer/prostatecancer/detailedguide/prostate-cancer-key-statistics

35. Chang S, McKiernan J. Genitourinary. In: Edge S, Byrd D, Compton C, Fritz A, Greene F, Trotti A, editors. AJCC Cancer Staging Manual. 7th ed. New York: Springer; 2010. p. 457–68.

36. Babaian RJ, Donnelly B, Bahn D, Baust JG, Dineen M, Ellis D, et al. Best practice statement on cryosurgery for the treatment of localized prostate cancer. J Urol. 2008 Nov;180(5):1993–2004.

37. Zisman A, Pantuck AJ, Cohen JK, Belldegrun AS. Prostate cryoablation using direct transperineal placement of ultrathin probes through a 17-gauge brachytherapy template-technique and preliminary results. Urology. 2001 Dec;58(6):988–93.

38. Han K-R, Cohen JK, Miller RJ, Pantuck AJ, Freitas DG, Cuevas CA, et al. Treatment of organ confined prostate cancer with third generation cryosurgery: preliminary multicenter experience. J Urol. 2003 Oct;170(4 Pt 1):1126–30.

39. Constantinou J, Feneley MR. PSA testing: an evolving relationship with prostate cancer screening. Prostate Cancer Prostatic Dis. 2005 Nov 29;9(1):6–13.

40. Onik G, Cobb C, Cohen J, Zabkar J, Porterfield B. US characteristics of frozen prostate. Radiology. 1988 Sep;168(3):629–31.

41. Onik GM, Cohen JK, Reyes GD, Rubinsky B, Chang Z, Baust J. Transrectal ultrasound-guided percutaneous radical cryosurgical ablation of the prostate. Cancer. 1993 Aug 15;72(4):1291–9.

42. Cohen JK, Miller RJ. Thermal protection of urethra during cryosurgery of prostate. Cryobiology. 1994 Jun;31(3):313–6.

43. Wong WS, Chinn DO, Chinn M, Chinn J, Tom WL, Tom WL. Cryosurgery as a treatment for prostate carcinoma: results and complications. Cancer. 1997 Mar 1;79(5):963–74.

44. Cohen JK. Cryosurgery of the Prostate: Techniques and Indications. Rev Urol. 2004;6(Suppl 4):S20–6.

45. Cresswell J, Asterling S, Chaudhary M, Sheikh N, Greene D. Third-generation cryotherapy for prostate cancer in the UK: a prospective study of the early outcomes in primary and recurrent disease. BJU Int. 2006 May 1;97(5):969–74.

46. Rossi MR, Tanaka D, Shimada K, Rabin Y. Computerized Planning of Prostate Cryosurgery Using Variable Cryoprobe Insertion Depth. Cryobiology. 2010 Feb;60(1):71–9.

47. Baissalov R, Sandison GA, Donnelly BJ, Saliken JC, McKinnon JG, Muldrew K, et al. A semi-empirical treatment planning model for optimization of multiprobe cryosurgery. Phys Med Biol. 2000 May;45(5):1085–98.

48. Baissalov R, Sandison GA, Reynolds D, Muldrew K. Simultaneous optimization of cryoprobe placement and thermal protocol for cryosurgery. Phys Med Biol. 2001 Jul;46(7):1799–814.

49. Keanini R, Rubinsky B. Optimization of multiprobe cryosurgery. J Heat Transf T ASME. 1992;114:796–802.

50. Lung DC, Stahovich TF, Rabin Y. Computerized planning for multiprobe cryosurgery using a force-field analogy. Comput Methods Biomech Biomed Engin. 2004 Apr;7(2):101–10.

51. Tanaka D, Shimada K, Rabin Y. Two-phase Computerized Planning of Cryosurgery Using Bubble-packing and Force-field Analogy. J Biomech Eng. 2006 Feb;128(1):49–58.

52. Tanaka D, Shimada K, Rossi MR, Rabin Y. Computerized planning of prostate cryosurgery with pullback operation. Comput Aided Surg Off J Int Soc Comput Aided Surg. 2008 Jan;13(1):1–13.

53. Tanaka D, Shimada K, Rossi MR, Rabin Y. Towards intra-operative computerized planning of prostate cryosurgery. Int J Med Robot Comput Assist Surg MRCAS. 2007 Mar;3:10–9.

54. Rossi MR, Tanaka D, Shimada K, Rabin Y. An Efficient Numerical Technique for Bioheat Simulations and its Application to Computerized Cryosurgery Planning. Comput Methods Programs Biomed. 2007 Jan;85(1):41–50.

55. Ziv A, Small SD, Wolpe PR. Patient safety and simulation-based medical education. Med Teach. 2000;22(5):489–95.

56. Scalese RJ, Obeso VT, Issenberg SB. Simulation technology for skills training and competency assessment in medical education. J Gen Intern Med. 2008;23(1 SUPPL.):46–9.

57. Bradley P. The history of simulation in medical education and possible future directions. Med Educ. 2006 Mar 1;40(3):254–62.

58. Aggarwal R, Black SA, Hance JR, Darzi A, Cheshire NJW. Virtual Reality Simulation Training can Improve Inexperienced Surgeons' Endovascular Skills. Eur J Vasc Endovasc Surg. 2006 Jun;31(6):588–93.

59. Larsen CR, Soerensen JL, Grantcharov TP, Dalsgaard T, Schouenborg L, Ottosen C, et al. Effect of virtual reality training on laparoscopic surgery: randomised controlled trial. BMJ. 2009 May 14;338:b1802–b1802.

60. Srivastava S, Youngblood PL, Rawn C, Hariri S, Heinrichs WL, Ladd AL. Initial evaluation of a shoulder arthroscopy simulator: establishing construct validity. J Shoulder Elb Surg Am Shoulder Elb Surg Al. 2004 Apr;13(2):196–205.

61. Jenkins S, Goel R, Morrell DS. Computer-assisted instruction versus traditional lecture for medical student teaching of dermatology morphology: A randomized control trial. J Am Acad Dermatol. 2008 Aug;59(2):255–9.

62. McNulty JA, Sonntag B, Sinacore JM. Evaluation of computer-aided instruction in a gross anatomy course: A six-year study. Anat Sci Educ. 2009 Jan 1;2(1):2–8.

63. Kopp V, Stark R, Fischer MR. Fostering diagnostic knowledge through computer-supported, case-based worked examples: effects of erroneous examples and feedback. Med Educ. 2008 Aug 1;42(8):823–9.

64. Cook DA, Triola MM. Virtual patients: a critical literature review and proposed next steps. Med Educ. 2009 Apr 1;43(4):303–11.

65. Corbett A, Koedinger KR, Anderson J. Intelligent Tutoring Systems. In: Helander M, Landauer T, Prabhu P, editors. Handbook of Human-Computer Interaction. Second. Elsevier Science BV; 1997.

66. Anderson JR, Lebiere C. The atomic components of thought. Mahwah, NJ: Erlbaum; 1998.

67. Ohlsson S. Constraint-Based Student Modeling. In: Greer JE, McCalla GI, editors. Student Modelling: The Key to Individualized Knowledge-Based Instruction. Springer Berlin Heidelberg; 1994. p. 167–89.

68. Koedinger K, Anderson J. Effective use of intelligent software in high school math classrooms. World Conference on Artifical Intelligence in Education. Charlottesville, VA; 1993. p. 241–8.

69. Gertner AS, VanLehn K. Andes: A Coached Problem Solving Environment for Physics. Proceedings of the 5th International Conference on Intelligent Tutoring Systems. London, UK; 2000. p. 133–42.

70. Mitrović A. Experiences in Implementing Constraint-Based Modeling in SQL-Tutor. In: Goettl BP, Halff HM, Redfield CL, Shute VJ, editors. Intelligent Tutoring Systems. Springer Berlin Heidelberg; 1998. p. 414–23.

71. Clancey W. The Handbook of Artificial Intelligence. Barr A, Feigenbaum E, editors. Los Altos, CA: William Kaufmann, Inc; 1982.

72. Eliot CR, Williams KA, Woolf BP. An intelligent learning environment for advanced cardiac life support. Proc AMIA Annu Fall Symp. 1996;7–11.

73. Azevedo R, Lajoie SP. The cognitive basis for the design of a mammography interpretation tutor. Int J Artif Intell Educ. 1998;9(1/2):32–44.

74. Sharples M, Jeffery NP, du Boulay B, Teather BA, Teather D, du Boulay GH. Structured computer-based training in the interpretation of neuroradiological images. Int J Med Inf. 2000 Dec 1;60(3):263–80.

75. Crowley RS, Naus GJ, Friedman CP. Development of visual diagnostic expertise in pathology. Proc AMIA Symp. 2001;125–9.

76. Evens M, Lee Y, Shim L, Woo C, Zhang Y, Michael JA, et al. CIRCSIM-Tutor: An Intelligent Tutoring System. 2002;

77. Sehrawat A, Shimada K, Rabin Y. Geometric deformation of three-dimensional prostate model with applications to computerized training of cryosurgery. Proc ASME Summer Bioeng Conf, Farmington, PA. 2011; 751–2.

78. Sehrawat A, Shimada K, Rabin Y. Geometric deformation models for application to the computerized training of cryosurgery. Biomedical Engineering Society (BMES) Annual Meeting, Atlanta, GA. 2012.

79. Sehrawat A, Shimada K, Rabin Y. Generating prostate models by means of geometric deformation with application to computerized training of cryosurgery. Int J Comput Assist Radiol Surg. 2013 Mar;8(2):301–12.

80. Kohn E. Invasion and Metastases. In: Hong W, Bast R, Hait W, Kufe D, Pollock R, editors. Holland-Frei Cancer Medicine. 8th ed. China: PMPH; 2010. p. 141–8.

81. Meiers I, Waters DJ, Bostwick DG. Preoperative prediction of multifocal prostate cancer and application of focal therapy: review 2007. Urology. 2007 Dec;70(6 Suppl):3–8.

82. Bosch JLHR, Tilling K, Bohnen AM, Bangma CH, Donovan JL. Establishing normal reference ranges for prostate volume change with age in the population-based Krimpen-study: prediction of future prostate volume in individual men. The Prostate. 2007 Dec 1;67(16):1816–24.

83. Prostate Cancer Treatment (PDQ®) - National Cancer Institute [Internet]. Available from: http://www.cancer.gov/cancertopics/pdq/treatment/prostate/Patient/page2

84. McNeal JE, Redwine EA, Freiha FS, Stamey TA. Zonal distribution of prostatic adenocarcinoma. Correlation with histologic pattern and direction of spread. Am J Surg Pathol. 1988 Dec;12(12):897–906.

85. Bostwick DG, Qian J, Hossain D. In: Non-neoplastic diseases of the prostate. Bostwick DG, Cheng L, editors. Urologic surgical pathology Elsevier Inc; China: 2008. pp. 381–442.

86. Villers A, McNeal JE, Redwine EA, Freiha FS, Stamey TA. The role of perineural space invasion in the local spread of prostatic adenocarcinoma. J Urol. 1989 Sep;142(3):763–8.

87. McNeal JE, Haillot O. Patterns of spread of adenocarcinoma in the prostate as related to cancer volume. The Prostate. 2001 Sep 15;49(1):48–57.

88. Ganzer R, Blana A, Gaumann A, Stolzenburg J-U, Rabenalt R, Bach T, et al. Topographical anatomy of periprostatic and capsular nerves: quantification and computerised planimetry. Eur Urol. 2008 Aug;54(2):353–60.

89. Keelan R, Shimada K, Rabin Y. Developing a Framework for Computerized Training of Cryosurgery Based on Finite Elements Analysis. Proc ASME Summer Bioeng Conf. 2011 Jun 22;749–50.

90. Furuhata T, Song I-H, Rabin Y, Shimada K. Interactive Prostate Shape Reconstruction from 3D TRUS Images. Int J of Comput Assist Radiol Surg. 2011—*submitted.*

91. Opell MB, Zeng J, Bauer JJ, Connelly RR, Zhang W, Sesterhenn IA, et al. Investigating the distribution of prostate cancer using three-dimensional computer simulation. Prostate Cancer Prostatic Dis. 2002;5(3):204–8.

92. Mun-Bo Shim, Murat Gunay, Kenji Shimada. Three-dimensional shape reconstruction of abdominal aortic aneurysm. Comput-Aided Des. 2009;41:555–65.

93. Sederberg T, Parry S. Free-form deformation of solid geometric models. ACM SIGGRAPH Comput Graph. 1986;20(4):151–60.

94. Gunay M, Shim M-B, Shimada K. Cost- and time-effective three-dimensional bone-shape reconstruction from X-ray images. Int J Med Robot Comput Assist Surg MRCAS. 2007 Dec;3(4):323–35.

95. Bardinet E, Cohen L, Ayache N. A parametric deformable model to fit unstructured 3d data. INRIA Tech Rep. 1995;2617.

96. Montagnat J, Delingette H. Globally constrained deformable models for 3D object reconstruction. Signal Process. 1997;71(2):173–86.

97. Battle XL, Le Rest C, Turzo A, Bizais Y. Three-dimensional attenuation map reconstruction using geometrical models and free-form deformations. IEEE Trans Med Imaging. 2000 May;19(5):404–11.

98. Coquillart S. Extended Free-form Deformation: A Sculpturing Tool for 3D Geometric Modeling. Proceedings of the 17th Annual Conference on Computer Graphics and Interactive Techniques. New York, NY, USA: ACM; 1990. p. 187–96.

99. MacCracken R, Joy KI. Free-form Deformations with Lattices of Arbitrary Topology. Proceedings of the 23rd Annual Conference on Computer Graphics and Interactive Techniques. New York, NY, USA: ACM; 1996. p. 181–8.

100. Xiao Y. Extended Free-Form Deformation [Internet]. Available from: http://classes.soe.ucsc.edu/cmps260/Winter03/proj/yx51866/projectReport.html

101. Rabin Y. Key Issues in Bioheat Transfer Simulations for the Application of Cryosurgery Planning. Cryobiology. 2008 Jun;56(3):248–50.

102. Rossi MR, Tanaka D, Shimada K, Rabin Y. Computerized Planning of Cryosurgery Using Bubble Packing: An Experimental Validation on a Phantom Material. Int J Heat Mass Transf. 2008 Nov;51(23-24):5671–8.

103. Sehrawat A, Shimada K, Rabin Y. Development of an Intelligent Tutoring System for Prostate Cryosurgery. CRYO2013-the 50th Annual Meeting of the Society for Cryobiology, N. Bethesda, DC. Cryobiology. 2013; 67(3):425-426.

104. Sehrawat A, Keelan R, Shimada K, Rabin Y. Interactive tutoring on a prostate model and prototype development. Annual Meeting of the American College of Cryosurgery, Key Largo, FL. Cryobiology. 2014 Aug;69(1):187.

105. Tanaka D, Shimada K, Rossi MR, Rabin Y. Cryosurgery planning using bubble packing in 3D. Comput Methods Biomech Biomed Engin. 2008 Apr;11(2):113–21.

106. Keelan R, Shimada K, Rabin Y. Imaging artifacts, training interface and computational challenges. Annual Meeting of the American College of Cryosurgery. Key Largo, FL. Cryobiology. 2014 Aug;69(1):187.

107. Ryan RM, Deci EL. Intrinsic and Extrinsic Motivations: Classic Definitions and New Directions. Contemp Educ Psychol. 2000 Jan;25(1):54–67.

108. Mann KV. Motivation in medical education: how theory can inform our practice. Acad Med J Assoc Am Med Coll. 1999 Mar;74(3):237–9.

109. Knowles M. The Adult Learner: A Neglected Species. Houston, TX: Gulf Publishing Company; 1973.

110. Sobral DT. What kind of motivation drives medical students' learning quests? Med Educ. 2004;38(9):950–7.

111. Mattick K, Knight L. The importance of vocational and social aspects of approaches to learning for medical students. Adv Health Sci Educ. 2009 Dec 1;14(5):629–44.

112. Schraagen JM, Chipman SF, Shalin VL. Cognitive Task Analysis. Psychology Press; 2000. 546 p.

Appendix A: Prostate Models

Nine prostate shapes were used in the tutor studies presented in Chapters 3 and 4. Four of these shapes served as base templates (Models 1, 4, 7, and 9), reconstructed from preclinical ultrasound scanning, and the remaining five were developed by applying global and localized deformation onto their corresponding base template. Table A.1 summarizes model dimensions along with the order in which models were presented during each tutor evaluation study. Figures A.1-A.3 display various views of each prostate and urethra model. The urethra model is unique for each base template and remains unchanged in the corresponding deformed prostate model presentation.

Table A.1: Description of prostate models used in tutor evaluation studies, including order in which models were presented, minimum and maximum dimensions, and volume.

		Case Order		Model Dimensions (mm)						
Model	**Base Model**	**Study 1**	**Study 2**	**[x_{min}, x_{max}]**	**[y_{min}, y_{max}]**	**[z_{min}, z_{max}]**	**Max X_{length}**	**Max Y_{length}**	**Max Z_{length}**	**Volume (cc)**
1	-	1	5	[-27.6, 21.8]	[-20.9, 12.3]	[-20.8, 23.8]	47.9	33.1	44.7	35.1
2	1	8	7	[-26.2, 21.9]	[-22.3, 12.8]	[-19.9, 21.4]	47.6	34.9	41.2	35.0
3	1	7	9	[-22, 19.7]	[-18.5, 17.7]	[-19.8, 24.5]	41.3	36.1	44.2	34.9
4	-	6	4	[-24.3, 26.3]	[-24.7, 11.3]	[-20.6, 21.4]	50.5	35.7	42.0	35.0
5	4	5	3	[-20.1, 23]	[-24, 12.2]	[-22.2, 23.2]	43.2	36.0	45.4	35.3
6	4	9	8	[-23.5, 23.6]	[-26.6, 11]	[-20.2, 21.7]	46.6	36.6	41.9	34.8
7	-	3	1	[-23.9, 23.8]	[-22.7, 10.8]	[-19.3, 22.5]	47.1	32.5	41.8	35.0
8	7	2	6	[-24.1, 24.7]	[-22.9, 9.3]	[-20.1, 24.4]	47.9	31.8	44.5	35.0
9	-	4	2	[-23, 24.7]	[-24.4, 10.8]	[-21, 20.7]	47.4	34.7	41.8	34.9

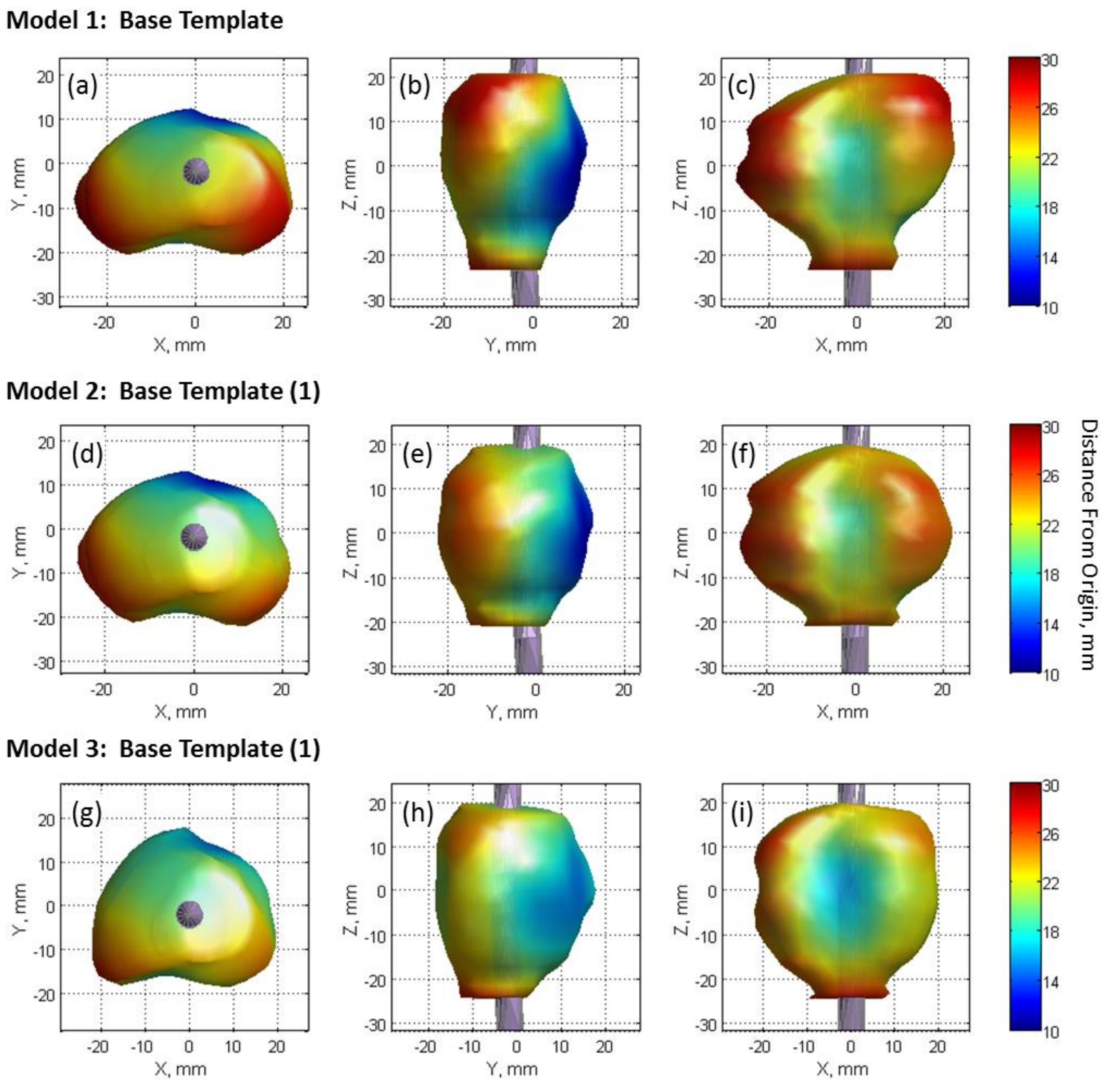

Figure A.1: Three-dimensional presentation of Models 1-3, where model color represents distance from model surface to origin. Model 1, (a)-(c), is a base template reconstructed using preclinical ultrasound scanning; Model 2, (d)-(f), was developed by geometrically deforming Model 1; Model 3, (g)-(i), was developed by geometrically deforming Model 1.

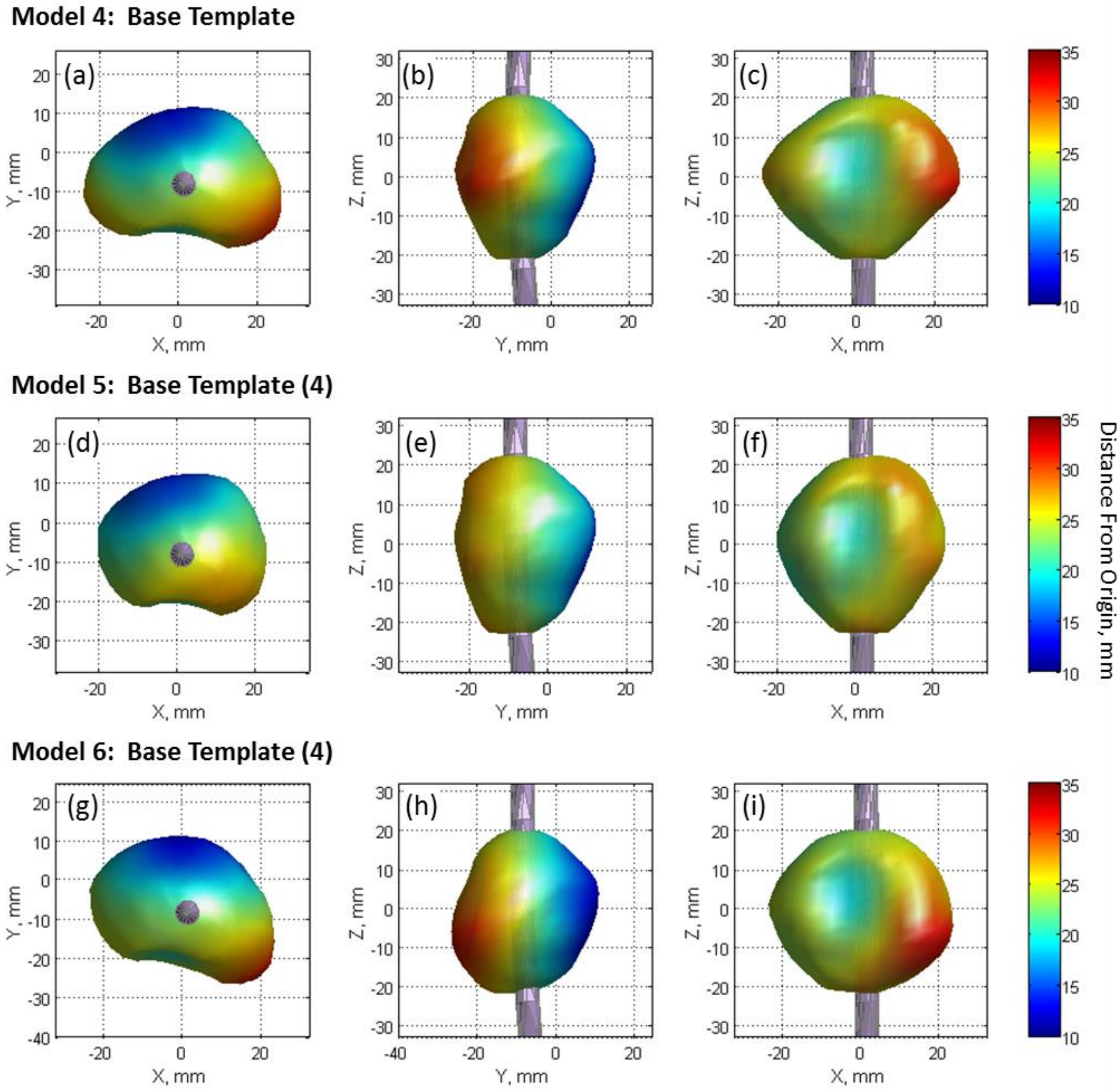

Figure A.2: Three-dimensional presentation of Models 4-6, where model color represents distance from model surface to origin. Model 4, (a)-(c), is a base template reconstructed using preclinical ultrasound scanning; Model 5, (d)-(f), was developed by geometrically deforming Model 4; Model 6, (g)-(i), was developed by geometrically deforming Model 4.

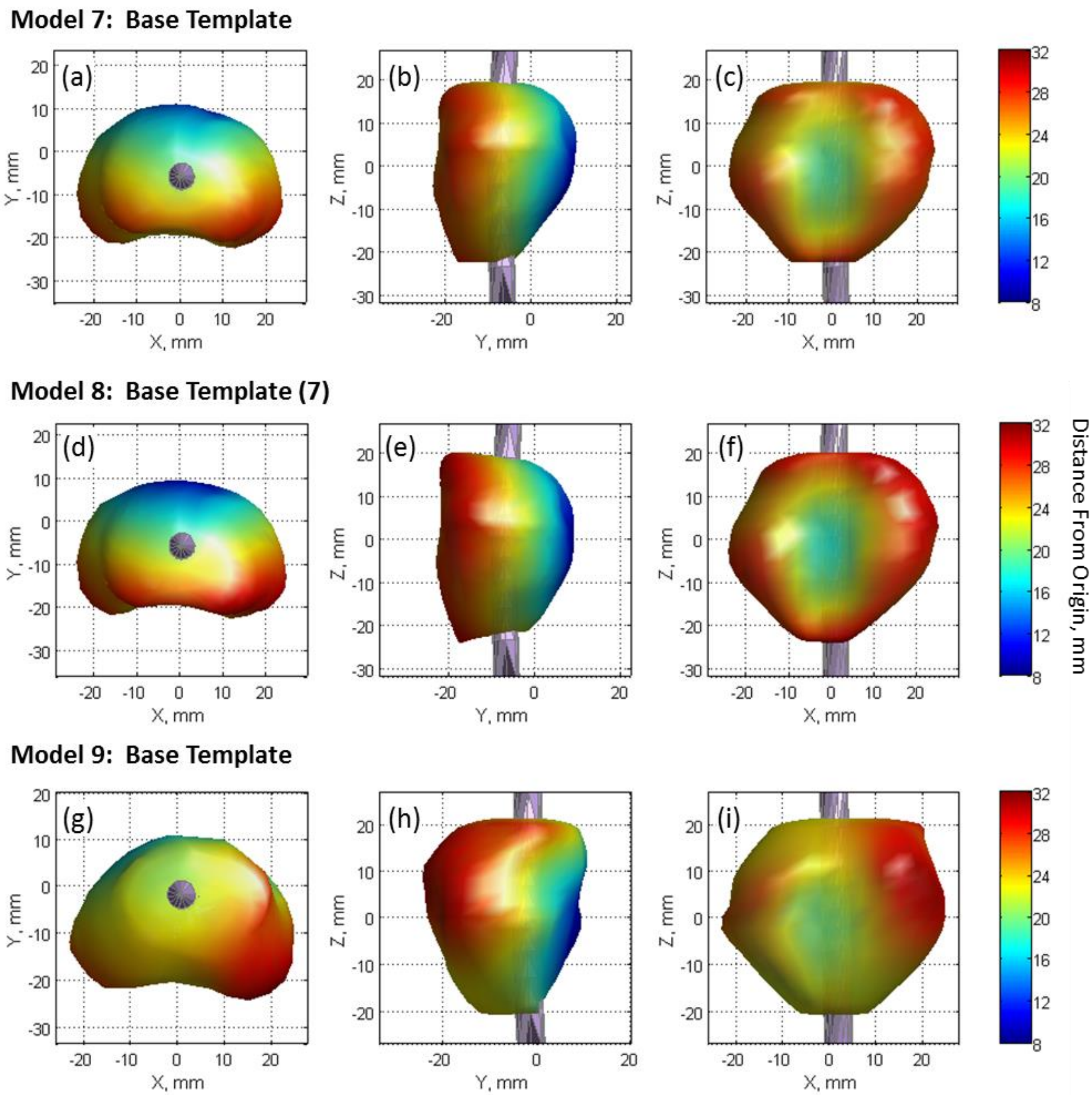

Figure A.3: Three-dimensional presentation of Models 7-9, where model color represents distance from model surface to origin. Model 7, (a)-(c), is a base template reconstructed using preclinical ultrasound scanning; Model 8, (d)-(f), was developed by geometrically deforming Model 7; Model 9, (g)-(i), is a base template reconstructed using preclinical ultrasound scanning.

Appendix B: User-Testing Guidelines

This section presents material used during the tutor evaluation studies, along with some general guidelines for designing and/or implementing user-studies.

Introduction: Contextualize system to be tested by presenting an introduction that ties in system application and long-term scope of the research so users understand what they are doing and why they are doing it. This way users understand that their contribution is significant and remain motivated. Figure B.1 displays screenshots of the presentation used to describe the cryosurgery procedure, including information about the tools, technique, and current accepted practices. The criteria used to evaluate a user-layout by the tutoring system was also reviewed. The introduction concluded with a short video demonstrating capabilities of cryosurgery computational tools to be included in the final training software—synthetic ultrasound imaging and real-time simulation of the freezing process.

System Introduction: When introducing a computerized system, it is important to remove the learning curve of the system from the actual study results. This can be achieved by providing hands-on demonstration of the system before initiating the study. When developing appropriate instruction, minimize assumptions about the user to be tested; user age, academic pedigree, etc. may be misleading when it comes to their base knowledge or ability to follow instruction. Use multiple mediums to repeat objective and critical instructions. In the studies presented in this thesis, instruction was verbally communicated and embedded into the tutoring system through text panels and pop-up warnings.

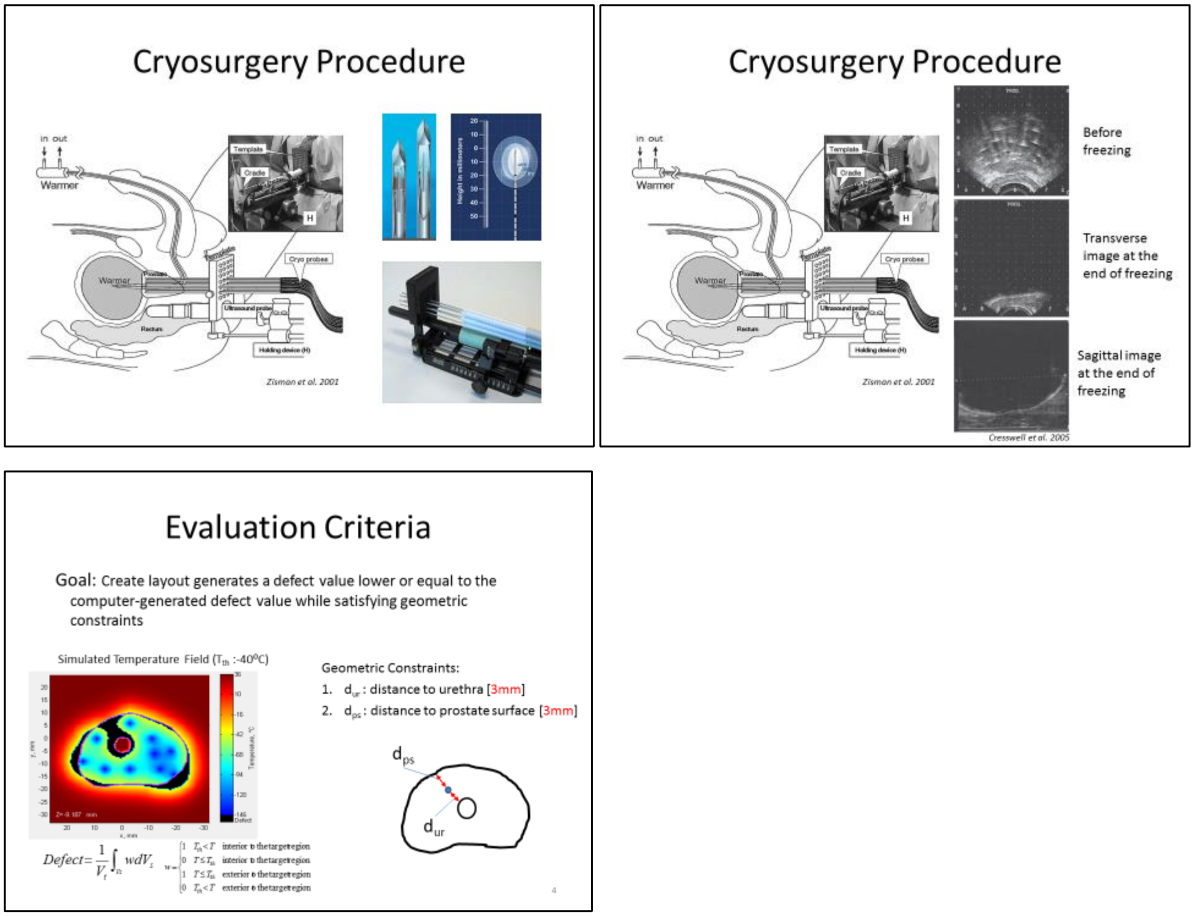

Figure B.1: Cryosurgery introduction and evaluation criteria presented prior to testing.

<u>User-Testing:</u> Carefully monitor the test session—walk around and observe how well users are following directions. This is especially helpful for users who may be unaware that their actions are incorrect. Additionally, placing a working prototype software in the hands of an untrained user may cause unexpected software/system crashes. Therefore, it is important to log every user-action/movement at the back-end such that in the event of a system crash, the researcher can determine where the user was in the training session and return the user to that state.

<u>Testing Follow-up:</u> Figure B.2 displays the questionnaire form given to users after the computerized training sessions. The questionnaire provides an opportunity to collect pertinent information about the user for further analysis and user-feedback on the tutoring system.

Cryosurgery ITS Questionnaire

1. Sex:
   ☐ Male
   ☐ Female

2. Age: _______________

3. Position:
   ☐ Medical Student Year:_______
   ☐ Resident Year:_______
   ☐ Fellow/Attending Year:_______

4. Sub-specialty, if applicable: ____________________________

5. What was your bachelor's degree concentration: __________________________

6. Rate your computation skills [1-5 -- novice-expert]:_________________

7. Do you have video gaming experience?
   ☐ No
   ☐ Yes, Year(s):______

8. Do you have experience using computerized surgical/medical training software?
   ☐ No
   ☐ Yes
   Please list software: ____
   ____
   ____

9. What was the hardest part of planning a cryoprobe layout?

10. What features of the Tutor did you find most useful?

11. What features of the Tutor were least useful?

12. Additional comments/suggestions:

Figure B.2: Questionnaire administered after user-testing.